



HAL
open science

Impact location in structures using elastic energy flow estimators with piezoelectric sensors

Xingjun Wang

► **To cite this version:**

Xingjun Wang. Impact location in structures using elastic energy flow estimators with piezoelectric sensors. Engineering Sciences [physics]. INSA Lyon, 2009. English. NNT : . tel-01777503

HAL Id: tel-01777503

<https://hal.science/tel-01777503>

Submitted on 25 Apr 2018

HAL is a multi-disciplinary open access archive for the deposit and dissemination of scientific research documents, whether they are published or not. The documents may come from teaching and research institutions in France or abroad, or from public or private research centers.

L'archive ouverte pluridisciplinaire **HAL**, est destinée au dépôt et à la diffusion de documents scientifiques de niveau recherche, publiés ou non, émanant des établissements d'enseignement et de recherche français ou étrangers, des laboratoires publics ou privés.

Impact location in structures using elastic energy flow estimators with piezoelectric sensors.

By

Xingjun WANG

A thesis submitted in fulfillment
of the requirements for the degree of

Doctor

School of doctorate: Electronic, Electrotechnic and Automatic (EEA)

INSA - Lyon

Lyon, France

21 December, 2009

Advisory Committee:

Prof. **OHAYON Georges** (reviewer)

CNAM de Paris

Prof. **ROUCHON Jean François** (reviewer)

EINSEEIHT de Toulouse UMR-CNRS

Prof. **PAPPALARDO Massimo** (Committee Member)

Università Roma

Prof. **GUYOMAR Daniel** (Advisor)

INSA de Lyon

Prof. **PETIT Lionel** (Co-advisor)

INSA de Lyon

LGEF Laboratory, Department of Electrical Engineering, INSA-Lyon

INSA Direction de la Recherche - Ecoles Doctorales – Quadriennal 2007-2010

SIGLE	ECOLE DOCTORALE	NOM ET COORDONNEES DU RESPONSABLE
CHIMIE	<u>CHIMIE DE LYON</u> http://sakura.cpe.fr/ED206 M. Jean Marc LANCELIN Insa : R. GOURDON	M. Jean Marc LANCELIN Université Claude Bernard Lyon 1 Bât CPE 43 bd du 11 novembre 1918 69622 VILLEURBANNE Cedex Tél : 04.72.43 13 95 Fax : lancelin@hikari.cpe.fr
E.E.A.	<u>ELECTRONIQUE,</u> <u>ELECTROTECHNIQUE, AUTOMATIQUE</u> http://www.insa-lyon.fr/eea M. Alain NICOLAS Insa : C. PLOSSU ede2a@insa-lyon.fr Secrétariat : M. LABOUNE AM. 64.43 – Fax : 64.54	M. Alain NICOLAS Ecole Centrale de Lyon Bâtiment H9 36 avenue Guy de Collongue 69134 ECULLY Tél : 04.72.18 60 97 Fax : 04 78 43 37 17 eea@ec-lyon.fr Secrétariat : M.C. HAVGOUDOUKIAN
E2M2	<u>EVOLUTION, ECOSYSTEME,</u> <u>MICROBIOLOGIE, MODELISATION</u> http://biomserv.univ-lyon1.fr/E2M2 M. Jean-Pierre FLANDROIS Insa : H. CHARLES	M. Jean-Pierre FLANDROIS CNRS UMR 5558 Université Claude Bernard Lyon 1 Bât G. Mendel 43 bd du 11 novembre 1918 69622 VILLEURBANNE Cédex Tél : 04.26 23 59 50 Fax 04 26 23 59 49 06 07 53 89 13 e2m2@biomserv.univ-lyon1.fr
EDISS	<u>INTERDISCIPLINAIRE</u> <u>SCIENCES-SANTE</u> Sec : Safia Boudjema M. Didier REVEL Insa : M. LAGARDE	M. Didier REVEL Hôpital Cardiologique de Lyon Bâtiment Central 28 Avenue Doyen Lépine 69500 BRON Tél : 04.72.68 49 09 Fax :04 72 35 49 16 Didier.revel@creatis.uni-lyon1.fr
INFOMATHS	<u>INFORMATIQUE ET MATHÉMATIQUES</u> http://infomaths.univ-lyon1.fr M. Alain MILLE Secrétariat : C. DAYEYAN	M. Alain MILLE Université Claude Bernard Lyon 1 LIRIS - INFOMATHS Bâtiment Nautibus 43 bd du 11 novembre 1918 69622 VILLEURBANNE Cedex Tél : 04.72. 44 82 94 Fax 04 72 43 13 10 infomaths@bat710.univ-lyon1.fr - alain.mille@liris.cnrs.fr
Matériaux	<u>MATERIAUX DE LYON</u> M. Jean Marc PELLETIER Secrétariat : C. BERNAVON 83.85	M. Jean Marc PELLETIER INSA de Lyon MATEIS Bâtiment Blaise Pascal 7 avenue Jean Capelle 69621 VILLEURBANNE Cédex Tél : 04.72.43 83 18 Fax 04 72 43 85 28 Jean-marc.Pelletier@insa-lyon.fr
MEGA	<u>MECANIQUE, ENERGETIQUE, GENIE</u> <u>CIVIL, ACOUSTIQUE</u> M. Jean Louis GUYADER Secrétariat : M. LABOUNE PM : 71.70 –Fax : 87.12	M. Jean Louis GUYADER INSA de Lyon Laboratoire de Vibrations et Acoustique Bâtiment Antoine de Saint Exupéry 25 bis avenue Jean Capelle 69621 VILLEURBANNE Cedex Tél :04.72.18.71.70 Fax : 04 72 43 72 37 mega@lva.insa-lyon.fr
ScSo	<u>ScSo*</u> M. OBADIA Lionel Insa : J. Y. TOUSSAINT	M. OBADIA Lionel Université Lyon 2 86 rue Pasteur 69365 LYON Cedex 07 Tél : 04.78.69.72.76 Fax : 04.37.28.04.48 Lionel.Obadia@univ-lyon2.fr

*ScSo : Histoire, Géographie, Aménagement, Urbanisme, Archéologie, Science politique, Sociologie, Anthropologie

Resumé

La détection et la quantification de chocs sur une structure mécanique reste une attente majeure dans de nombreuses thématiques, notamment celle du contrôle de santé structurel (Health monitoring). Les domaines les plus demandeurs sont sans nul doute l'aéronautique et l'aérospatiale où l'utilisation de plus en plus fréquente de structures composites rend leur suivi et leur contrôle de santé indispensables pour d'évidentes raisons de performances et de sécurités de fonctionnement.

Savoir détecter et localiser des chocs, c'est avant tout savoir dresser un historique des impacts générés sur la structures et permettre ainsi de gérer au mieux le risque d'apparition d'endommagements structurels (casse, délaminage, déformation...).

L'objectif central de ces travaux de thèse a porté sur la détection d'impact par l'estimation du flux d'énergie élastique induit (vecteur de Poynting) lors du choc.

Ces estimateurs sont déduits des tensions électriques fournies par des éléments piézoélectriques collés sur la structure.

Le chapitre introductif dresse un état de l'art des techniques de détection d'impact. La pertinence des présents travaux est alors justifiée en premier lieu par le besoin de disposer de techniques simples à mettre en œuvre et basées sur des estimateurs mathématiques ne nécessitant pas de systèmes de calculs complexes. Ceci dans le but ultime de pouvoir proposer des techniques à très faibles besoins énergétiques, pouvant donc être *autoalimentables*.

Dans le **1^{er} chapitre**, la méthode à été évaluée théoriquement et expérimentalement sur une structure 1D (poutre) accueillant un réseau de capteurs piézoélectriques uniformément répartis. Le flux énergétique peut alors être estimé à partir de la différentielle de l'énergie électrique extraite par 2 capteurs consécutifs. Cette différentielle s'annule si l'impact a eu lieu sur la zone délimitée par les 2 capteurs, sinon son signe indique la localisation (*i.e.* gauche ou droite) de l'impact.

Cette technique simple à mettre en oeuvre et totalement passive, possède néanmoins une résolution faible car limitée à la distance inter-capteurs du réseau.

La suite des travaux à consister à étendre ce concept de détection à des structures 2D (type plaques ou coques) plus représentatives des structures

communément utilisées dans les domaines d'application visés.

Afin d'avoir les outils théoriques requis, **le 3^{ème} chapitre** est consacré au calcul de la réponse impulsionnelle liant la force d'impact à la tension sur les éléments piézoélectriques en considérant une plaque mince infinie. La réponse à un choc quelconque s'obtient en convoluant la réponse impulsionnelle par une force représentative du choc.

Dans le 4^{ème} chapitre, un estimateur de la direction du vecteur de Poynting est d'abord théoriquement établi à partir de la tension d'éléments piézoélectriques. Ceux-ci adoptent ici un arrangement géométrique en maille, délimitant ainsi une surface fermée unitaire. Si le choc a lieu à l'extérieur de la maille, l'estimateur est nul car l'intégrale temporelle du flux au travers de la surface est nul (flux entrant = flux sortant). Dans le cas contraire, l'estimateur est non nul.

Cette approche est validée par des résultats expérimentaux obtenus sur une plaque métallique de grande dimension (120 x 80 cm²).

Le **chapitre 5** introduit un nouvel estimateur du vecteur de Poynting plus performant que celui introduit précédemment.

Le but ici est de disposer non seulement d'une information concernant la direction du flux, mais également d'estimer l'amplitude de ce flux, et de pouvoir au final quantifier pleinement l'impact.

Une nouvelle approche théorique est donc développée pour approximer au mieux le vecteur de Poynting, toujours à l'aide des tensions générées par les capteurs piézoélectriques.

Les simulations et les résultats expérimentaux obtenus sont concordants et ouvrent d'intéressantes perspectives.

En **conclusion**, ces travaux ont montré qu'il est envisageable de développer des estimateurs du flux d'énergie élastique induit par un choc sur une structure élastique et de pouvoir en tirer des informations concernant sa localisation, voire son amplitude. L'approche théorique est complexe et nécessite une connaissance globale des divers couplages mis en jeu.

Quoi qu'il en soit, ces techniques, de part leur simplicité de mise en œuvre et leur

Resumé

faible demande de moyens de calcul, constituent une proposition intéressante pour de futures techniques de détection d'impact passives ayant de plus la faculté d'être *autoalimentables* ; autrement dit, ayant la faculté de puiser directement dans les vibrations de la structure l'énergie suffisante pour assurer le calcul de l'estimateur et sa transmission par liaison sans fils.

Acknowledgements

Acknowledgements

I would like to express my sincere gratitude and appreciation to two of my advisors Pro. Daniel Guyomar, Professor and Pro. Lionel Petit.

I owe profound debt of gratitude to Pro. Daniel Guyomar who gives me a chance to study this thesis, for his sense of responsibility, enlightening guidance, and incredible patience during the whole course of my studying.

I would like to thank to Pro. Lionel Petit for his kindness support during this work.

I would like to thank to Kaori Yuse who give me many advises on writing science paper.

I would also like to express my heartfelt gratefulness to my teammate Lallart Mickael for his kindness support during this work.

The experimental work could not have progressed as quickly without the support of Defromerie Frederic.

I would like to thank to Evelyne Dorieux, secretary of Laboratory, for her supporting.

I would also like to express my gratefulness to my colleagues (Thibaut, Adil, Christophe, Abdelowahed, Saber, Rabah, Akram, Chatchai, Pierre-Jean, Jiawei, Kaixiang, Hongying, Masae, Dan, Qin...)

I will not be able to list the names of all whom I feel grateful to, but I would like to express my gratitude to all of the members of LGEF, scientific and administrative for their help and support during my work.

Finally, I would like to take this opportunity to express my deepest thanks to my family for their endless encouragement and affection.

Nomenclature

P	polarization
T	stress
D	piezoelectric strain constant
E	electric field
S	strain
D_d	electrical displacement
s^E	elastic compliance
k	coupling factor
M	lineic mass
K	lineic stiffness
u_x	longitudinal displacement
u_z	flexural displacement
C_0	clamped capacitance
ϵ^S	permittivity of the piezoelement
e	voltage coefficient
A	surface of the piezoelement
l	thickness of the piezoelement
L	length of the plate
W	width of the plate
u_z	structural displacement (deflection)
I_{out}	outgoing current from the piezo-element
Δ	Laplacian poerator
m	surface density
D	bending stiffness
β	damping factor
q	applied load
$F_{ext}(x, t)$	applied force
k_x, k_y	spatial frequency along the x and y axis
Y	Young modulus
θ	Inclination angle
ν	Poisson ratio

Nomenclature

H	Plate thickness
ζ	Damping coefficient
P_x, P_y	Poynting vector in x and y direction
E_E	Electric field
V	piezovoltage
M_p	lineic mass of the part of the beam where a piezoelement is bonded
K_p	Stiffness of the part of the beam where a piezoelement is bonded
c_p	blocked pizo capacitance.

Contents

Chapter 1 Generalities.....8

1.1 Introduction.....8

1.2 Motivation for impact identification9

1.3 Overview of impact detection techniques9

1.3.1 Identification of temporal response of an impact force 10

1.3.1.1 Deconvolution technique..... 10

1.3.1.1.1 Deconvolution in the time domain 10

1.3.1.1.2 Deconvolution in the frequency domain..... 11

1.3.1.1.3 Identification of the transfer function 12

1.3.1.2 Other techniques..... 13

1.3.2 Estimation of impact force location 13

1.3.2.1 Impact location in beams..... 14

1.3.2.2 Impact location in plates 16

1.4 Motivation of the present works 17

1.5 Generalities on piezoelectric systems 20

1.5.1 Constitutive equations.....20

1.5.2 A wide range of forms.....22

1.6 Conclusion25

2 Preliminary results on beam.....26

2.1 Introduction.....26

2.2 Principle27

2.3 Modelling.....28

2.3.1 Lumped model28

2.3.2 Energetic balance30

2.4 Performance Discussion.....32

2.5 Numerical analysis-finite element simulation32

2.6 Experimental Results41

2.6.1 Experimental Set-up.....41

2.6.2 Results & Discussion42

2.7 Conclusion43

3 Transient bending wave modeling in an infinite plate with bonded piezoelectric inserts44

3.1 Introduction.....44

3.2 Impulse response modelling: theoretical approach.....45

3.2.1 Determination of the displacement under pulse force45

Contents

3.2.2	Derivation of the piezoelectric sensor voltage.....	50
3.3	Simulations-Numerical analysis	52
3.4	Comparison with finite element simulation.....	56
3.5	Comparison with experimental measurement.....	59
3.5.1	Experimental set-up	59
3.5.2	Results & Discussion	61
3.6	Conclusion	61
4	Force detection using energy flow direction estimator with piezoelectric sensors ..	63
4.1	Introduction.....	63
4.2	Principle	64
4.3	Theoretical approach.....	66
4.4	Expression of the energy density difference	66
4.5	Poynting vector and piezoelectric sensor outputs.....	69
4.6	Impact area location detection with piezoelectric sensors output.....	73
4.7	Numerical simulation validation.....	76
4.7.1	Impact location and q value determination	76
4.7.2	q -estimator value with different location inside	81
4.8	Experimental validation	83
4.8.1	Experimental set-up	83
4.8.2	Result & Discussion.....	84
4.9	Conclusion	87
5	Force detection using energy flow estimator with piezoelectric sensors.....	88
5.1	Introduction.....	88
5.2	Principles.....	89
5.3	Poynting vector applied with bending wave	90
5.4	Numerical simulation based on Poynting vector	94
5.5	Approximation of Poynting vector and piezoelectric sensors outputs....	98
5.6	Numerical simulation and experimental results based on piezoelectric sensors outputs	105
5.6.1	Numerical simulation.....	105
5.6.2	Experimental set-up	106
5.6.3	Result & Discussion.....	106
5.7	Conclusion & Further Work	115
5.8	Anisotropic plate	115
6	Conclusions.....	119

Introduction

Detection and quantification of impacts on elastic structure stays a major preoccupation in many fields, especially for Structural Health Monitoring (SHM). Aerospace and aeronautic are probably the more applicant industry sectors because the increasingly use of composite material enforces an obligatory monitoring for security survey.

Detecting impacts permits to prevent and supervise the risk of structural damage such as deformation, delamination, breakage...

This work concerns with the impact detection based on induced elastic energy flow estimators. These quantities are here deduced from voltage of a piezoelements network embedded on the structure.

The **introduction** is a state of the art in impact detection techniques. The basic common idea in these works is to indirectly estimate the impact force (amplitude and location) by convolution techniques from measurements of mechanical responses such as displacement, acceleration, and strain. These techniques generally require high computation capabilities, noise treatments and an estimation of the transfer function.

The pertinence of the present work is then justified by the need of a simplest approach using light calculation mathematical estimators in order to develop a low-power technique.

In **chapter 2**, a new method is theoretically introduced and experimentally evaluate for a 1D structure (beam), exploiting electric response of a piezoelectric sensors network. The energy flow is estimated from the energy differential of 2 consecutive sensors. This differential is nil if the impact is inside of the area delimited by the 2 sensors, otherwise its sign indicates the impact location (*i.e.* left or right of the area).

This simple technique, easy to implement and totally passive, has a low spatial resolution limited by the inter-sensors distance.

The 3rd chapter is devoted to the impulse response determination of an infinite plate in order to have the theoretical tools useful to estimate the impact force from the

piezoelectric sensor voltage. The response from a particular impact is derived from the convolution of this impulse response by the representative impact force.

.

In chapter 4, an estimator of the Poynting vector direction is theoretically established from the voltage of piezoelectric elements for a 3D structure. These elements have a specific geometrical meshed arrangement, thus delimiting an unitary closed surface of energy flow integration. If the impact is outside of this closed area, the estimator is nil because the integration in time of the flow is nil (ingoing flow=outgoing flow).

In the contrary case, the estimator is not nil.

This approach is validated by experimental results obtained with a large metallic plate (120 x 80 cm²).

In chapter 5, a new estimator of the Poynting vector is introduced. In addition of the energy flow direction, this estimator gives additional information on the energy flow amplitude in order to fully quantify the impact.

A new theoretical approach is developed here in order to refine the approximation of the Poynting vector by the piezoelectric sensor voltage. Simulations issues from this new model and experiments are in good agreement and then open new design perspectives.

In conclusion, these works show that new estimators of the energy flow induced by an impact can give informations on its location and even on its amplitude. The theoretical approach stays complex and needs a global knowledge of the relating mutiphysic couplings.

However, these techniques are simples, easy to implement and do not have a high calculation capacity requirement. They are a new interesting offer for future passive impact detection techniques with moreover the capacity to be self-powered.

Chapter 1 Generalities

1.1 Introduction

This chapter introduces the generalities concerning the impact detection techniques. The existing ways of research on this topic are presented and finally the principle of our approach, based on the energy flow estimation, is introduced. At the end, some basics generalities on piezoelectric systems are given.

1.2 Motivation for impact identification

Damage due to an external impact is a major preoccupation for structure design in many domains (aerospace, aircraft, automobile, building engineering...). Detecting damages is then essential to guarantee performances and security in such structures. In that way, many Structural Health Monitoring (SHM) approaches¹ have been developed. For example, ultrasonic inspections such as A-Scan, B-Scan, C-Scan or Lamb Wave techniques²⁻³⁻⁴⁻⁵ detect damages in metallic or composite structures with high efficiency. But most of these techniques are built around time-consuming and/or *high need of memory* algorithms and finally, they cannot be performed in real-time. To lighten the process, the structure health monitoring is often operated by periodical inspections rather than a continuous inspection. Another drawback of the SHM techniques is that an only eventual damage caused by impact is detected and not the impact itself. Yet it is important to have an impact history, even if they don't induced detectable damage, because it permit to predict damage occurrence. This point largely justify the need of impact detection techniques, not for supplant SHM ones but rather to complete them.

Numerous works have been carried out on impact location estimation. The basic concept relies on a combination of innovative sensors, advanced analytical techniques and artificial intelligence to provide a continual real time health assessment of a structure. When an impact occurs, these smart structures using information from the sensors can determine its location and eventually its amplitude. Exploiting the structural response to infer other information about the structure is referred to as an inverse problem. Before introduce our new technique, an overview of the various types of inverse problem is introduced in following part.

1.3 Overview of impact detection techniques

When considering the mechanics of structures deformations, the variation of the applied force is one of the most critical factors. The force applied to a structure cannot be measured directly but indirectly by the induced deformations variations. In order to overcome this difficulty, lots of researchers have studied this subject during several decades. This section will present a review of methods of inverse analysis for the indirect measurement of impact force.

The basic idea is to indirectly estimate the impact force from measurements of mechanical responses such as displacement, acceleration, and strain...

To completely define the impact force, it requires knowing its temporal response and its location.

1.3.1 Identification of temporal response of an impact force

The simplest approaches generally employed are based on deconvolution techniques.

1.3.1.1 Deconvolution technique

If the elastic behaviour of the structure can be considered as linear during the impact process, the response $e(t, r)$ at a particular point is given by the linear convolution of the impact force $f(t)$ by the impulse response function of the linear system $h(t)$:

$$e(t, r) = \int_0^t h(t - \tau, r) f(\tau) d\tau \quad (1.1)$$

It is assumed here that $f(t), h(t), e(t)$ equal to zero when $t < 0$. This supposed that the impulse response $h(t)$ is known and that the response $e(t)$ can be measured. In that case, the impact force $f(t)$ is obtained by the deconvolution of (1.1).

1.3.1.1.1 Deconvolution in the time domain

The equation (1.1) is expressed in the time domain as

$$e = h * f \quad (1.2)$$

where e and f are vectors composed of discrete values of $e(t)$ and $f(t)$. h is a matrix composed of discrete values of $h(t)$. The impact force history can be obtained by solving equation (1.2). From this approach, Goodier *et al*⁶ obtained the impact force from the strain measured at a point on the surface of structure. Doyle⁷ (1984) also estimated the impact force acting on a beam from the bending strain measured by strain gauges. In these studies, the impact force is obtained by solving equation (1.2) using Gaussian elimination. But these conventional Gaussian elimination methods can lead to severely noisy or unstable measurements. The h -matrix coefficients is often ill-conditioned, small errors in the response vector e induces large errors in vector f . For this reason the above approach is not so effective to obtain an accurate and stable

estimation of the impact force.

To overcome this problem of noise amplification, the least-squares method had been used in several works. Chang and Sun⁸ made the number of equations greater than the number of unknowns in equation (1.2) by imposing a response duration measurement longer than the impact force one. They solved this least-squares problem by the conjugate gradient method, which is an iterative optimization technique. But, too much iteration may cause an unstable estimation for the same reason as in conventional methods. Chang and Sun did not specify the iteration number.

The least-squares method was also used in Wu *et al*⁹ works. They considered several responses records at multiple locations simultaneously. To get a stable estimation, they consider the non-negative impact force (compressive or zero force). This problem with the non-negativity constraint was solved by an iterative optimization technique named the gradient projection method. Yen and Wu¹⁰ demonstrated the efficiency of the non-negativity constraint. In their next works, Wu *et al* carried a numerical simulation for a laminated plate and showed that this technique can improve the estimation pertinence, even when the response records are very noisy.

They also showed that too many iterations cause an unstable estimation. They proposed a criterion for the optimal iteration number, which makes an accurate and stable estimation. But, the criterion is only qualitative.

Tanka and Ohkami¹¹ proposed a technique using Truncated Singular Value Decomposition (TSVD) to detect the impact force acting on a pipe from its response measured by an accelerometer.

Fan Jiangling *et al* proposed a technique which estimates multiple periodical impact force from single point response in time domain¹².

1.3.1.1.2 Deconvolution in the frequency domain

Another basic technique is to transform the convolution in the time domain into frequency domain using Fourier transforms as:

$$E(w) = H(w)F(w) \quad (1.3)$$

When the transfer function $H(w)$ is known, the impact force can be estimated by evaluating the Fourier Transform of the measured response. The advantage of this technique is to reduce the computational task compared to that required in time

domain.

Holzer¹³ is the one of precursor to use the frequency domain deconvolution. His method involves the use of a short load cell and a fiber optics displacement transducer. The analysis of the force/time data allows signal correction for the effect of the dynamic characteristic of the force measurement system. The method involves frequency transformation of the force data by a Fast Fourier Transform algorithm, and can correct the dynamic ringing of the load cell and the phase lag of the recording system

Doyle¹⁴ claimed that frequency domain is better than time domain deconvolution because of simplicity. Some researchers also applied this technique on various structural components (Doyle¹⁵⁻¹⁶⁻¹⁷ Martim and Doyle¹⁸ Rizzi and Doyle¹⁹).

In practical computation, the data vector has a finite length, but Fourier Transforms are defined by infinite integrals. Thus, it causes a discontinuity at the end of the data, which is leakage. An exponential window $\exp(-\gamma t)$ applied to the data can reduce the leakage.

Inoue et al²⁰⁻²¹ have used this technique to estimate impact force on a beam and plate. A Fourier transform with an exponential window is the same as Laplace transform²²⁻²³. Inoue & al²⁴ used Tikhonov regularization to numerical Laplace inversion to improve the accuracy of the estimation.

It should be note that a small noise involved in the response data may cause a large change in deconvolution results. Wiener filter was used to overcome this problem by Inoue et al²⁵. Wiener filter is an optimal inverse system to reduce the amount of noise by comparison with an estimation of the desired noiseless signal. They demonstrated the effectiveness of the Wiener filter by numerical simulations on a rod.

Kishimoto & al²⁶ also showed the effectiveness of the Wiener filter on cantilever beam impact detection.

In addition, lots of researchers have used deconvolution in the frequency domain such as Whiston²⁷, Jordan and Whiston²⁸, Bateman *et al*²⁹ Kim and Lyon³⁰, Lin and Bapat³¹, McCarthy and Lyon³²

1.3.1.1.3 Identification of the transfer function

The perfect knowledge of the transfer function $h(t)$ is essential to obtain a precise estimation of the impact force.

There are basically three approaches to have the transfer function: by theoretical analysis, by experimental analysis, or by numerical analysis. Each of them has some advantages and disadvantages.

The theoretical analysis approach needs a precise modelling of the structure including significant parameters (shape, size, boundaries conditions, etc...). This generally stays a difficult approach because numerous parameters are hard to identify, and generally many approximations are indispensable.

In experimental identification, the transfer function is obtained by a calibration procedure, as described for example in³³⁻³⁴⁻³⁵. However, this also has many difficulties because small errors in the calibration data cause significant errors in the transfer function. Thus, it makes an unstable estimation of impact force.

The numerical analysis is another way for the transfer function estimation. This approach also needs experimental investigations and is difficult to carry³⁶.

1.3.1.2 Other techniques

Other techniques exist for the impact force detection. The most significant are given here:

The Sum of Weighted Acceleration Technique (SWAT) was proposed by Bateman *et al*³⁷. However, the main disadvantage of SWAT is the difficulty of determining the weighting factors.

A Neural network technique was also proposed³⁸. It can be easily applied in the case of nonlinear response. The estimation process is very simple. The parameters of the network must be determined appropriately to get an accurate estimation. In addition, a larger number of data are required to train the network adequately.

1.3.2 Estimation of impact force location

To estimate the impact location is basically a nonlinear problem even in elastic structures. In most of the researches, the main approach is that the impact location can be obtained from the velocities of stress waves and from their arrival times at several points of the structure. However, it is not easy to determine the wave velocities and arrival time in complex shapes because of waves reflections and dispersions. The majority of the proposed methods are developed for basic structures as beams or

plates.

1.3.2.1 Impact location in beams

In the field of estimation of force location, some effective methods have been proposed. For example, the identification methods based on infinite beam using Timoshenko theory³⁹.

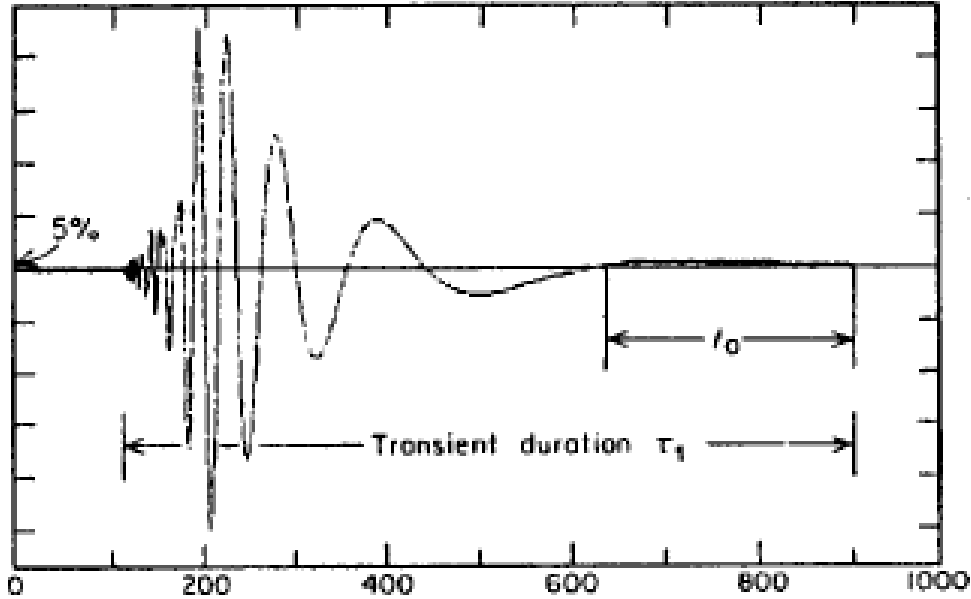


Figure 1.1. Beam acceleration response under impulse force.

The beam response to an impulse force is shown in Figure 1.1 (from⁴⁰). The high frequency compounds (fast wave) propagate velocity close to the shear velocity c_s in Timoshenko theory. Information on impact location are carried by the slowest significant component velocity $c(w_0)$. This component is observed at the pseudo-pulsation $w_0 (= \frac{\pi}{t_0})$ where t_0 is roughly estimated as shown in Figure 1.1.

The response to impulse force of τ_1 -duration can be calculated as:

$$\frac{x}{c_{w_0}} - \frac{x}{c_s} = \tau_1 \quad (1.4)$$

where x is the distance from the impact location to the measuring point.

Solving Equation (1.4), x can be obtained as:

$$x = \tau_1 \frac{c_s c(w_0)}{c_s - c(w_0)} \quad (1.5)$$

Relation (1.5) provides the distance from the impact location. However, the main restriction of this approach is that the impact force must be pulse-type and that human intervention is required for determinate the slowest pulsation component and the duration time τ_1 , which makes the approach not so simple. Based on Bernoulli-Euler beam theory, Doyle⁴¹ proposed other technique to determine the impact location. The phase information obtained from a spectral analysis of the dispersive waves is used here to locate the source of the waves. Choi & Chang⁴² have proposed an impact load identification method using distributed built-in sensors. The identification system consists of a system model and a response comparator. The system model characterizes the dynamic response of the structure subject to a known impact force. The comparator compares the measured sensor outputs with the estimated measurements from the model and predicts the location and force history of the impact. If the given experimental results are satisfactory, there are a large number of variables to optimize, which might cause difficulties in the optimization process.

To overcome the shortcoming of the above techniques, Doyle⁴³ improved his initial technique based on the spectral-element method by combined it with a stochastic genetic algorithm to give a scheme that can locate the source of structural impacts.

In this approach, two independent estimations are carried from two responses by deconvolution where the transfer function is predicted by Timoshenko theory. These two estimations were well coinciding if the impact location estimation is correct.

A genetic algorithm was considered to search for a global maximum of the correlation. A genetic algorithm (GA) is a research technique used in computing to find exact or approximate solutions to optimization and search problems.

Martin & Doyle⁴⁴ used this technique on a frame structure. First, they developed a method to predict the transfer function as a function of estimated impact location. Second, they proposed another objective function based on the differences between two estimations of the impact force. However, an appropriate tuning of parameters is essential for obtaining a sufficient fast convergence of the searching process.

Inoue & al⁴⁵ proposed a technique that did not rely on beam theory. In the prior research⁴⁶, it was shown that if a propagating pulse in a dispersive medium is recorded at a point, the arrival time of each frequency component of the pulse at that point can be estimated by a time-frequency analysis with the help of wavelet transform. The main advantage of this approach is that the impact location estimation

is only performed from experimental records without using beam theory. That is the reason this approach is easy to apply in other structures. Inoue & al. proposed a technique, which employs the arrival time of each frequency component of a pulse detected by means of wavelet, transform⁴⁷. There is also an energy extraction-based algorithm has been proposed⁴⁸⁻⁴⁹.

1.3.2.2 Impact location in plates

The oldest works on impact location in plate must probably be attributed to Yen and Wu⁵⁰⁻⁵¹. They proposed a technique from the strain responses at particular points on isotropic plates based on Greens's functions. The impact location can be obtained to transverse impact from strain responses measured at multiple points on the plate.

Ohkami and Tanaka⁵² developed a two-step technique based on classical plate theory. First, they determine an elliptic region that may contain the true impact location. Secondly, it is linked with the estimation on the impulse force history. Unfortunately, human interventions are required both in determining the elliptic region and in selecting a final estimation of the impact location.

Gaul & Hurlebaus⁵³ proposed an experimental method for detecting flexural waves in plates by the use of piezoelectric films. They solved a simple system of nonlinear equations based on arrival times of flexural waves at several points of a plate. The advantages of the approach are its accuracy. However, it should be possible to extend this approach to composite material.

A triangulation procedure incorporating a Genetic Algorithm (GA) to localize the impact location was proposed by Coverly & Staszewski⁵⁴ and Haywood & al⁵⁵. They demonstrated the promising potential of GA in impact load identification. Unfortunately, they only considered the impact location in these researches. There was no mention about how to identify the temporal impact force.

Gang Yan and Li Zhou⁵⁶ provide a GA-based approach to identify the impact location and reconstruct the impact force history simultaneously in composite panel.

Base on minimizing the error between measured strains responses in PZT sensors and numerically evaluated ones, a technique for force location was proposed⁵⁷. Not only these theoretical approaches have been developed, many experimental works also exist, mainly acoustic or stress-strain methods using optical fibers or PZT as sensor

materials⁵⁸⁻⁵⁹.

Shin⁶⁰ proposed a technique using modal displacement and accelerometers information.

Another method introduced by Akhavan & al⁶¹.use fiber optic strain sensor data as inputs to a neural network to obtain contact force history. They had designed and built an instrumented drop-weight impact tower to facilitate the measurement of contact force during an impact event. The impact head assembly incorporates a load cell to measure the contact forces experimentally. An in-house finite-element program is used to establish the validity of the fiber optic sensor contact force response. The finite-element model is based on a higher-order shear deformation theory and accounts for geometric nonlinearity.

1.4 Motivation of the present works

The previously introduced existing approaches for impact detection generally require high capabilities for computation, noise treatments and sometimes human interventions. Moreover, they have high electric power consumption, which is not the actual tendency for low-power systems especially for the embedded systems domain.

The motivation of present work gives raise in the need for a simple, low -power method to identify impact. The main goal here is not to increase the resolution of detection, but rather to have a method making the compromise between an acceptable detection resolution, an *easy to implement* computation algorithm and a low power requirement. The principle of the approach is to estimate the elastic energy flow induced by an impact in a structure with the help of piezoelectric sensors network.

Previous works⁶²⁻⁶³⁻⁶⁴ discuss on the energy flow in the structure but have not extended the work to impact location estimation.

The main difficulty in our approach is to reasonably estimate the power flow characterised by the Pointyng vector with the help of the electrical response of the embedded piezoelements.

This work has been done through various progressive steps:

In a first step, the work focuses on simple 1D problem. It has been shown that a specific shunted piezoelectric network bonded on the structure (Figure 1.2) could permit to determine the energy flow direction.

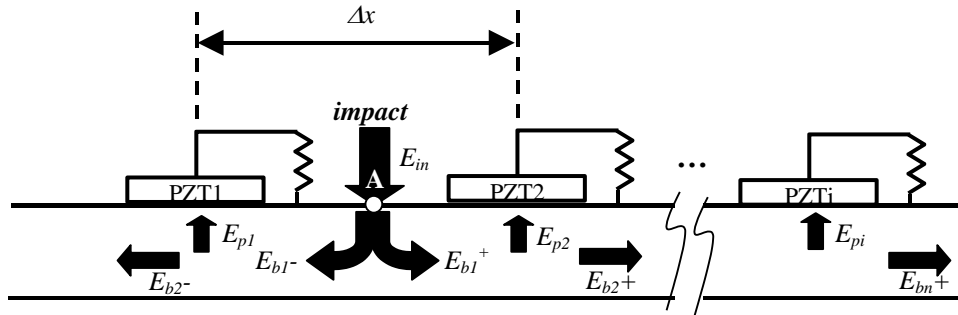


Figure 1.2 sensor network for the detection of the energy flow direction in a 1D structure.

In the second step, the problem is extended to a 2D problem (infinite plate).

Considering a closed surface (S) (Figure 1.3a), when the impact is located inside frame surface S (I -point), the mechanical energy flows out the structural surface. The time domain integral of this outgoing energy is then positive with energy.

In the case of an outside frame impact (O -point), the induced energy quantity flows in and out through the closed surface (S). The out going energy quantity and energy losses in the structure consist ingoing energy. The time domain integral is then nil, considering a lossless plate.

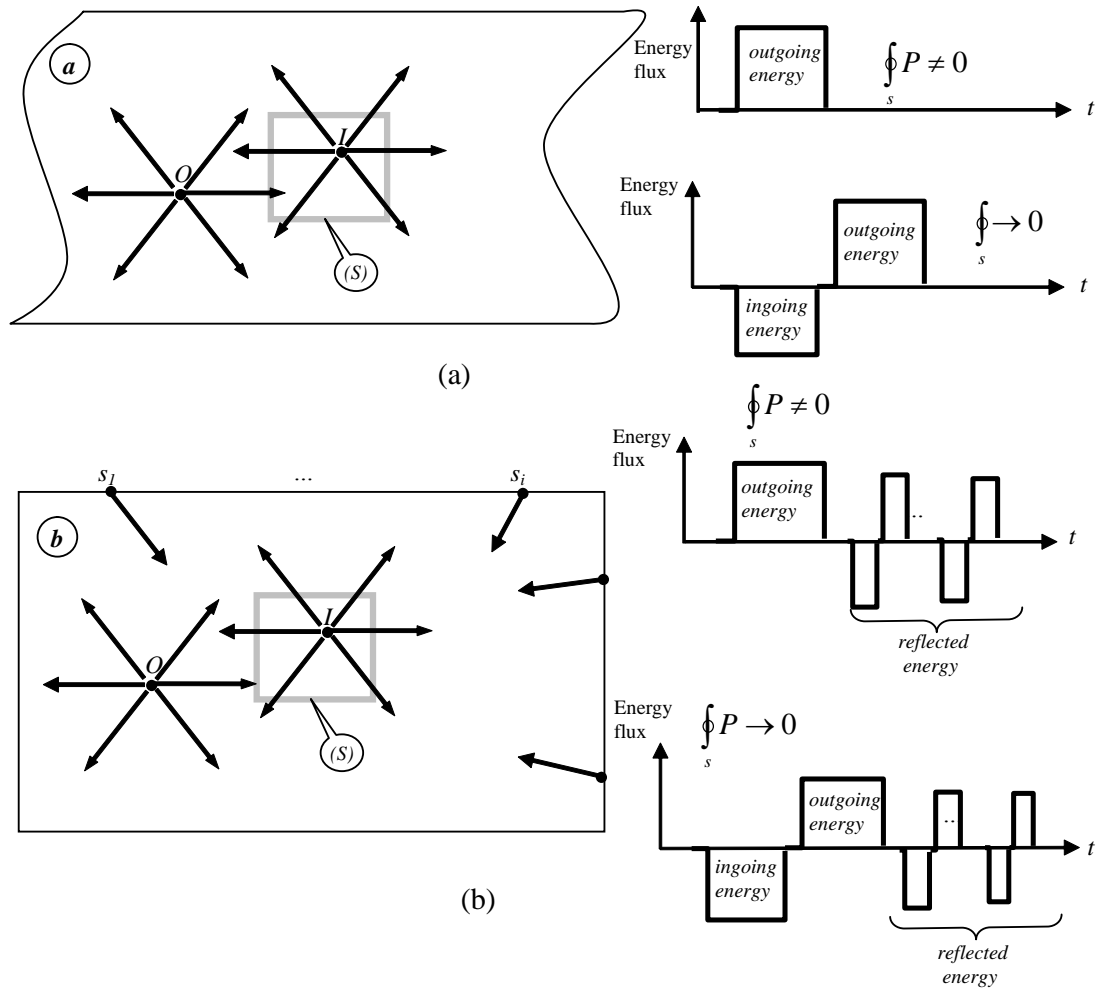


Figure 1.3: principle of the energy flux expressed by Poynting vector in an infinite structure (a) without consideration of losses. Sum of energy flux trough the surface (S) is null for an outside impact (O-point) and not null for an inside impact (I-point). For a finite structure (b), reflection on the boundaries induce secondary sources (s1..si) with a null associated energy flow.

In the case of a finite plate, the reflection phenomenon on plate edges has to be taken into account (Figure 1.3b) by considering them as secondary external sources. The flow associated to the reflected energy leads to a null value and hence does not degrade the initial information carried by the energy flow associated to the initial impact. Our works had thus focused on the development of a technique based on this approach. The basic idea is firstly to use a closed piezoelectric sensor and secondly, to estimate the energy flow trough this closed sensor from the piezoelectric sensor voltage induced by impact.

1.5 Generalities on piezoelectric systems

Many books and papers deal with piezoelectricity and we don't give here more details. We just give here the useful relation for the present work. After introducing the general constitutive equations for a piezoelectric element, main equations for a sensor deforming in bending mode is given, because it corresponds to the case funded in this work: piezoelectric sensors embedded on a bending beam or plate.

We finally show the interest in using piezoelectric technology for impact detection in terms of integration and performances.

1.5.1 Constitutive equations

The general constitutive equations for an anisotropic piezomaterial are given in (1.6) and (1.7).

$$E_i = \beta_{ij}^T D_j - g_{mi} T_m \quad (1.6)$$

$$S_i = s_{ij}^E T_j + d_{mi} E_m \quad (1.7)$$

Where

- S is the vector of deformations
- T is the vector of stress consists of 6 components $T_i = 1 \dots 6$
- E is the electric field vector with 3 components $E_i = 1 \dots 3$
- D_d is the electric displacement field vector of 3 components $D_i = 1 \dots 3$
- s^E is compliance of 6X6 matrix at constant electric field.
- d is 3X6 matrix of piezoelectric charge coefficients.
- g is 3X6 matrix of piezoelectric voltage coefficients.
- $\beta^T = \frac{1}{\varepsilon^T}$ where ε^T is the 3X3 matrix of dielectric constants measured at

constant stress

The Equation (1.6) denotes the direct piezoelectric effect, where an electric field E arises under a mechanical solicitation T . This direct effect is exploited in sensing applications. The reverse piezoelectric effect is represented by (1.7): when an external electric field E is applied on the piezoelement, it deformed itself. This indirect effect

is exploited in actuation applications.

Our task mainly concerns with bending sensors (Figure 1.4). The piezoelement is poled in the 3-direction. The 2 electroded faces are parallel arranged along the 1-direction. We supposed here that the strain in the 3-direction are negligible compared to the 1-direction one. This permits to say that only lateral deformation (1-direction) induces the electric field E .

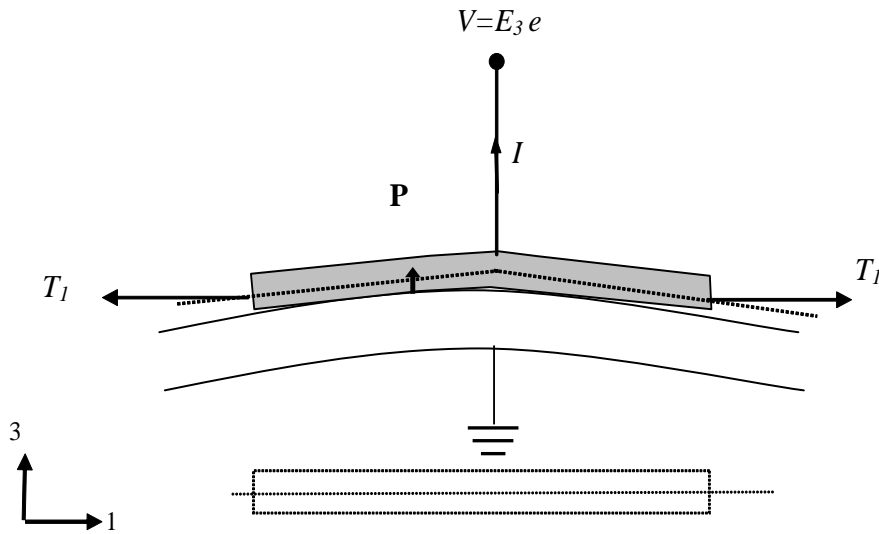


Figure 1.4. Piezoelectric element used as bending sensor.

In that case, the relation (1.6) becomes:

$$E_3 = \beta_{33}^T D_3 - g_{31} T_1 - g_{32} T_2 - g_{33} T_3 \quad (1.8)$$

It should be note that T_3 equals to zero for flexural wave.

If the sensor is in open-circuit condition, the open voltage is:

$$V_3 = -g_{31} T_1 e \quad (1.9)$$

1.5.2 A wide range of forms

Piezoelectric materials exist under four primary forms: massive ceramics, single crystals, fibers or films. These 4 primary forms can be directly integrated into the structure or they can be used in advanced systems such as summarized Figure 1.5

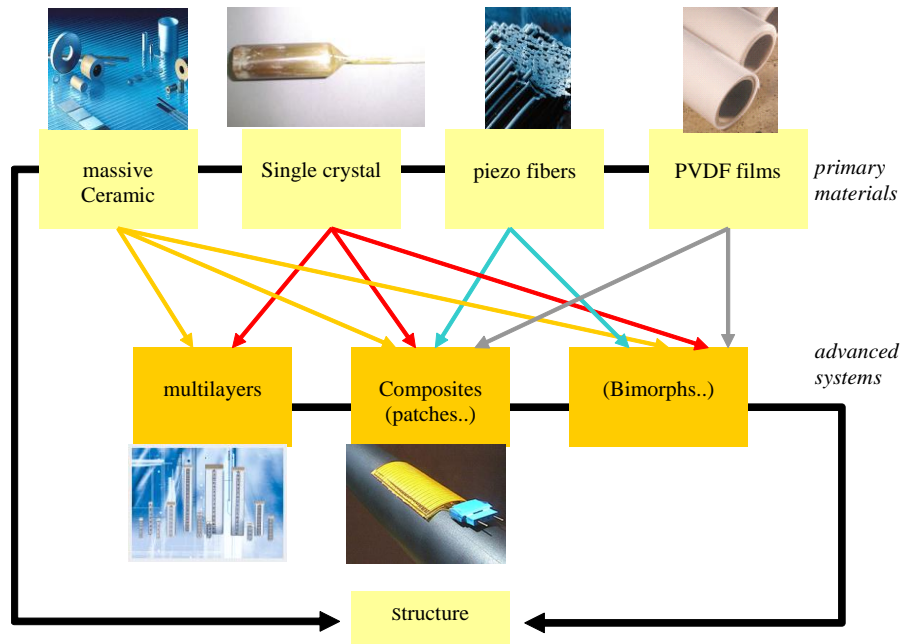


Figure 1.5. primary forms of piezoelectric material

This large choice of piezoelectric materials or systems permits to have an adapted response in terms of integration for the wanted applications. This point is crucial for impact detection techniques because the piezoelectric sensors are the core of the detection system. If massive ceramics are often an adapted solution, piezofibers, films or composites *floppy* patches are very promising alternatives, especially for integration in structures deforming in bending mode.

We focus here on the 2 common used piezoelement for sensing applications:

- **Massive ceramics**

These materials exist under a multitude of geometries. Columns, tubes, plates are hence commonly available in industry standards (figure 1.9).



Figure 1.6: Massive ceramic: industrial standard materials.

Thus, there are widely application. There are hard and soft ceramics. Hard ceramics are more difficulty changed by electrical fields than soft ceramics. The piezoelectric properties depend upon the thermoelectric treatment by sintering and then polarization under the influence of an electrical direct current field. The most common piezoelectric ceramic is lead zirconate titanate, $\text{Pb}(\text{Zr},\text{Ti})\text{O}_3$ (PZT). Because of many years of practical using, it can be made to almost any shape, high stiffness, and high dielectric constant. In addition, PZT is relatively inexpensive compared with PVDF. It is sensitive to low tensile.

- **Piezoelectric fibers**

Piezoelectric fibers are manufactured by various methods, e.g. extrusion, viscous suspension spinning process. Basic applications of piezoelectric fibers include 1-3 composites, which are aligned fibers embedded in a polymer matrix (figure 1.10).

The advantages of fibers are low acoustic impedance and high piezoelectric coefficients. In addition, many works focus on a newly developed active fiber composites (AFC), which have a big potential benefits over conventional piezoelectric sensing and actuating devices.

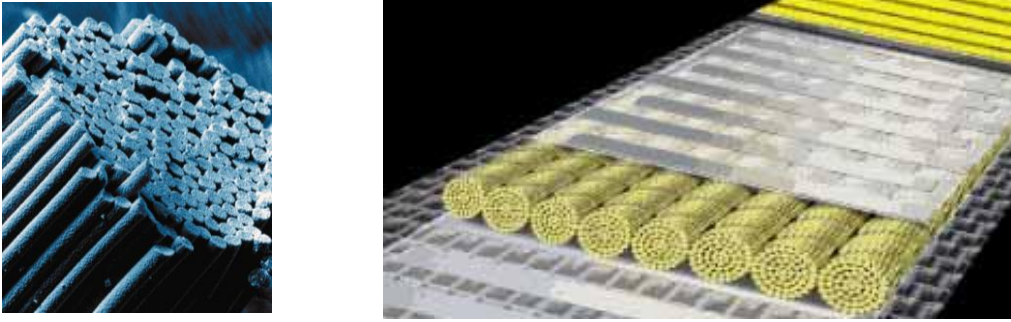


Figure 1.7. piezoelectric fibers (a) and an example of integration (b)

These kinds of piezoelectric systems are a very seductive solution for impact detection sensor network because they can be directly integrated in structures, especially in composites structures. The average values of the piezoelectric characteristics for the various primary forms are summarized in Table 1.1. Only characteristics are linked to the 31-mode (lateral mode) because it is generally the solicited mode in structural bending deformations, which directly concerns the present work.

Table 1.1. Average values of piezoelectric charge coefficient d_{31} , piezoelectric voltage coefficient g_{31} coupling coefficient k_{31} and mechanical factor quality Q_m for primary materials in 31-mode (lateral mode)

type	d_{31} 10^{-12} m/V	g_{31} 10^{-3} V.m/N	k_{31} %	Q_m	ϵ_{33}
hard PZT	-100	-10	-35	>1000	1150
soft PZT	-200	-15	-37	100	1850
PVDF Film	-30	-200	-	10	2 ~ 5
fiber	-60	-10			
Single crystals PMN-PT	-1500		85	100~200	3000~5000
Cellulose electroactive paper EAPap ⁶⁵	-	-0.03	-	-	

If the d_{31} coefficient denotes the actuation material abilities, the g_{31} coefficient characterizes the sensing material abilities. Even if PVDF film is a good candidate for sensing applications, massive PZT ceramics are used in the current work due to their easy implementation for experimental set-up.

1.6 Conclusion

This chapter presents the objectives of this thesis and the some basic generalities on piezoelectric systems.

In order to develop an easy to implement low power technique, a new method is introduced.

The starting point of our work is that the impact detection can be given by an estimation of the pointing vector, which represents the energy flow in an elastic structure. This new estimator is deduced from voltage response of piezoelectric sensor embedded or bonded on the structure.

2 Preliminary results on beam

2.1 Introduction

In this chapter, the possibility to detect impact by estimating the energy flow is validated in a simple 1D problem. The proposed technique consists in estimating the energy flow evolution in a monitored beam through a network of resistively shunted piezoelectric inserts.. These sensors do not need any external power supply.

The impact location is simply deduced from a dissipated energy comparison given by the shunted resistor voltage.

The first part of this chapter presents the principle of this method. Second part introduces the theoretical approach. Final part, theoretical and experimental measurements are carried out to demonstrate the method.

2.2 Principle

This study considers a one-dimensional beam with resistively shunted piezoelectric elements bonded on the structure as shown Figure 2.1. Besides, the beam is considered as lossless and infinite. The piezoelements are uniformly bonded on the beam with a Δx step. Considering an impact at the point A on the beam, the longitudinal waves, as well as the induced energy (E_{in}) flow generated by this force would propagate in opposite directions (E_{in+} and E_{in-}) along the beam. Going through a piezoelectric insert (PZT_i), a part of the mechanical energy (E_i) is extracted and converted into electrical energy (E_{pi}) and finally dissipated in the resistor. Thus, the energy of the wave decreases each time it passes a piezoelectric insert i and can be estimated as, assuming that each shunted piezoelectric insert has the same conversion ratio:

$$E_{bn-} = E_{n-1} - E_{pi} \quad (2.1)$$

Considering that the 2 induced energy flows are identical ($E_{inl+} = E_{inl-}$), the force location can be estimated by simply comparing the dissipated energy by each resistor. Effectively, the gradient energy ($E_{p1} - E_{p2}$) of 2 consecutive piezoelements would be nil only in the case where they surrounded the impacted area.

The impact spatial resolution of the proposed technique stays lower than Δx its performance relies on its fast processing and on the fact that the sensors do not need any external power.

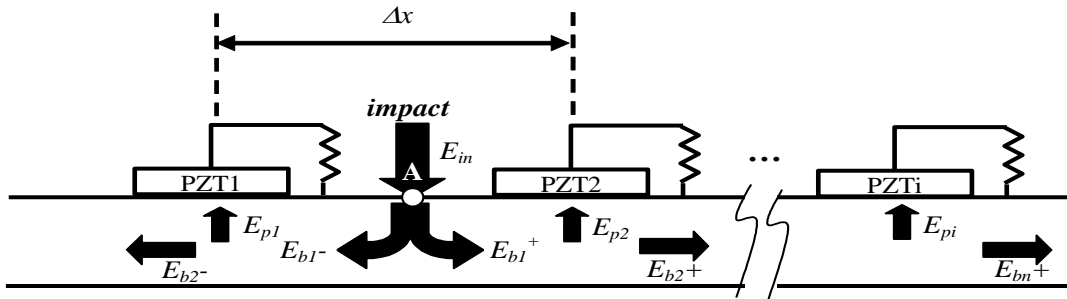


Figure 2.1: The studied structure. The PZT elements are uniformly bound on the beam with a Δx – step. E_{in} is the stored energy in the beam due to the impact at the point A.

E_{pi} is the energy extracted by the i -element and dissipated in the resistor. E_b is the mechanical energy in the beam.

2.3 Modelling

2.3.1 Lumped model

The nondispersive wave propagation in an infinite lossless beam can be modeled using spring-mass systems as shown in Figure 2. 2. These simple assumptions are sufficient to enlighten the basic principles of the detection technique. The beam is split in 2 kind of section:

- Simple mechanical section corresponding to the beam area without bonded piezoelement
- Composite section corresponding to the beam area with bonded piezoelement

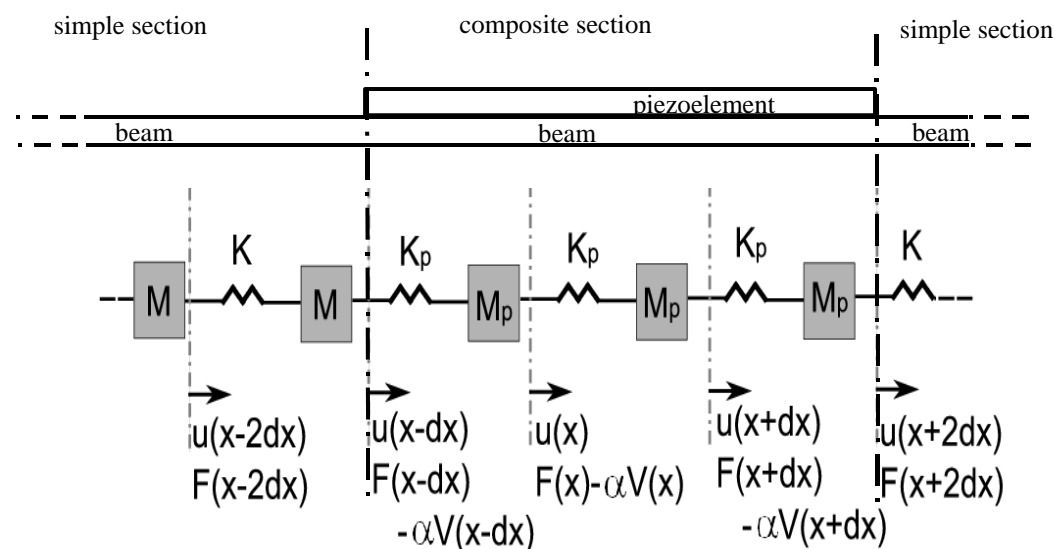


Figure 2. 2: Spring-Mass representation of an infinite beam.

K and M are respectively the stiffness and the lineic mass of an simple (mechanical) section (only beam)

K_p and M_p are respectively the stiffness and the lineic mass of a composite section (beam + piezoelement).

Chapter 2 Preliminary results on beam

Table 2.1: Nomenclature of the lumped model

M	lineic mass
K	stiffness
u_x	longitudinal displacement
V	piezovoltage
M_p	lineic mass where a piezoelement is bonded
K_p	stiffness where a piezoelement is bonded

Considered that the piezoelectric inserts does not significantly modify the local stiffness and mass of the structure, one can assume that M_p and K_p are equals to M and K respectively. Applying the fundamental dynamic equation and using Taylor expansion thus yields Equation (2.2) for non-piezoelectric parts and Equation (2.3) for piezoelectric parts, with α the force factor of the piezoelement defined as Equation (2.4), where e , A and l are defined as the voltage coefficient, the surface and the thickness of the piezoelement. Because there are the second derivative of x with respect to displacement u , Figure 2. 2 has u_x , $u_{(x-dx)}$, $u_{(x+dx)}$ three part in composite section.

$$\begin{aligned} M\ddot{u}_x(x,t) &= K[u_x(x+dx,t) + u_x(x-dx,t) - 2u_x(x,t)] & (2.2) \\ &= K(dx)^2 \frac{\partial^2 u_x(x,t)}{\partial x^2} \end{aligned}$$

$$M\ddot{u}_x(x,t) = K(dx)^2 \frac{\partial^2 u_x(x,t)}{\partial x^2} - \alpha \frac{\partial V(x,t)}{\partial x} dx \quad (2.3)$$

$$\alpha = \frac{eA}{l} \quad (2.4)$$

$$I_{out} = -C_0 \dot{V} + \alpha \dot{u}_x \quad (2.5)$$

The current flowing out of the piezoelements can be derived from the macroscopic piezoelectric equations yielding Equation (2.5), with C_0 the clamped capacitance defined as Equation (2.6), with ε^s the permittivity of the piezoelement. The resistive shunt thus leads to Equation (2.7), with R the value of the resistor.

$$C_0 = \frac{\varepsilon^s A}{l} \quad (2.6)$$

$$-C_0 \dot{V} + \alpha \dot{u}_x = \frac{V}{R} \quad (2.7)$$

2.3.2 Energetic balance

The purpose of this section is to expose the dissipated energy over the two different sections of the system. The energy stored by the structure is given by Equation (2.8), where $F_{ext}(x, t)$ are the external applied force.

$$E_{in} = \int_{-\infty}^{+\infty} F_{ext}(x, t) \dot{u}_x(x, t) dt \quad (2.8)$$

$$E_{p,n} = \int_{-\infty}^{+\infty} \frac{(V(x_n, t))^2}{R} dt \quad (2.9)$$

$$\Delta E_{pn,n+1} = \frac{1}{R} \int_{-\infty}^{+\infty} (V(x_{n+1}, t)^2 - V(x_n, t)^2) dt \quad (2.10)$$

Because a resistor is connected to the piezoelement (giving Equation (2.7)), the energy E_p can be written as Equation (2.9). Consequently this energy extraction reduces the wave energy available for the next parts of the beam.

Differentiating the energy over two consecutive piezoelements thus gives Equation (2.10). Therefore, the Equation (2.10) that performs a differentiation of the energy is almost null considering the two shunted patches that are closed to the impact location. The location estimation of the wave source can be done by determining the zero crossing of that the first criterion. The reason is the first two shunted patches

absorb more energy than the other patches. Therefore, from the origin of the wave, the energy dissipated through the shunt resistor is a decreasing value of the distance from the patch to the energy source. Therefore, the criterion (2.10) that performs a differentiation of the dissipated energy is null considering the two shunted patches that are closest to the impact source. Because, the energy decrease with the distance and the each patch absorbs a part of the mechanical energy of the wave, the criterion reaches a minimal and a maximal value for the next set of patches, then the absolute value decreases as shown in Figure 2.3.

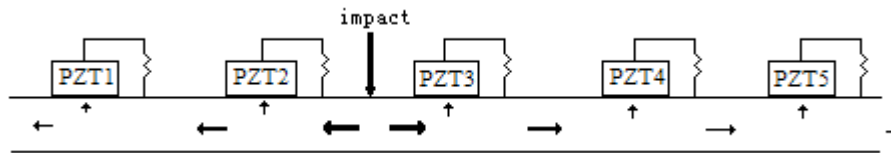


Figure 2.3 Energy flow in the beam, differentiating the energy over sensor 1 to 2 is negative ($\Delta E_{p12} < 0$), sensor 2 to 3 is null ($\Delta E_{p23} = 0$), 3 to 4 and 4 to 5 is positive

$$(\Delta E_{p23} > \Delta E_{p34} > \Delta E_{p45})$$

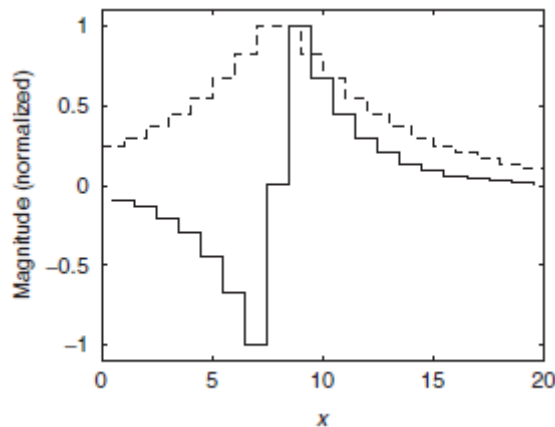


Figure 2.4 Normalized evolutions of the extracted energy (dotted) and the proposed criterion (plain)—force location at $x_0=7.5$.

It should be note that the signum of the criterion depends both on the wave direction and the direction the estimation is performed. If the wave and the criterion are the same direction (*resp. opposite*), the criterion is positive (*resp. negative*). Figure 2.4

shows the evolution of the extracted energy and the criterion (2.10) for a wave propagating from the point $x_0=7.5$.

The patches are assumed to be placed at integer values of x . As expected, the criterion is null near impact location, then reaches a minimal and maximal values, and starts decreasing in absolute value, with a signum depending on the wave direction and criterion direction.

2.4 Performance Discussion

This technique is not so precise compared to standard method because the impact location estimation accuracy is given by the inter-piezo size Δx . But, it is much faster and computationally efficient. It is necessary to note that all received signals are not processed by any filters. The noise influence is quite limited. In addition, there is no need of external power supply to the sensors. Finally, taking into account drifts in the coupling coefficient caused by the bonding is simple by adjusting the associated shunted resistance the energy extraction ration for each piezoelectric insert.

2.5 Numerical analysis-finite element simulation

Simulations using numerical Finite Element Analysis have been carried out in order to confirm the model. The modeled beam (Figure 2.5) received by five identical bonded piezoelectric patches. The dimensions and the physical properties are given in Table 2.2. The poling direction for the PZT patches is on the y -direction.

The beam with surface mounted piezoelectric patches is meshed (zoomed view in Figure 2.6) using the commercial FE code ANSYS 9.0. The structure is meshed with six nodes plane quadratic elements. The patches are meshed with PLANE13, and the beam with PLANE42 (Figure 2.6). PLANE13 is defined by four nodes with up to four degrees of freedom per node (x and y directions and the electric potential V for piezoelectric elements). Moreover, CIRCU94 elements are used to model the resistors, which are connected to each piezoelement electrode. The mechanical boundary conditions of the structure are clamped at both end of the beam (all degrees of

Chapter 2 Preliminary results on beam

freedom equal to zero). Moreover, the electrical potential is forced to zero on interface between PZT and the beam. A force with a frequency band of 500 kHz in is applied to the beam. As illustration, the Figure 2.7 shows the PZT2 voltage when an impact is applied in part 0.

Table 2.2: FEM simulation parameters

Parameter	Value (SI)	Parameter	Value (SI)
Resistivity	1	Density	7850
Length of the piezoelements	$2 \cdot 10^{-2}$	Length of the beam	4.74
Thickness of the piezoelements	$3 \cdot 10^{-4}$	Thickness of the beam	$3 \cdot 10^{-2}$
Relative permittivity	1142	Elasticity	$195 \cdot 10^9$
Voltage coefficient	-6.18		

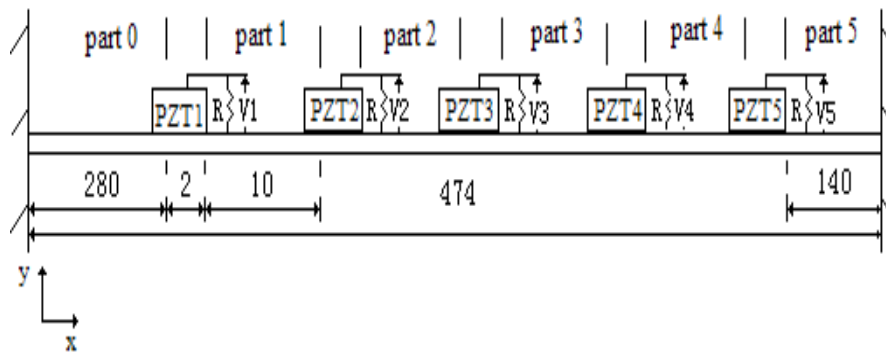


Figure 2.5: The simulated model. Dimensions are in mm



Figure 2.6: Meshing of the structure (Zoomed area)

Chapter 2 Preliminary results on beam

In order to evaluate the force location, the criterion Equation (2.10) is calculated along the x-axis. The force is applied on nodes of parts 0 to 5, and the results are shown in Figure 2.5. The black dots represent the energy differentiation over sensor n and sensor $n+1$. As expected, the source of the impact is quite well estimated by the zero crossing of the criterion. Moreover, if all the values of $\Delta E_{n,n+1}$ are positive (*resp.* negative), the force location is found to be within part 5 (*resp.* part 0). When the impact source is within the scanning range, the criterion crosses the zero value in the impact area, and then reaches an extremum and decrease in absolute value, with the signum depending on the criterion and energy flow directions (Figure 2.8).

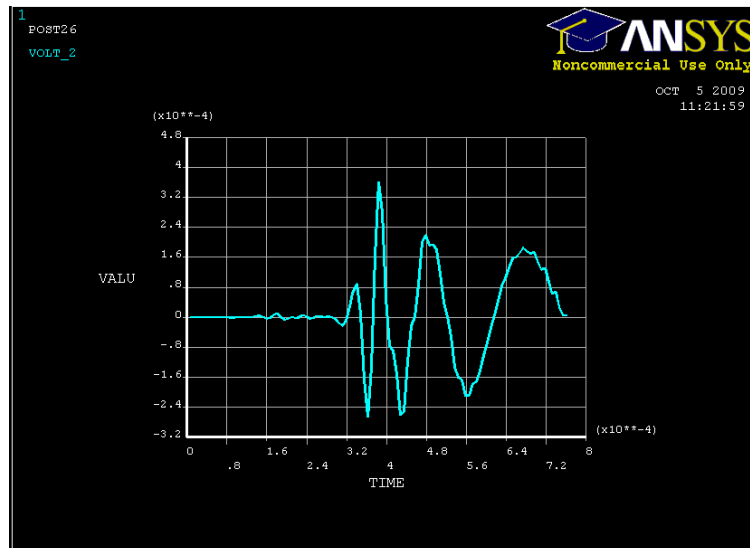
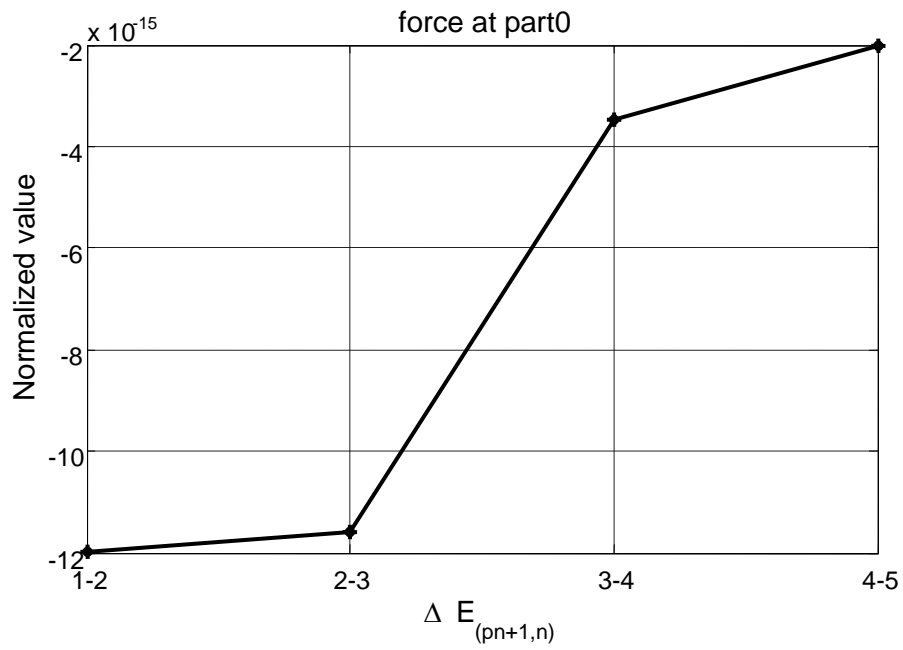
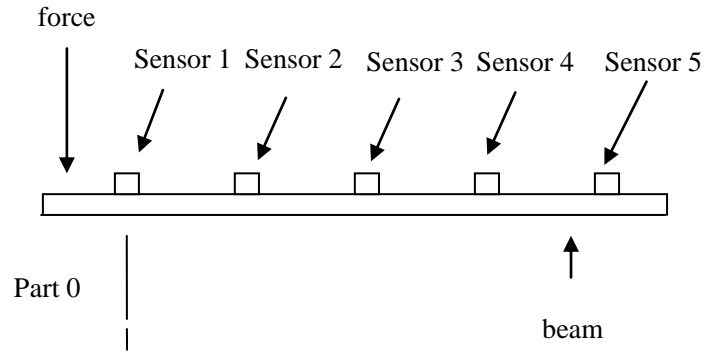
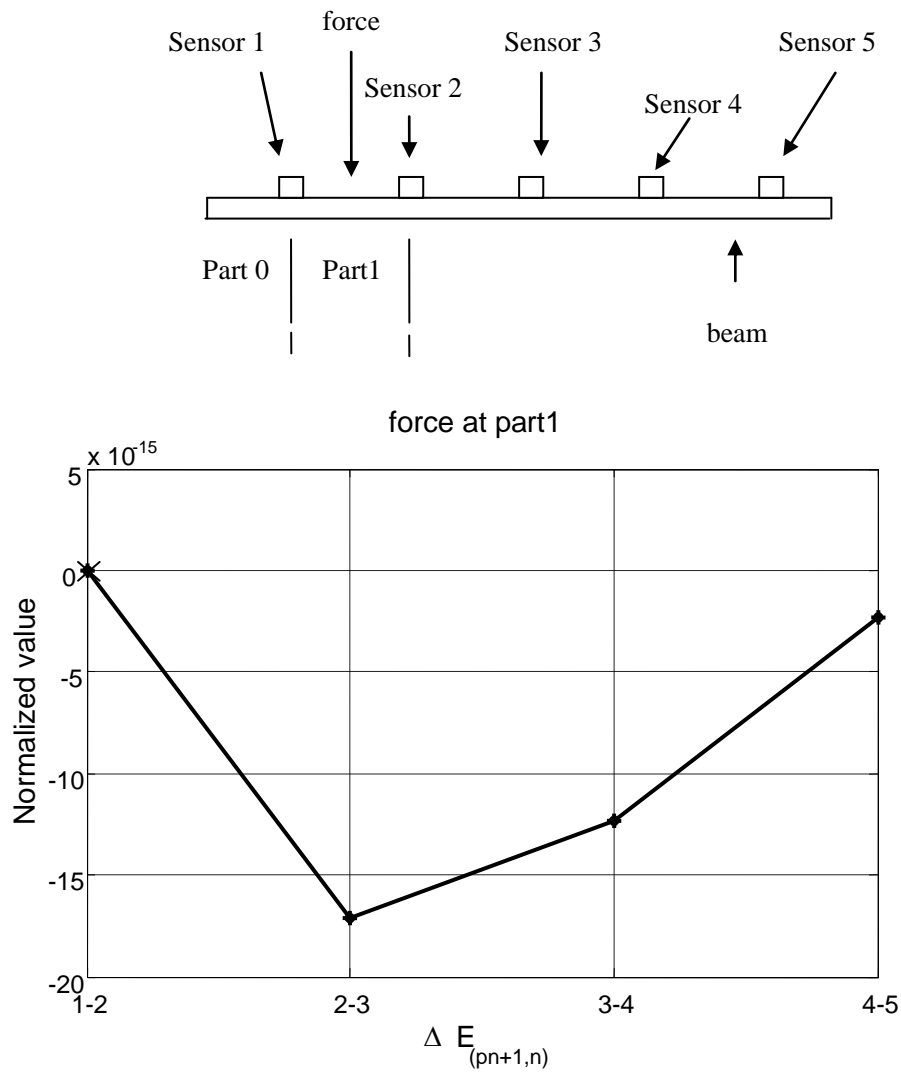


Figure 2.7: Example of a sensor (PZT2) response for an impact in part 0.

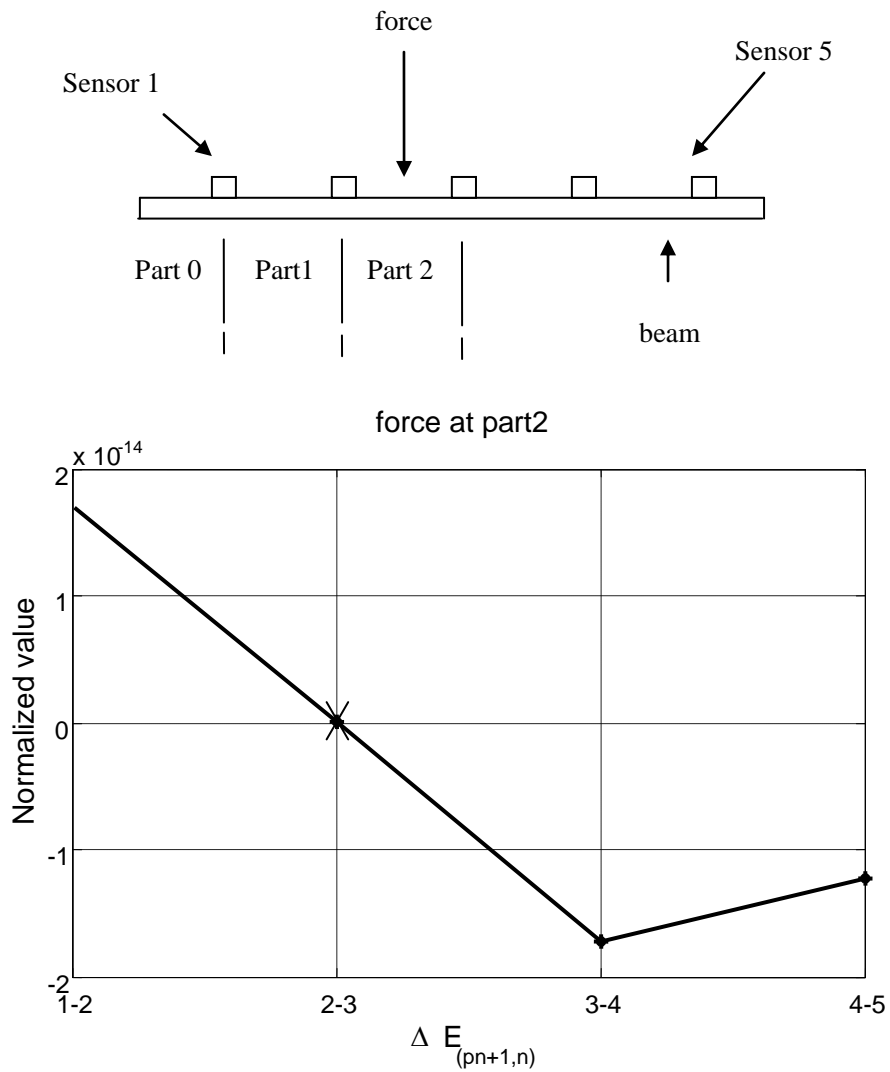


- (a) Force is applied at part 0, all the $\Delta E_{(pn+1,n)}$ is negative, minimal value is $\Delta E_{p_{21}}$ and the absolute value decreases with distance.

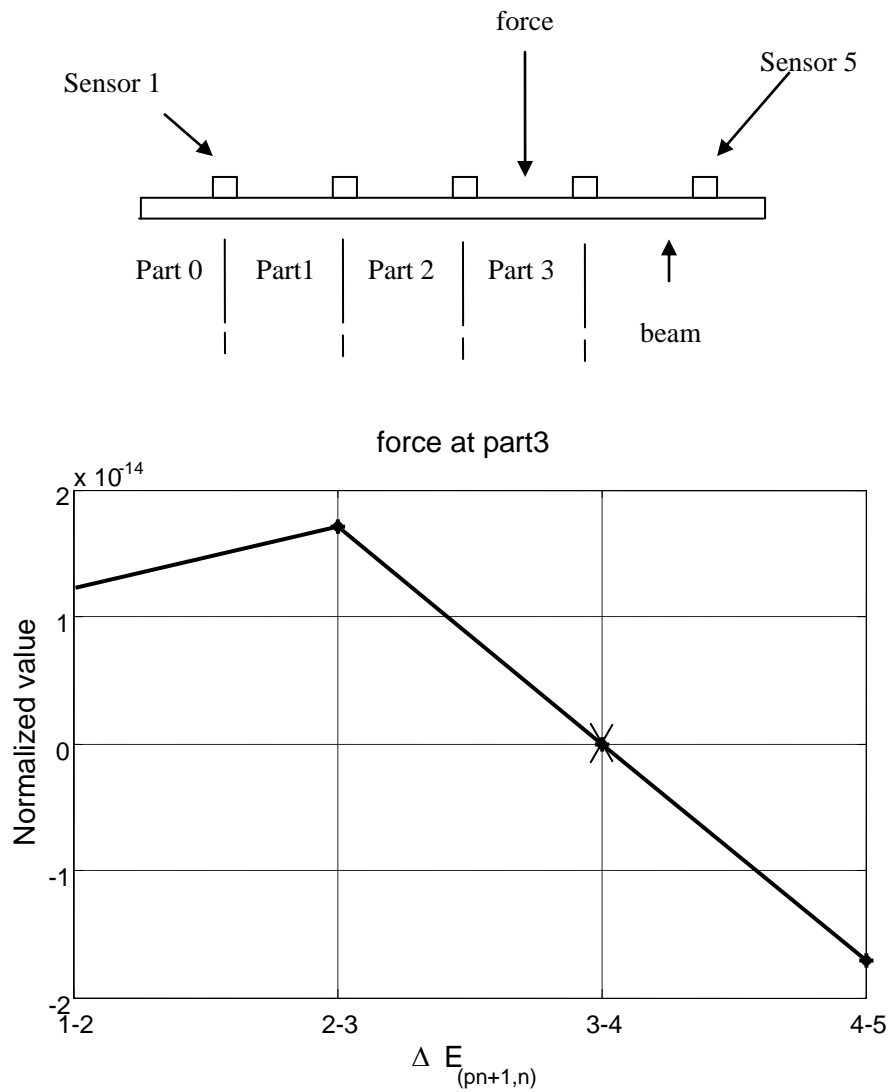


(b) Force is applied at part 1, $\Delta E_{21} = 0$, others $\Delta E_{pn+1,n}$ are negative, minimal value is

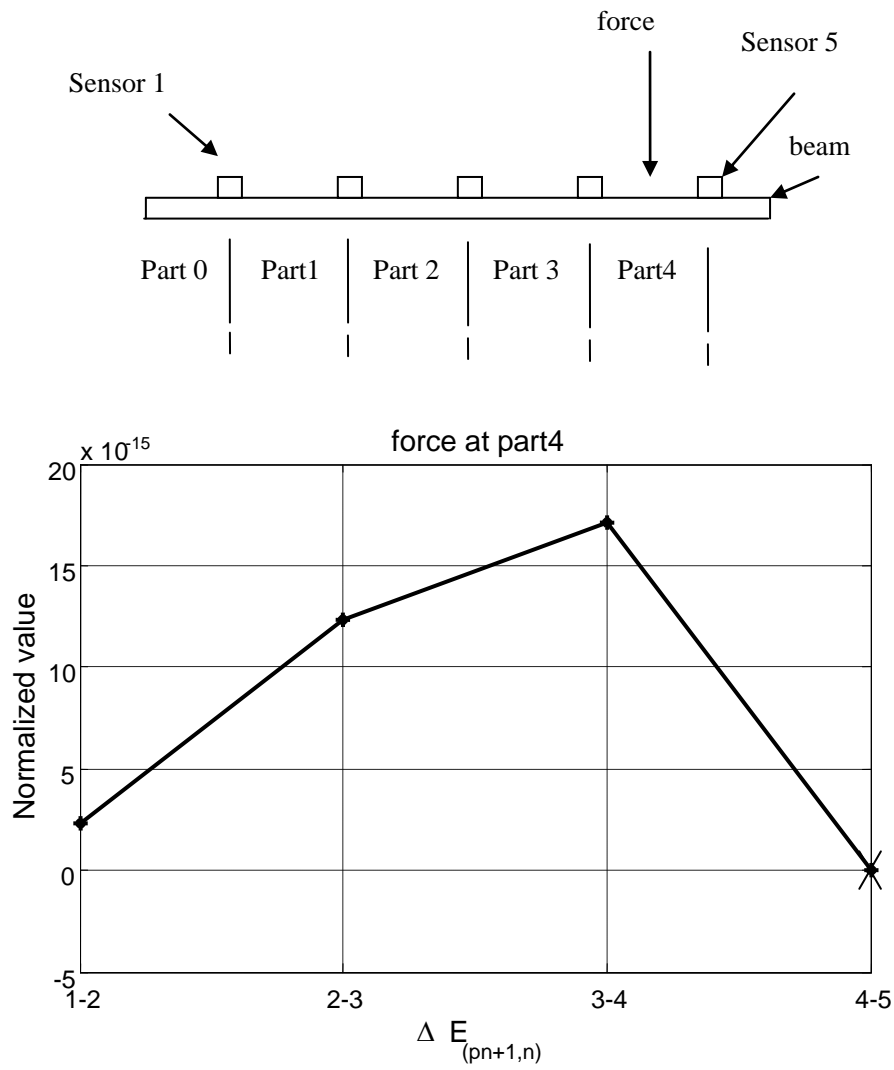
ΔE_{p32} and the absolute value decreases with distance.



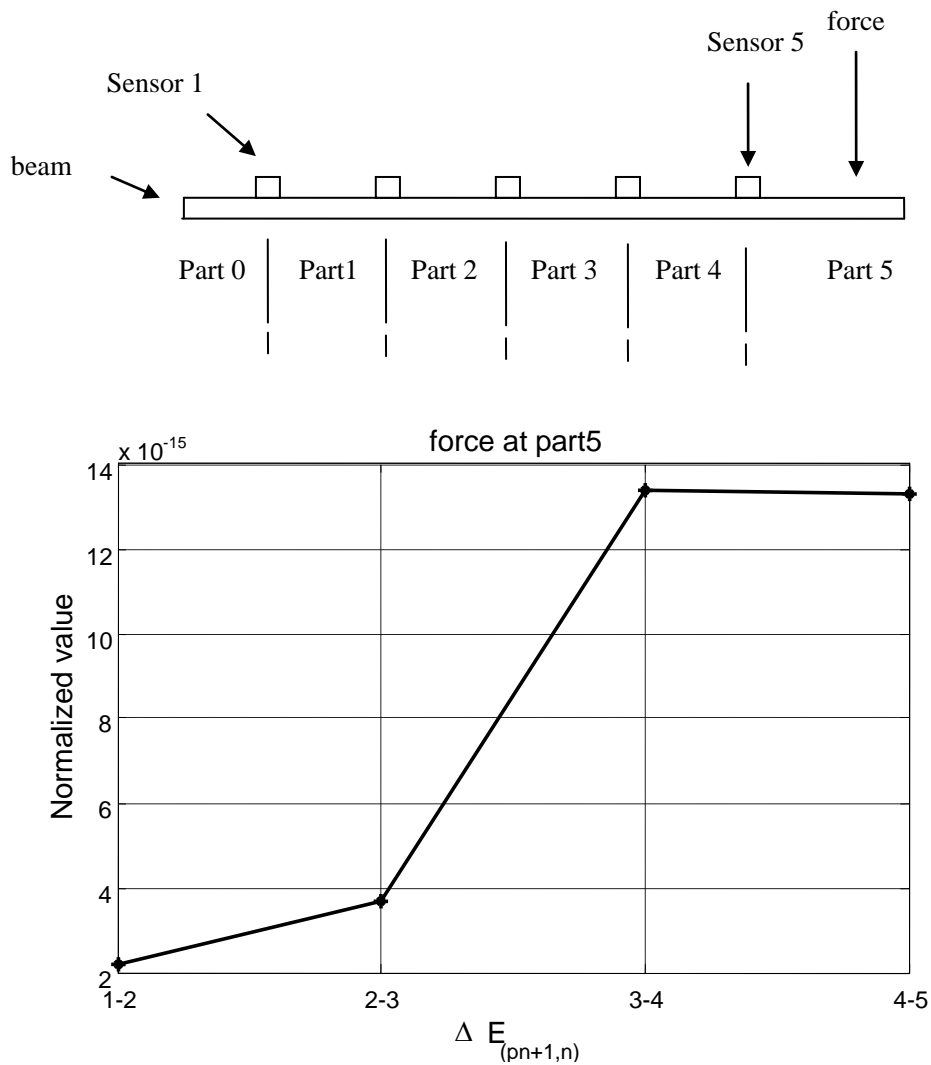
(c) Force is applied at part 2, $\Delta E_{p21} > 0$, $\Delta E_{p32} = 0$; The others $\Delta E_{pn+1,n}$ are negative, minimal value is ΔE_{p32} and maximum value is ΔE_{p21} .



(d) Force is applied at part 3, $\Delta E_{p32} > \Delta E_{p21} > 0$, $\Delta E_{p43} = 0$. The others $\Delta E_{pn+1,n}$ are negative, minimal value is ΔE_{p54} and maximum value is ΔE_{p32} .



(e) Force is applied at part 4, $\Delta E_{p43} > \Delta E_{p32} > \Delta E_{p21} > 0$, $\Delta E_{p54} = 0$



(f) Force is applied at part 5, all the $\Delta E_{pn+1,n}$ are positive. The maximum value is ΔE_{p54} and decreases with the distance.

Figure 2.8: simulation results: 2-1 means ΔE_{p21} (the differentiating energy over sensor 2 and 1 (Figure 2.5)). As the same, 3-2, 4-3, 5-4 mean ($\Delta E_{p32}, \Delta E_{p43}, \Delta E_{p54}$)

2.6 Experimental Results

2.6.1 Experimental Set-up

Experimental measurements were done considering a $350 \times 50 \times 3 \text{ mm}^3$ Bulk Molding Compound (BMC) beam to confirm the proposed method. Seven resistively shunted piezoelectric inserts (PZT *P-18 Saint-Gobain*) are bonded onto the upper surface of the beam (Figure 2.9). The dimension of inserts is $30 \times 3 \times 0.5 \text{ mm}^3$ and each separated by a distance $\Delta x = 40 \text{ mm}$. Because of the variability of the bonding condition, the coupling of each piezoelectric insert is quite different. The value of each resistor has been tuned to have the same ratio of extracted energy for each piezoelectric patch. The experimental parameters are shown in Table 2.3, except for the value of the resistance, which is tuned to equalize the energy extraction ration due to the bonding.

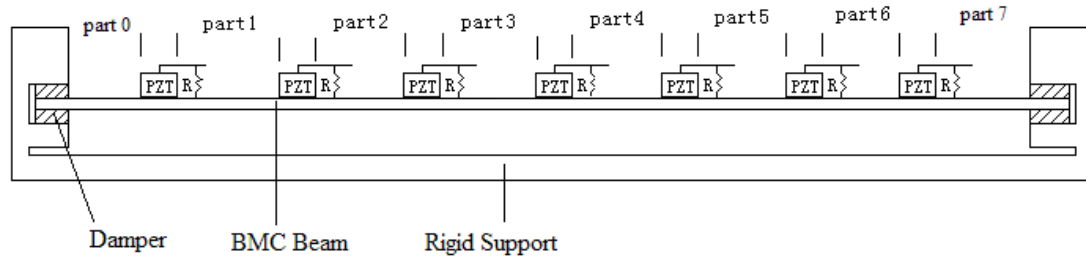


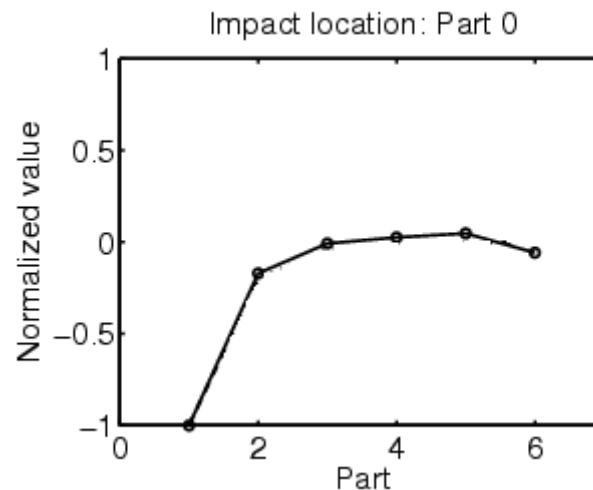
Figure 2.9 Experimental set-up

Table 2.3: Experimental parameters

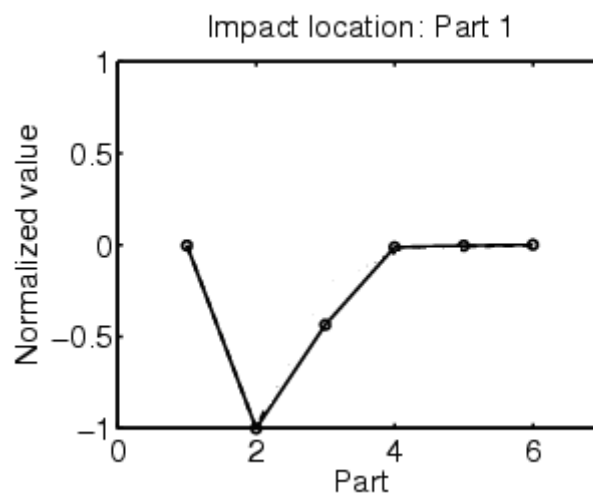
Beam parameters		Piezoelectric parameters				Other parameters
M	K	l	ϵ^s	e	s_0	ω
210 g.m^{-1}	$1,75 \text{ MN.m}^{-2}$	3 mm	$1142 .\epsilon_0$	-6.18 C.m^{-1}	12.10^{-5} m^2	$1000.10^3 \pi \text{ rad.s}^{-1}$

2.6.2 Results & Discussion

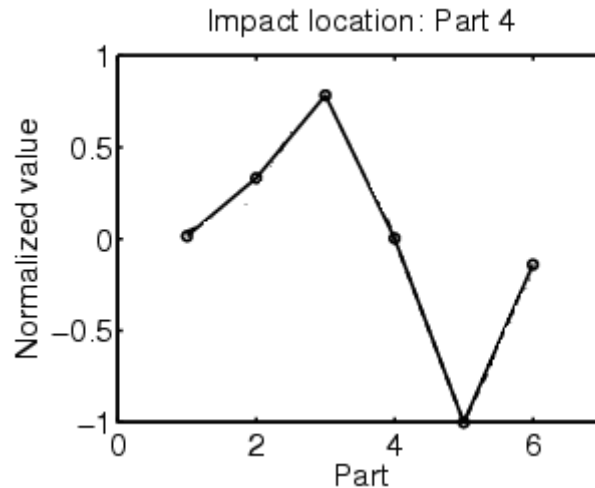
The impact is generated by a source moveable piezoelectric patch excited in a sinus-burst-mode (10 periods at a frequency of 530 KHz), corresponding to the beam first flexural mode. Experiment results are shown in Figure 2.10. Results demonstrate that the location of impact is quite well estimated by the zero crossing of the criterion, and follows theoretical predictions in a similar fashion, with a response depending on criterion and wave directions. In addition, although the internal damping coefficient can be quite small, it gives rather precise information of the impact location. Comparison between experimentally with simulation results, these results shows a good agreement to accurately estimate the impact location.



(a)



(b)



(c)

Figure 2.10: Experimental (plain) and results for the proposed criterion using a-530KHz piezoelectric moveable source.

2.7 Conclusion

We suggest here that impact location can be performed by estimating the energy flow in the structure with the help of a network of piezoelectric sensors.

The principles of the method rely on the comparison of the extracted electrical energy by each sensor. The piezoelectric elements can be perceived as local electromechanical dampers that give insight of the energy flow. This research considers infinite lossless and 1-D beam. Following chapter would consider 2-D structure, which is more useful in reality situation. In addition, there are also some other field of investigative such as multiple impacts, resistive shunts, inductive or nonlinear shunts. This study considers infinite lossless beam, as well as resistive shunt. Future work considering a lossy finite beam would lead to a more realistic model, and therefore to a finer impact location estimation. Besides, it is believed that taking into account internal losses in the beam can predict more accurately the impact location by extrapolation.

3 Transient bending wave modeling in an infinite plate with bonded piezoelectric inserts

3.1 Introduction

In previous chapter proposed a simple efficient technique to evaluate the impact location in a 1D structure (beam). Estimating the location and energy of impacts in plate can be obtained with the same approach, that is to say in estimating the energy flow in the structure. But, the knowledge of the piezoelement electric response is a non trivial problem for a 2D structure. However, when dealing with mechanical wave propagation, a common approach consists in using numerical methods that are often time-consuming.

This chapter proposes a new approach using a Fourier transform for modeling the impulse response of an infinite plate with surface-bonded piezoelectric elements. This step is requisite to deduce the relationship between energy flow and piezoelectric response.

The proposed analytical formulation therefore allows bypassing numerical analysis drawbacks, in this specific case, while giving the response for the whole time and space domains. The proposed model relies on flexural wave decomposition over the spatial frequency domain and corresponds to a time generalization of the angular spectrum theory, thus introducing flexural wave propagation as a time-varying spatial filter. The inverse Fourier transform is then applied and leads to the impulse response in the physical domain. From this model is also derived an analytical expression of the impulse voltage response of piezoelectric transducers. The predicted impulse response is then compared to FEM simulation and experimental measurements in order to asses the model.

3.2 Impulse response modelling: theoretical approach

In this study, a two-dimensional lossy plate with piezoelement bonded on its surface as shown in Figure 3.1 is considered. This Section leads to establish the solution of the flexural traveling wave generated by a pulse force.

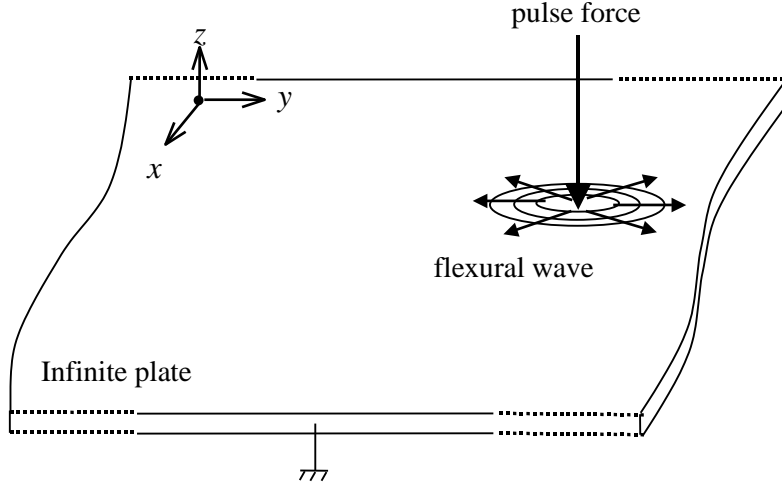


Figure 3.1: Schematics of the considered infinite plate

3.2.1 Determination of the displacement under pulse force

The general equation for linear flexural wave in thin undamped plates is well-known and can be found in Timoshenko⁶⁶ for example and follows the equation:

$$m\ddot{u}_z + D\Delta^2 u_z = q(x, y, t) \quad (3.1)$$

where

u_z is the flexural displacement

$q(x, y, t)$ is the applied load.

Δ is the Laplacian operator

m is defined as the surface mass density

D represents the bending stiffness that can be expressed as a function of the Young modulus Y , the Poisson ratio ν and the plate thickness h by:

$$D = \frac{Yh^3}{12(1-\nu^2)} \quad (3.2)$$

We may also consider that losses occur in the plate. Assuming losses that depend only

Chapter 3 Transient bending wave modeling in an infinite plate with bonded piezoelectric inserts

on the displacement time derivative leads to the modified motion equation:

$$m\ddot{u}_z + \beta\dot{u}_z + D\Delta^2 u_z = q(x, y, t) \quad (3.3)$$

where β is the damping factor.

In order to get the impulse response of the system, the space-domain Fourier transform is applied to Equation (3.3), along the x and y axis, which leads to (Guyomar and Powers, 1984⁶⁷, Guyomar and Power, 1985⁶⁸):

$$m\ddot{\tilde{u}}_z + \beta\dot{\tilde{u}}_z + D(k_x^2 + k_y^2)^2 \tilde{u}_z = \tilde{q}(k_x, k_y, t) \quad (3.4)$$

where :

\tilde{u}_z and $\tilde{q}(K_x, K_y, t)$ are respectively the expression of the flexural displacement and the load in the space-domain Fourier transform

k_x , k_y are the wave vectors along the x and y axis,

Therefore, if the applied load is a pulse excitation, $q(x, y, t)$ can be expressed as:

$$q(x, y, t) = \delta(x)\delta(y)\delta(t) \quad (3.5)$$

where δ is the delta distribution. This leads to the spatial Fourier decomposition of the load:

$$\tilde{q}(k_x, k_y, t) = \delta(t) \quad (3.6)$$

Therefore the spatial frequency domain equation of motion (3.4) turns to:

$$m\ddot{\tilde{u}}_z + \beta\dot{\tilde{u}}_z + D(k_x^2 + k_y^2)^2 \tilde{u}_z = \delta(t) \quad (3.7)$$

Such equation is a well-known second order system, whose elementary solution is given by:

$$\tilde{u}_z(k_x, k_y, t) = \frac{1}{m} \frac{1}{\gamma k^2 \sqrt{1 - \zeta^2}} e^{-\zeta \gamma k^2 t} \sin(\gamma k^2 t \sqrt{1 - \zeta^2}) \quad (3.8)$$

with the coefficients γ , k^2 and ζ defined as:

$$\gamma = \sqrt{\frac{D}{m}} ; k^2 = k_x^2 + k_y^2 ; \zeta = \frac{\beta}{2m\gamma k^2} \quad (3.9)$$

It is interesting to note that Equation (3.8) shows that the propagation acts as a spatial low-pass filter, with a strong reduction of high spatial frequency components, and whose the cut-off frequency is decreasing with the time. This last observation partly

Chapter 3 Transient bending wave modeling in an infinite plate with bonded piezoelectric inserts

expresses the dispersive nature of the wave.

We knowing the expression of $\tilde{u}(K_x, K_y, t)$. A 2D inversed Fourier transform leads to the expression of the flexural wave in the physical space (x, y, t) .

$$u_z(x, y, t) = \frac{1}{m\sqrt{2\pi}} \int_{-\infty}^{\infty} \int_{-\infty}^{\infty} \frac{1}{\gamma k^2 \sqrt{1-\zeta^2}} e^{-\zeta \gamma k^2 t} \sin(\gamma k^2 t \sqrt{1-\zeta^2}) e^{i(k_x x + k_y y)} dk_x dk_y \quad (3.10)$$

Consequence, this integral can be done by switching from Cartesian coordinates (k_y, k_x) and (x, y) to cylindrical coordinates (k, ϕ) and (r, θ) respectively:

$$u_z(r, \theta, t) = \frac{1}{m\sqrt{2\pi}} \int_{-\infty}^{\infty} \int_{-\infty}^{\infty} \frac{1}{\gamma k^2 \sqrt{1-\zeta^2}} e^{-\zeta \gamma k^2 t} \sin(\gamma k^2 t \sqrt{1-\zeta^2}) e^{i\gamma k \sin(\theta + \phi)} k d\phi dk \quad (3.11)$$

where θ and ϕ are obtain from:

$$\begin{aligned} x &= r \cos(\theta) & ; & & y &= r \sin(\theta) \\ k_x &= k \sin(\phi) & ; & & k_y &= k \cos(\phi) \end{aligned} \quad (3.12)$$

Using Bessel functions of the first kind, Equation (3.11) becomes:

$$u_z(r, \theta, t) = \frac{\sqrt{2\pi}}{m} \int_0^{\infty} \frac{1}{\gamma k^2 \sqrt{1-\zeta^2}} e^{-\zeta \gamma k^2 t} \sin(\gamma k^2 t \sqrt{1-\zeta^2}) k J_0(rk) dk \quad (3.13)$$

Expanding the sine term of this expression using Euler's formula and deriving according to the time leads to:

$$\begin{aligned} \dot{u}_z(r, \theta, t) &= \frac{\sqrt{2\pi}}{m\gamma\sqrt{1-\zeta^2}} \frac{1}{2i} \left[\int_0^{\infty} -(\zeta\gamma - j\gamma\sqrt{1-\zeta^2}) \cdot \right. \\ &\quad \left. e^{-k^2 t (\zeta\gamma - j\gamma\sqrt{1-\zeta^2})} k J_0(rk) dk \right. \\ &\quad \left. + \int_0^{\infty} (\zeta\gamma + j\gamma\sqrt{1-\zeta^2}) e^{-k^2 t (\zeta\gamma + j\gamma\sqrt{1-\zeta^2})} k J_0(rk) dk \right] \end{aligned} \quad (3.14)$$

Therefore, referring to [Abramowitz and Stegun, 1964]⁶⁹ (Equation (11.4.29)), the

Chapter 3 Transient bending wave modeling in an infinite plate with bonded piezoelectric inserts

expression of the flexural phase velocity yields:

$$\dot{u}_z(r, \theta, t) = \frac{1}{2tm} \sqrt{\frac{2\pi m}{D(1-\zeta^2)}} e^{-\frac{r^2\zeta}{4t}\sqrt{\frac{m}{D}}} \sin\left(\frac{r^2}{4t}\sqrt{\frac{m}{D}}(1-\zeta^2)\right) \quad (3.15)$$

The flexural displacement resulting from a pulse force can be obtained by integrating Equation (3.15) over the time domain $u_z = \int_0^t \dot{u}_z(r, z) dt$. The response $\dot{u}_z|_{arb}$ for any arbitrary excitation $q(t)$ is then simply obtained using a straight convolution between the impulse response $u_{z(impr)}$ and the arbitrary driving.

$$\dot{u}_z(r, \theta, t)|_{arb} = \dot{u}_{z(impr)}(r, \theta, t) * q(r, \theta, t) \quad (3.16)$$

One can note that the impulse response is independent from the angular value θ , which is a logical consequence of the wave propagation through an isotropic structure. This can also be observed in Equation (3.15) where the wave instantaneous frequency depends on the product (r^2/t^2) , demonstrating the dispersive nature of the wave. Particularly, as $t \rightarrow 0$ the instantaneous frequency tends to ∞ . This is a strong limitation when using classical numerical analysis due to the fine spatial and time meshing required.

The wave expression may also be rewritten as:

$$\begin{aligned} \dot{u}_z(r, \theta, t)|_{arb} &= \frac{1}{r^2} \frac{r^2}{2tm} \sqrt{\frac{2\pi m}{D(1-\zeta^2)}} e^{-\frac{r^2\zeta}{4t}\sqrt{\frac{m}{D}}} \sin\left(\frac{r^2}{4t}\sqrt{\frac{m}{D}}(1-\zeta^2)\right) \quad (3.17) \\ &= \frac{1}{r^2} f\left(\frac{r^2}{t}\right) \end{aligned}$$

where $f\left(\frac{r^2}{t}\right) = \frac{r^2}{t} \frac{1}{2m} \sqrt{\frac{2\pi m}{D(1-\zeta^2)}} e^{-\frac{r^2\zeta}{4t}\sqrt{\frac{m}{D}}} \sin\left(\frac{r^2}{4t}\sqrt{\frac{m}{D}}(1-\zeta^2)\right)$.

When t tends to zero, the term $e^{-\frac{r^2\zeta}{4t}\sqrt{\frac{m}{D}}}$ tends to zero too and the sign of term $\sin\left(\frac{r^2}{4t}\sqrt{\frac{m}{D}}(1-\zeta^2)\right)$ change quickly.

It is interdependence between space and time domains (which is not the case when dealing with classical propagation). The coefficient $1/r^2$ expresses the energy conservation theorem.

Chapter 3 Transient bending wave modeling in an infinite plate with bonded piezoelectric inserts

As well, this expression shows that the wave propagation is dependent to the scaling factor r^2/t , and consequently it is possible to obtain the whole response in the spatial and time domain as soon as the response at a given location or for a given time instant is known.

As shown in the Figure 3.1, when an impact is applied at the origin (0, 0), two points of the phase velocity are obtained in Figure 3.2 (0.2, 0.2) and Figure 3.3 (0.4, 0.4). The time to reach maximum value in Figure 3.2 is close to 0.01 second and that in Figure 3.3 is close to 0.04 second. The reason is that the distance between impact location and measure point is two times different. Because of the scaling factor r^2/t , the Figure 3.2 scale down Figure 3.3.

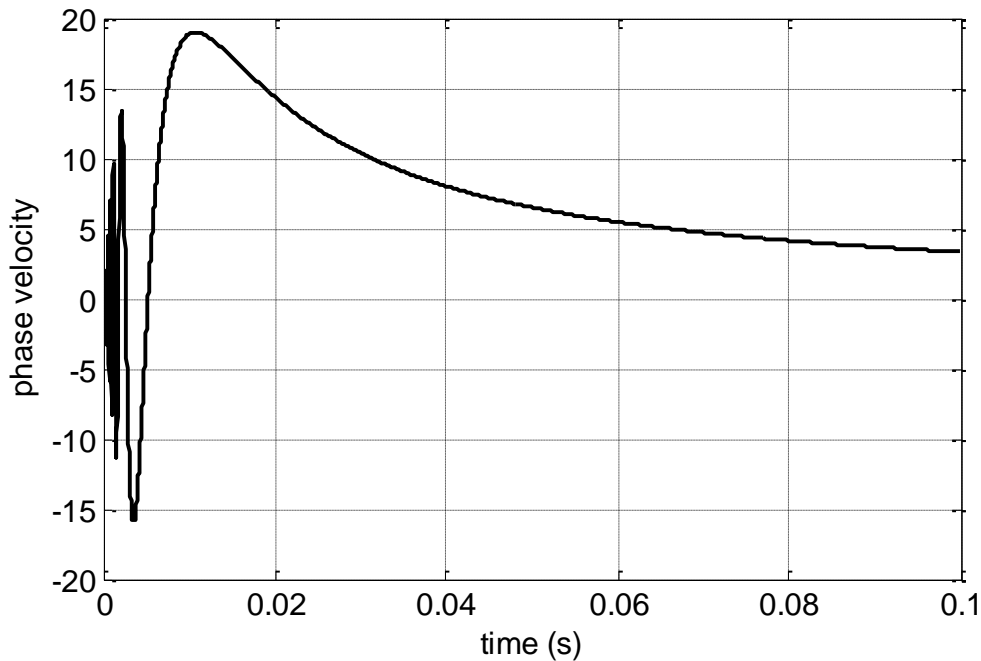


Figure 3.2: Impulse response at the point (0.2, 0.2)

-- impact is applied at origin (0, 0)

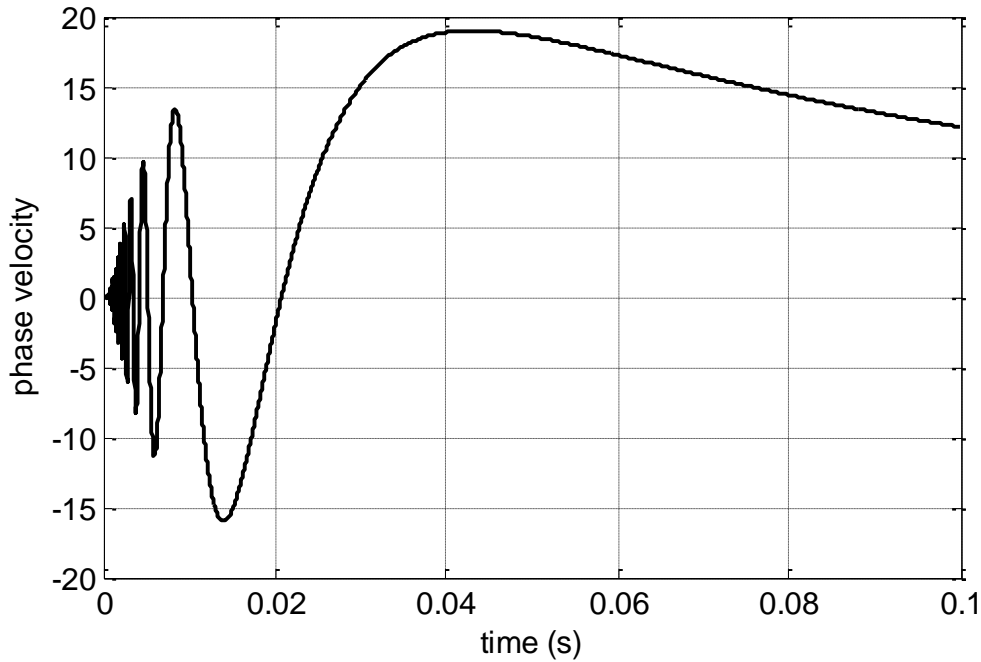


Figure 3.3: Impulse response at the point (0.4, 0.4)
impact is applied at origin (0, 0)

Equation (3.15) can also be expressed in the Cartesian coordinates as a function of x and y as:

$$\dot{u}_z(x, y, t) = \frac{1}{2tm} \sqrt{\frac{2\pi m}{D(1-\zeta^2)}} \cdot e^{-\frac{(x^2+y^2)\zeta}{4t} \sqrt{\frac{m}{D}}} \sin\left(\frac{(x^2+y^2)}{4t} \sqrt{\frac{m}{D}(1-\zeta^2)}\right) \quad (3.18)$$

3.2.2 Derivation of the piezoelectric sensor voltage

This part exposes the derivation of the voltage of a piezoelectric element bonded on the structure. The principles of the analysis consist in using the previously calculated flexural displacement velocity in order to estimate the piezovoltage in Cartesian coordinates. It will also be assumed that the piezoelement does not modify the local behavior of the structure (negligible effect of the added mass and stiffness).

The piezoelectric voltage can be derived considering the constitutive piezoelectric

Chapter 3 Transient bending wave modeling in an infinite plate with bonded piezoelectric inserts

equations and the previous assumptions, giving the electric induction field D_d along the z -axis as a function of the electric field E_E along the z -axis and the strain as:

$$D_{dE} = \epsilon_{33}^S E_E + e_{31} (S_{xx} + S_{yy} + S_{zz}) \quad (3.19)$$

with ϵ_{33}^S and e_{31} defined as the permittivity of the piezoelement and piezoelectric coefficient respectively. For bending wave, we assume that the strain is zero inside the plate ($S_{zz} = 0$)

Let us now consider the specific arrangement of the piezoelectric sensor, as given Figure 3.4

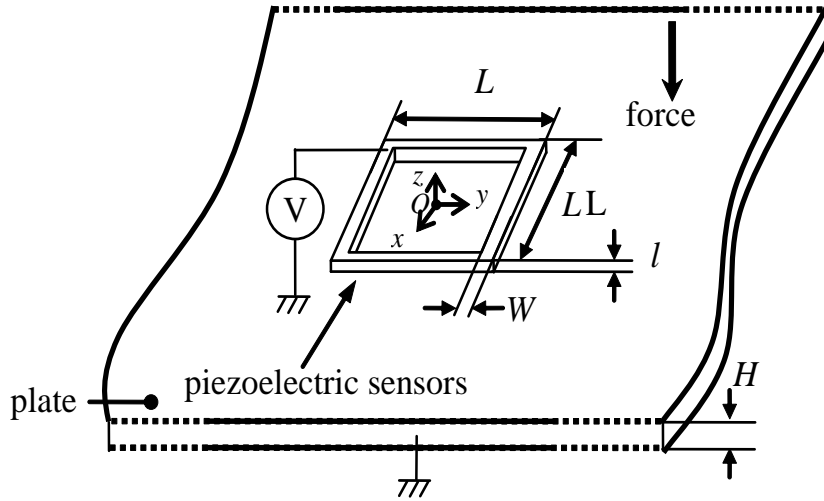


Figure 3.4: Schematics of the considered structure with surface-bonded piezoelectric element

Considering a constant electric field over the piezoelectric element, Equation (3.19) therefore turns this expression to:

$$D_{dE} = \epsilon_{33}^S \frac{V}{l} - e_{31} \frac{h}{2} \frac{1-2\nu}{1-\nu} \left(\frac{\partial^2 u_x}{\partial x^2} + \frac{\partial^2 u_z}{\partial y^2} \right) \quad (3.20)$$

with V the voltage across the piezoelectric element and l its thickness.

The current I flowing out the piezoelectric element is obtained using the relationship between the electric induction field and the current:

$$I = \int_A \dot{D}_d dA \quad (3.21)$$

where A is the surface of the piezoelectric element.

In open-circuit condition the current I is null, and considering null initial conditions of

Chapter 3 Transient bending wave modeling in an infinite plate with bonded piezoelectric inserts

the voltage and the second-order derivative of u_x and u_y leads to the expression of the voltage as

$$\begin{aligned} \int_A \epsilon_{33}^S \frac{\dot{V}}{l} - e_{31} \frac{h}{2} \frac{1-2\nu}{1-\nu} \left(\frac{\partial^2 \dot{u}_z}{\partial x^2} + \frac{\partial^2 \dot{u}_z}{\partial y^2} \right) dA &= 0 \\ \int_A \epsilon_{33}^S \frac{\dot{V}}{l} - e_{31} \frac{h}{2} \frac{1-2\nu}{1-\nu} \left(\frac{\partial^2 \dot{u}_z}{\partial x^2} + \frac{\partial^2 \dot{u}_z}{\partial y^2} \right) dA &= 0 \\ \int_A \epsilon_{33}^S \frac{V}{l} - e_{31} \frac{h}{2} \frac{1-2\nu}{1-\nu} \left(\frac{\partial^2 u_z}{\partial x^2} + \frac{\partial^2 u_z}{\partial y^2} \right) dA &= Q_0 \end{aligned} \quad (3.22)$$

(Assuming electric quantity is null with time is zero $Q_0 = 0$):

$$V = k \int_A \left(\frac{\partial^2 u_z}{\partial x^2} + \frac{\partial^2 u_z}{\partial y^2} \right) dA \quad (3.23)$$

with $k = \frac{le_{31}h}{2\epsilon_{33}^S A} \left(\frac{1-2\nu}{1-\nu} \right) = \frac{e_{31}h(1-2\nu)}{2c_p(1-\nu)}$ c_p is blocked pizo capacitance.

Finally, the impulse response is calculated in 2 steps: knowing the impact characteristics, the displacement is firstly derived from Eq.(3.18). The resulting piezoelectric voltage is then calculated with the help of Eq.(3.21) and (3.22).

3.3 Simulations-Numerical analysis

The propagation of impulse bending waves is simulated with the help of *Matlab*® software in a infinite plate (Figure 3.4) with the physical properties and dimensions given in Table 3.1 and Table 3. 2 The sensor is a square piezoelectric element poled in the Oz direction.

Table 3.1: Simulation parameters of the plate

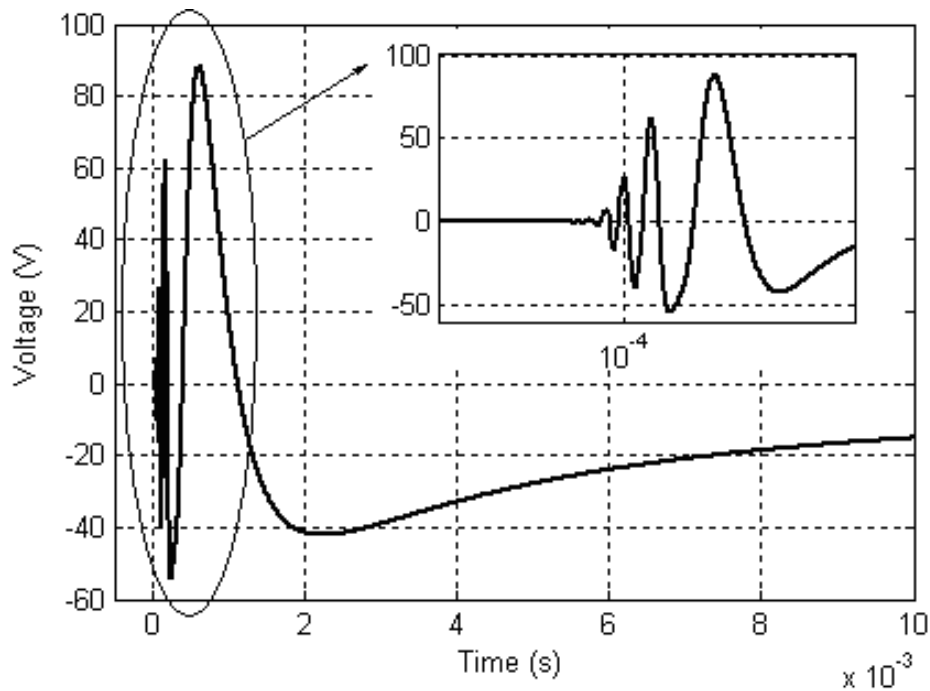
Parameter	Value
Surface density m	6.4 $Kg.m^{-2}$
Young modulus Y	195 GPa
Thickness h	0.8 mm
Poisson ration ν	0.33
Damping coefficient ζ	0.08

Chapter 3 Transient bending wave modeling in an infinite plate with bonded piezoelectric inserts

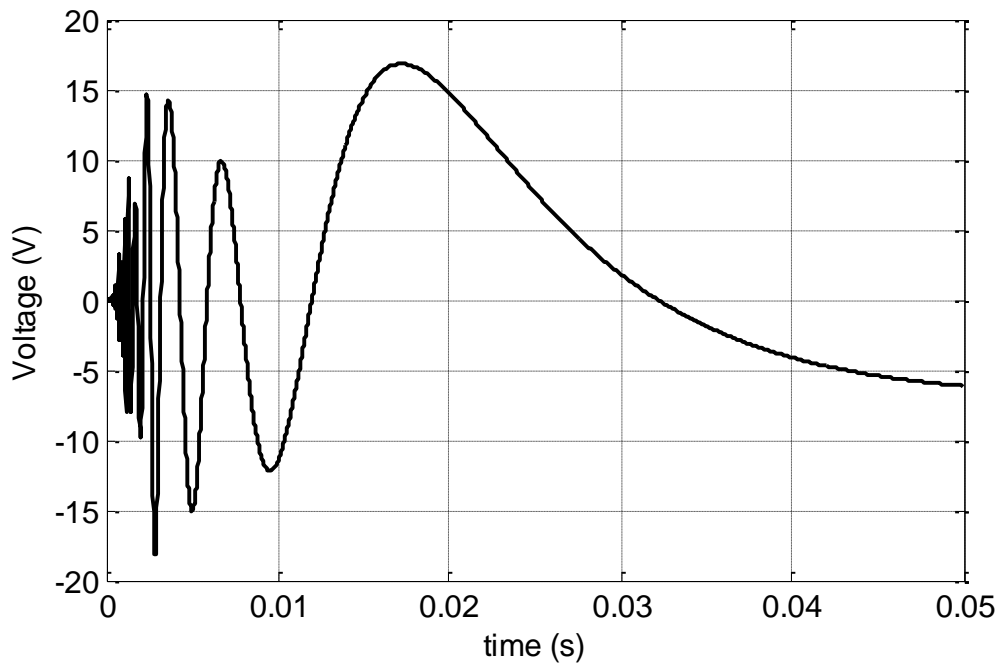
Table 3. 2: Simulation parameters of the piezoelectric element

Parameter	Value
Length L	180 mm
Width W	20 mm
Thickness l	1 mm
Voltage coefficient e_{31}	-4.3 C.m^{-1}
Relative permittivity $\epsilon_{33}^s / \epsilon_0$	1142

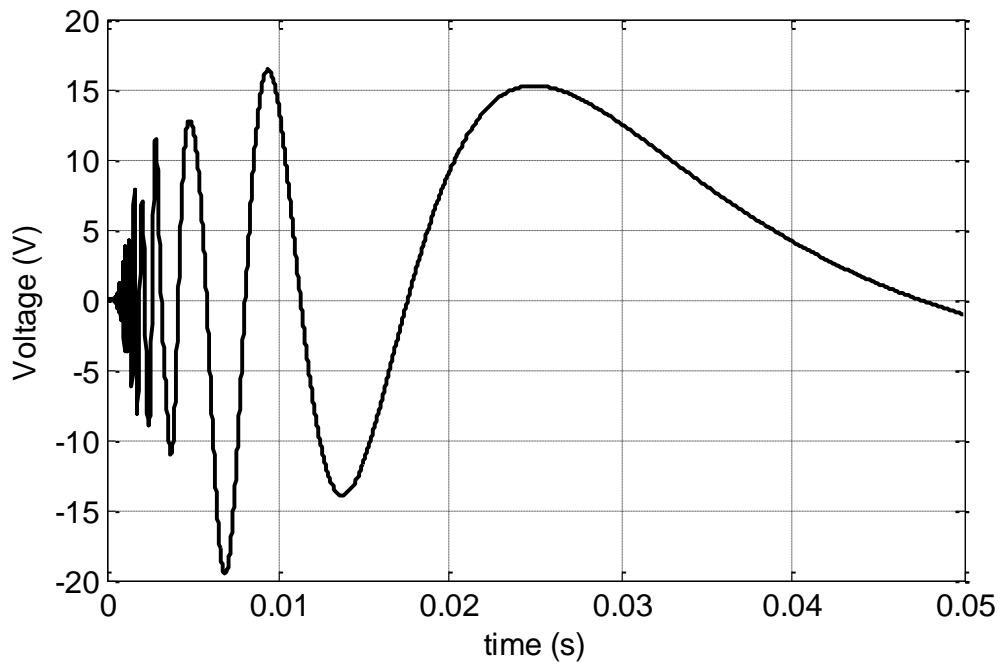
The Figure 3.5 depicts the evolution of the voltage as a function of the time when a unitary pulse force is applied at the origin. Other excitation cases in different locations can of course be considered. The instantaneous frequency decreases as a function of time due to the presence of the dispersive $\sin\left(\frac{1}{t}\right)$ term in Eq (3.18). However, the spatial filtering performed by the insert (and represented by the surface integral in Equation (3.22)) significantly changes the envelope of the response. From the time delay in Figure 3.5, it can also be shown that the propagation nature is also well described by the model.



(a) Voltage response to for pulse force excitation at the origin (0, 0)
 --force inside surface of the structural



(b) Voltage response to a pulse force excitation at the (0.25, 0.25)
--force outside surface of the structural



(c) Voltage response to a pulse force excitation at the (0.35, 0.3)
--force outside surface of the structural

Figure 3.5: Voltage response to a pulse force excitation at different location

In the general case, the excitation force is a low-velocity impact, and therefore the high frequency components of the impulse response edge are filtered. Finally we

Chapter 3 Transient bending wave modeling in an infinite plate with bonded piezoelectric inserts

choose here an n-period burst waveform as a representative impact.

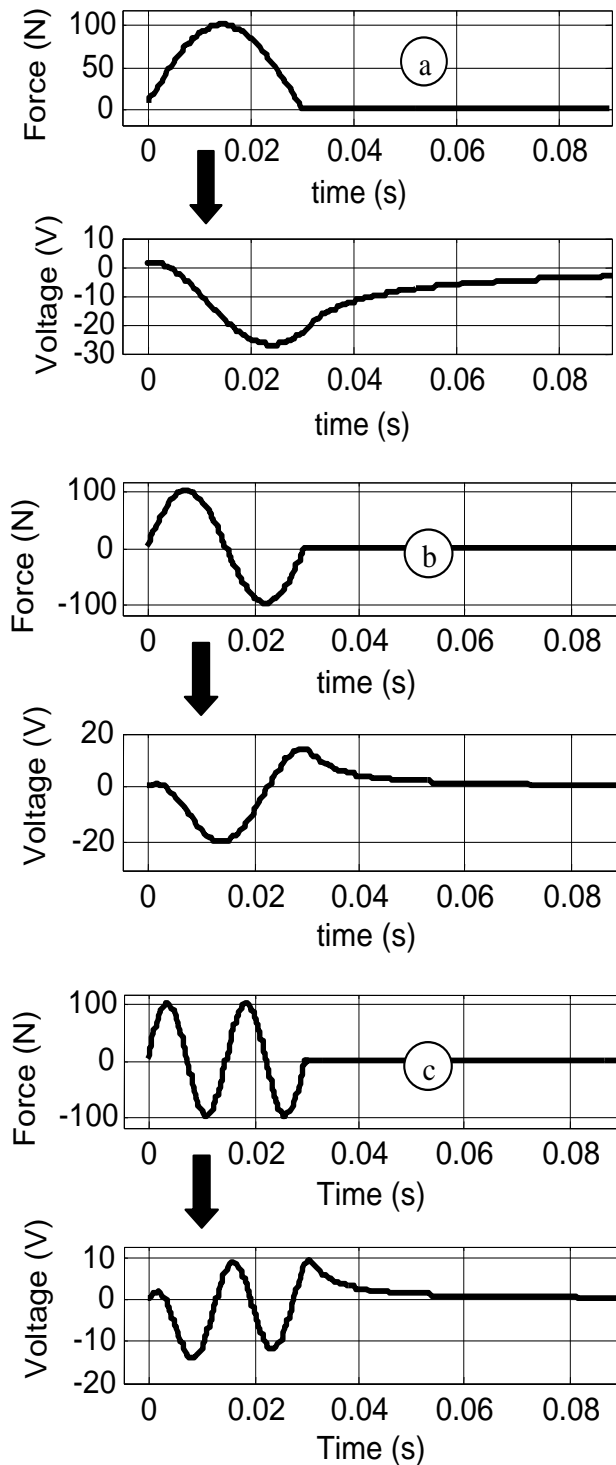


Figure 3.6: Simulated sensor voltage for a half period-burst impact (a), 1 period-burst impact (b) and 2 periods-burst impact (c). The impact location coordinates are (0, 0).

3.4 Comparison with finite element simulation

In order to validate the model, this Section proposes a comparison between predicted voltage response from the model with the one obtained by numerical analysis through the use of Finite Element Method (FEM) with the commercial software ANSYS. The plate and the piezoelectric elements are modeled using the SOLID5 and SOLID45 elements, respectively. As well, performance discussion about computation requirements of the proposed method will be exposed.

In the case of the FEM analysis, the infinite dimension condition is fulfilled by the use of a plate with very large dimensions, preventing reflection phenomena in the transient stage in the considered spatial domain.

Secondly, the ratio a/h (ratio between length and thickness of the plate) is chosen high [Ventsel and Krauthammer, 2001]⁷⁰, to respect thin plate conditions (Kirchhoff's plate theory). In this way, the vertical shear strains γ_{xy} and γ_{yz} are negligible. The dimensions of the plate FEM model are summarized in table Table 3.3

Table 3.3 Dimensions (in mm) of the FEM model

plate (Length X Width X Thickness H)	2500 X 2000 X 1
piezoelement square size (side L X Width W X Thickness l)	40 X 40 X 1 X 0.5

The simulated model is shown in Figure 3.7. Other parameters are those used in the previous simulations.

Transient analysis was achieved considering a burst impact force located at point I (inside frame) or point O (outside frame). As example, the evolution of the plate deformation is shown in Figure 3. 8 for an outside impact at different time. Finally, the piezovoltage evolution can be deduced from these simulations. Figure 3.9 and Figure 3.10 respectively show the comparison between the two resolutions methods when the excitation is a 5-kHz, one cycle sine burst applied at the location (13mm, -13mm) (*i.e.* inside the piezoelectric element location) and when the excitation is a 5-kHz, one cycle sine burst applied at the location (-110mm, 38mm) (*i.e.* outside the

Chapter 3 Transient bending wave modeling in an infinite plate with bonded piezoelectric inserts

piezoelectric element location). The analytical solution is obtained by convolution of

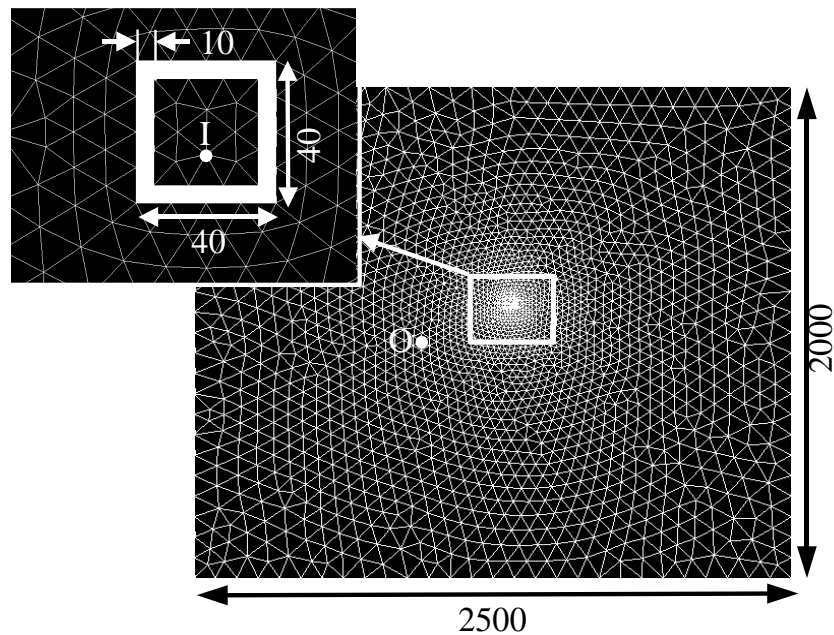


Figure 3.7: Meshed plate and piezoelectric element-I point is the inside point impact and O point is the output point impact

the force waveform with the impulse response at the given position. These Figures show a good agreement between the predicted voltage from the FEM analysis and from the proposed analytical model, both in terms of frequencies and magnitude. In Figure 3.10, the divergence at $t=0.7 \text{ ms}$ is explained by the finite FEM meshing that induces a reflection.

In terms of computational requirements, the FEM resolution takes more than 10 minutes for 60 points, while the derivation of the voltage using the analytical model lasts only 30 seconds for 3000 points, demonstrating the performances of the exposed analysis.

Chapter 3 Transient bending wave modeling in an infinite plate with bonded piezoelectric inserts

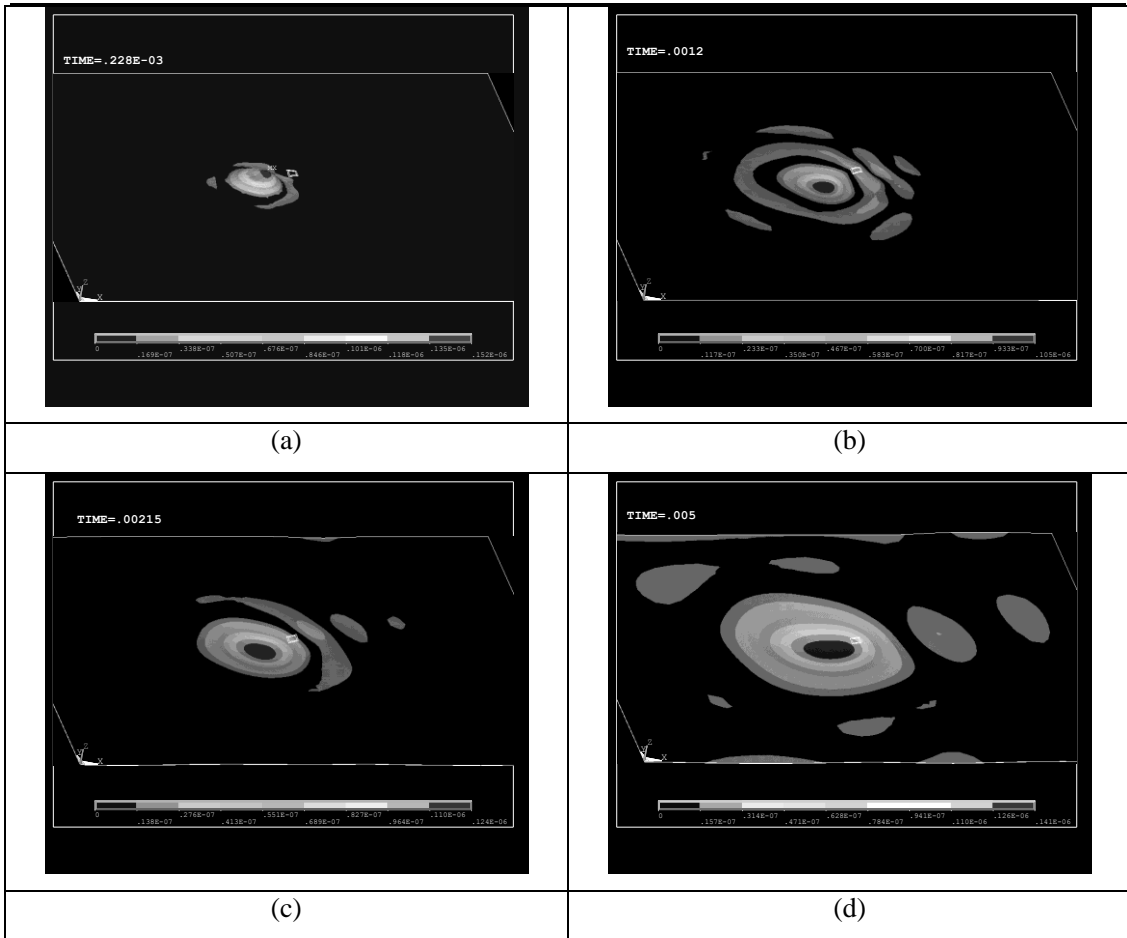


Figure 3. 8: Deformation of the plate obtained with the FEM for an outside impact at different time ($t = 0.228\text{ms}$ (a); 1.2ms (b); 2.15ms (c) and 5ms (d))

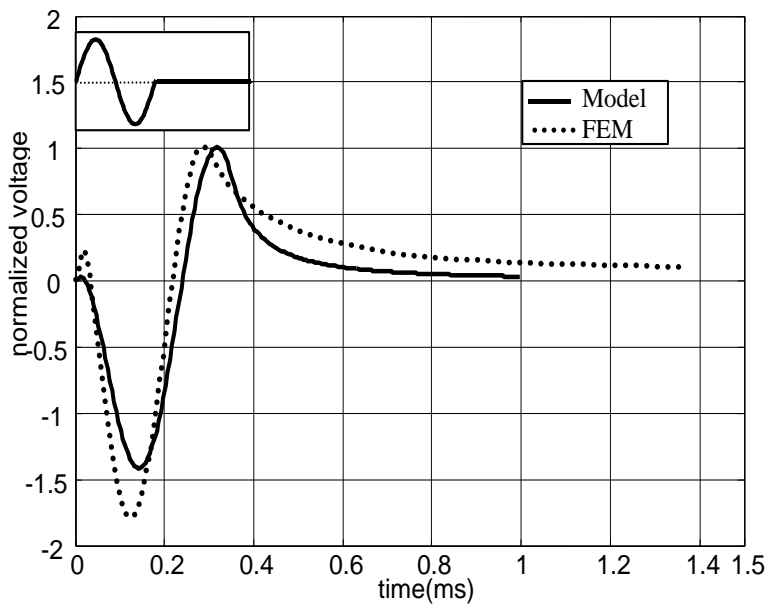


Figure 3.9: Comparison between FEM and analytical model for a burst force inside the piezo frame

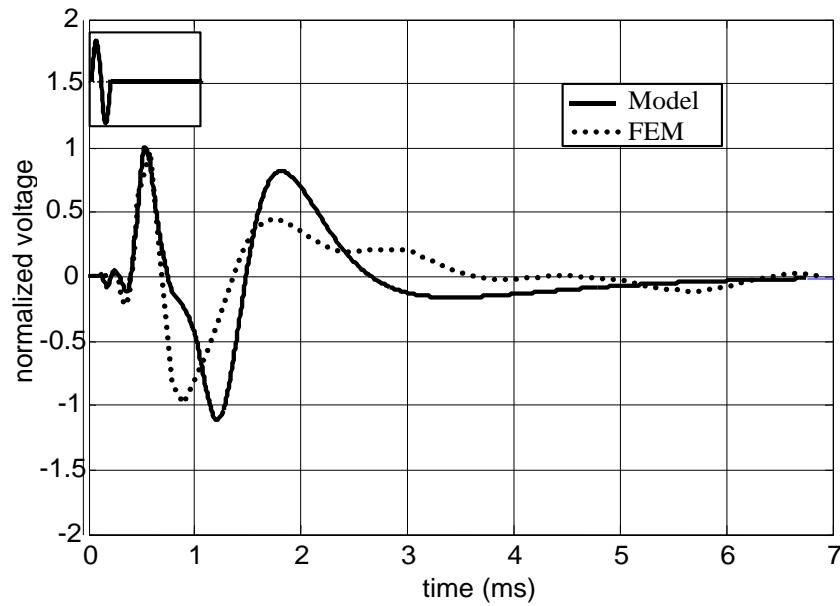


Figure 3.10: Comparison between FEM and analytical model for a burst force outside the piezo frame

3.5 Comparison with experimental measurement

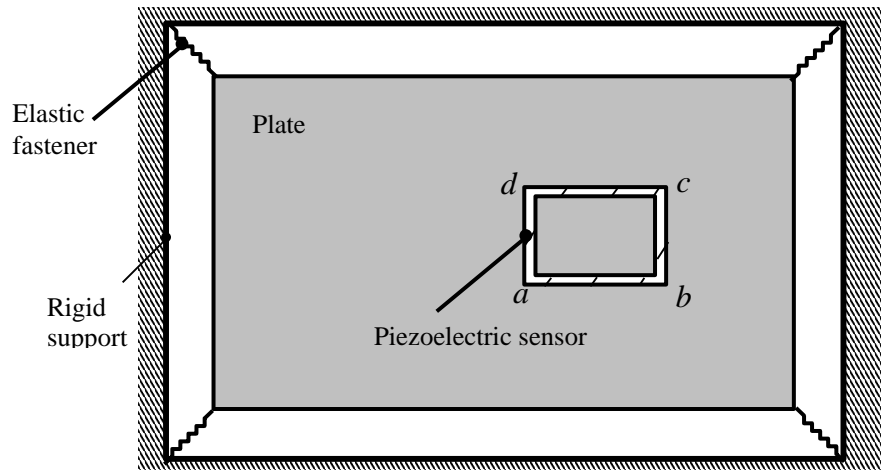
This Section exposes the comparison of resolution using the previously exposed analytical model, FEM predictions, and experimental measurements made on a thin plate.

3.5.1 Experimental set-up

The experimental set-up consists of a steel thin plate with surface-bonded piezoelectric devices. The plate is suspended vertically at its four corners by elastic fasteners. Experimental parameters are the same to the ones of previous simulations except for the following factors. The plate is finite with dimensions of $1.2m \times 0.8m$. The piezoelectric sensor thickness is $0.5mm$. The frame formed by the piezoelectric sensors is made of 16 pieces, 4 on each side. The 16 elements are connected to each other in parallel. These elements are used as sensors. Therefore, they should not modify the behavior of the structure. Actually, the voltage sensors are composed by several parts so that there is flexibility on bending mode. Each part is small enough

Chapter 3 Transient bending wave modeling in an infinite plate with bonded piezoelectric inserts

compared to plate dimensions and the mass is negligible. Thus, the modification of structure factors might be ignored. The driving force is generated by the use of an impulse hammer (*Dytran-5850B*). The range of force is 50-8000 *lbs*. The output voltage of the connected piezoelectric sensors is observed and recorded using an oscilloscope. The signals are not processed by any filters or the environmental noises handled.



(a) schema



(b) experiment set up

Figure 3.11: the experimental set-up. Plate dimension is $1200 \times 800 \times 0.1 \text{ mm}^3$.

3.5.2 Results & Discussion

The Figure 3.12 depicts the comparison between FEM and analytical predictions with the experimentally measured voltage on the square sensor. This Figure shows a good agreement between predictions and experimental results on the transient stage. At $t_1 = 28ms$, the reflections on the plate boundaries make the analytical model diverging from other responses. In a first approximation, this is not a blocking point because it is considered that reflections induce a nil wave flow through a closed surface (Figure 3.11 *abcd*). So we can consider here that only transient response (for $t < t_1$) gives information about wave flow.

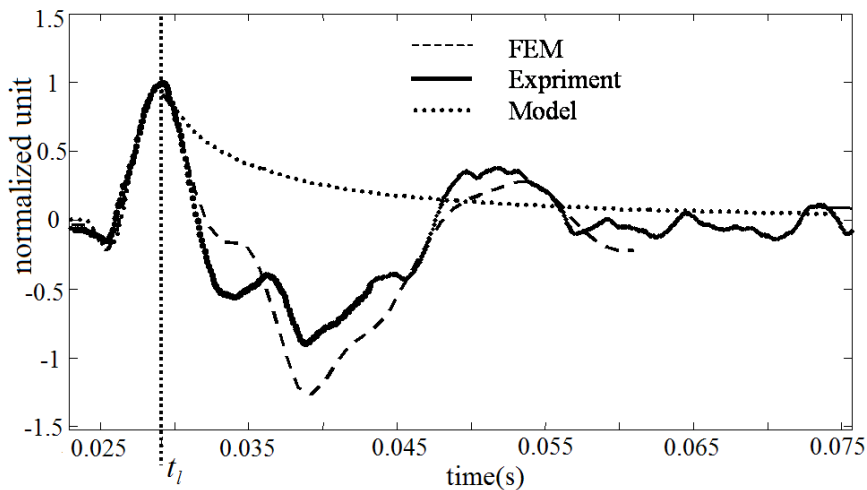


Figure 3.12: Experimental results and analytical and FEM prediction for a force applied at location (0, 0)

3.6 Conclusion

This chapter introduces a new analytical model for the wave propagation problem using the Fourier transform formalism. This model allows a computationally efficient way for determining the displacement response of an infinite thin plate submitted to a given force excitation, as well as an analytical formulation of the voltage response when piezoelectric element are bonded to the plate.

This model is valid for arbitrary time signal and arbitrary sensor shapes whatever the

Chapter 3 Transient bending wave modeling in an infinite plate with bonded piezoelectric inserts

spectrum of the excitation. Comparison with FEM analysis and experimental measurements shows that the proposed model gives a good prediction of the transient state of the wave propagation, taking into account phenomena such as dispersion and time of travel.

4 Force detection using energy flow direction estimator with piezoelectric sensors

4.1 Introduction

The last chapter proposed a model of an analytical expression of the piezoelectric transducers impulse voltage response in the whole time and space domains.

This chapter proposes to develop a new detection technique exploiting this piezoelectric output voltage.

As well known in the three-dimensional theory of elasticity, the Poynting vector (*P-vector*) represents the three-dimensional energy flow in a elastic media.

Here, the basic idea is to deduce in a first step an estimator of the power flow (*i.e.* *P-vector*) direction from the sensor voltage response.

We voluntary limit the analysis to the *P-vector* direction estimation.

This approach is conducted in three different steps:

- First, the energy flow theoretical analysis is proposed with the Poynting vector. Then, knowing this theoretical expression, an estimator is derived from the electric response. It should be note that this new estimator does not estimate the energy flow amplitude (*i.e.* Poynting vector amplitude) but only its direction.
- Secondly, numerical simulations are performed to verify the above theory with piezoelectric sensor outputs.

Finally, the experimental confirmation of the theory is demonstrated using piezoelectric sensors integrated on a thin steel plate. All the received signals here are not processed by any filters and no environmental noises need to be handled with special care. The most important advantages of the present method are the low energy requirement and the simplicity. Besides, there is another important advantage. Any boundary limit must be concerned. It means that the structural change does not effect for identification.

4.2 Principle

For lossy system, the value of the energy density is a decreasing function of the distance from the impact location. Considering a 1D-propagation, the energy flow direction can be obtained from the sign value of the energy density difference estimated by piezoelectric sensors, as shown in Figure 4.1a. One can easily appreciate that an arrangement in 2 sensor clusters (1&2; 3&4) permits to localize an impact, in considering again a 1D propagation (Figure 4.1b). In other words, if an impact occurs inside of the area delimiting by the 2 clusters (*I*-point), the energy density differences ΔE_{12} and ΔE_{34} of the 2 clusters are opposite sign terms. Effectively, cluster (1&2) sees a *Right* impact where cluster (3&4) sees a *Left* impact.

Conversely, an outside impact (*O*-point) leads to energy density differences ΔE_{12} and ΔE_{34} of the same sign.

The sum of this 2 energy density differences then gives information (Inside or Outside) on the impact localization. Effectively, an Inside impact induces a sum result leading to zero where an Outside impact leading to no-zero result.

The extension to a 2D propagation (Figure 4.1c) can be intuitively done by placing 2 others clusters (5&6; 7&8) perpendicular to the 2 primary clusters.

It will be shown thereafter that this specific arrangement permits to detect the direction of the flow energy.

Chapter 4 Force detection using energy flow direction estimator with piezoelectric sensors

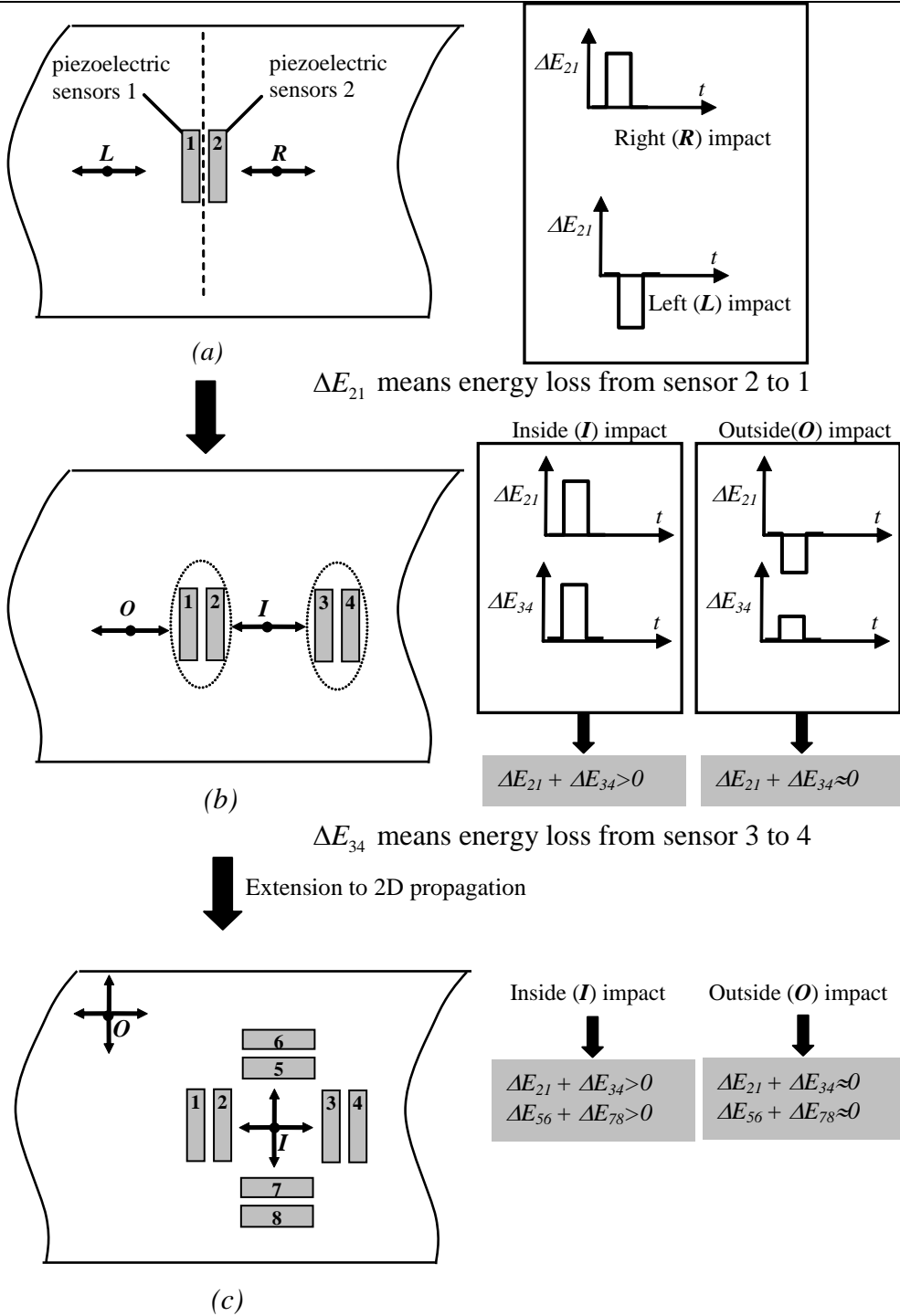


Figure 4.1. (a) detection of energy flow direction for 1D propagation; (b) impact detection (Inside or Outside) for 1D propagation. When force is applied in the area I , energy loss from sensor 2 to 1 and 3 to 4 are positive. When force is applied in the area O , energy loss from sensor 2 to 1 is negative, sensor 3 to 4 is positive. (c) extension for a 2D propagation .

ΔE_{ij} is the energy density difference from sensor i to sensor j .

4.3 Theoretical approach

Two main theoretical steps are needed to obtain the link between the impact location (inside or outside) and the piezoelectric sensor electric outputs:

- Express the energy density difference by the Poynting vector approach.
- link this energy density difference with the piezoelectric sensor outputs.

4.4 Expression of the energy density difference

In order to estimate the spatial derivative of the Poynting vector, the energy flow vector for a lossy infinite isotropic plate is firstly established. The strain components in cylindrical coordinates are given by ::

$$S_r = \frac{\partial u_r}{\partial r} \quad (4.1)$$

$$S_\theta = \frac{u_r}{r} + \frac{1}{r} \frac{\partial u_\theta}{\partial \theta}$$

$$S_{r\theta} = \frac{1}{r} \frac{\partial u_r}{\partial \theta} + \frac{\partial u_\theta}{\partial r} - \frac{u_\theta}{r}$$

Where s_i is the strain component in the i direction

u_i is the displacement component in the i direction

r , the radial distance

θ is the incident angle of the Poynting vector (i.e energy lfux)

The stress components are:

$$T_{rr} = \frac{E}{1-\nu^2} \left(\frac{\partial u_r}{\partial r} + \nu \frac{u_r}{r} \right) \quad (4.2)$$

$$T_{\theta\theta} = \frac{E}{1-\nu^2} \left(\frac{u_r}{r} + \nu \frac{\partial u_r}{\partial r} \right)$$

$$T_{r\theta} = \frac{E}{2(1+\nu)} \left(\frac{1}{r} \frac{\partial u_r}{\partial \theta} - \frac{\partial u_\theta}{\partial r} - \frac{u_\theta}{r} \right)$$

where E is the Young modulus and ν is the Poisson ratio.

The general equation of energy flow vector for an isotropic elastic medium can be expressed by the Poynting vector P_r as (Romano et al, 1990⁷¹) :

Chapter 4 Force detection using energy flow direction estimator with piezoelectric sensors

$$P_r = -(T_{rr}\dot{u}_r + T_{r\theta}\dot{u}_\theta + T_{rz}\dot{u}_z) \quad (4.3)$$

we consider here an axisymmetric problem to simplify the theoretical approach. This involves that the components $T_{r\theta}$ and T_{rz} are zero.

Assuming the strain T_{zz} is zero:

$$u_r = -z \frac{\partial u_z}{\partial r} \quad (4.4)$$

where z is the half thickness of the plate. Thus, from Equations (4.2) (4.3) (4.4) the Poynting vector can be expressed as a function of plate deflection:

$$\begin{aligned} P_r &= -\frac{E}{1-\nu^2} z^2 \left(\frac{\partial^2 u_z}{\partial r^2} + \frac{\nu}{r} \frac{\partial u_z}{\partial r} \right) \frac{\partial \dot{u}_z}{\partial r} \\ &= \frac{E}{1-\nu^2} z^2 \left(\frac{1}{r} \frac{\partial}{\partial r} \left(r \frac{\partial u_z}{\partial r} \right) \right) \frac{\partial \dot{u}_z}{\partial r} \end{aligned} \quad (4.5)$$

The value of the derivative of the displacement in the space domain $\frac{\partial^2 u_z}{\partial r^2}$ is

assumed to be larger than the displacement divided by distance $\frac{1}{r} \frac{\partial u_z}{\partial r}$.

Besides, the energy flow can be considered as parallel lines as shown in Figure 4.2. Because the incident angle θ is minuteness changed. Since incident angle θ is constant when radial distance r is great, the first term of Equation (4.5) becomes much larger than the second one. By neglecting this second term, Equation (4.5) becomes:

$$P_r \approx -\frac{z^2 E}{1-\nu^2} \frac{\partial^2 u_z}{\partial r^2} \frac{\partial \dot{u}_z}{\partial r} \quad (4.6)$$

The Figure 4.2 shows an example of a force effect to a certain area $abcd$, when the force is applied at the far bottom left outside. The ingoing energy can be expressed as:

$$P_{in} = \int_a^b P_r \cos \theta dr + \int_a^d P_r \sin \theta dr \quad (4.7)$$

with $(0 \leq \theta \leq \frac{\pi}{2})$.

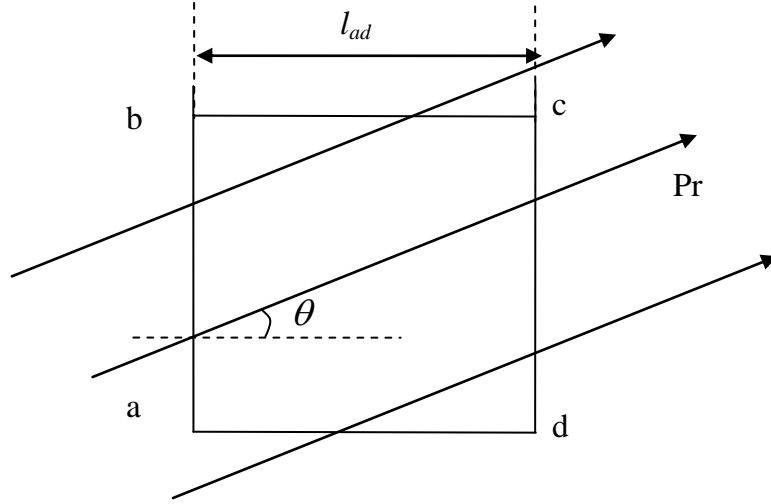


Figure 4.2: Integrated surface-1

As well, the outgoing energy flow can be expressed:

$$P_{out} = \int_a^c P_r \cos \theta dr + \int_b^c P_r \sin \theta dr \quad (4.8)$$

The ingoing energy minus the outgoing energy equals the total energy difference:

$$P_{in-out} = \int_a^b P_r \cos \theta dr - \int_d^c P_r \cos \theta dr + \int_a^d P_r \sin \theta dr - \int_b^c P_r \sin \theta dr \quad (4.9)$$

The right term of Equation (4.9) has two components; $\int_a^b P_r \cos \theta dr - \int_d^c P_r \cos \theta dr$

and $\int_a^d P_r \sin \theta dr - \int_b^c P_r \sin \theta dr$

For clarity reasons, only the first one will be investigated. It is possible because the 2 components are independent and the second one can be obtained by a similar analysis.

As Figure 4.3 shows, Equation (4.10) can be obtained from Equation (4.9) when inclination angle θ equals to 0.

$$\begin{aligned} P_{in-out} &= \int_a^b P_r dr - \int_d^c P_r dr \quad (4.10) \\ &= \left(-l_{ab} \frac{z^2 E}{1-\nu^2} \left(\frac{\partial^2 u_z}{\partial r^2} \frac{\partial \dot{u}_z}{\partial t} \right) \Big|_{r=r_1} \right) - \left(-l_{ab} \frac{z^2 E}{1-\nu^2} \left(\frac{\partial^2 u_z}{\partial r^2} \frac{\partial \dot{u}_z}{\partial t} \right) \Big|_{r=r_2} \right) \\ &= A \left(\frac{\partial^2 u_z}{\partial r^2} \frac{\partial \dot{u}_z}{\partial r} \Big|_{r=r_2} - \frac{\partial^2 u_z}{\partial r^2} \frac{\partial \dot{u}_z}{\partial r} \Big|_{r=r_1} \right) \end{aligned}$$

Where :

- l_{ab} is the vertical length of the considered surface.
- the coefficient A is :

$$A = l_{ab} \frac{z^2 E}{1 - \nu^2} \quad (4.11)$$

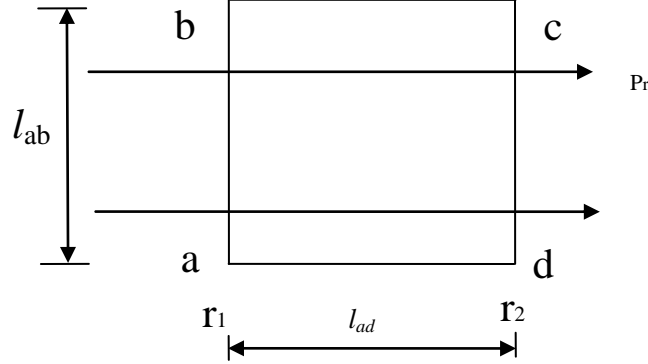


Figure 4.3: Integrated surface for an incident angle $\theta = 0$

Finally, the energy difference can be approximated as:

$$P_{in-out} = A \cdot l_{ab} \frac{\left(\frac{\partial^2 u_z}{\partial r^2} \frac{\partial \dot{u}_z}{\partial r} \Big|_{r=r2} - \frac{\partial^2 u_z}{\partial r^2} \frac{\partial \dot{u}_z}{\partial r} \Big|_{r=r1} \right)}{l_{ab}} \quad (4.12)$$

$$\approx A l_{ab} \left(\frac{\partial^3 u_z}{\partial r^3} \frac{\partial \dot{u}_z}{\partial r} + \frac{\partial^2 u_z}{\partial r^2} \frac{\partial^2 \dot{u}_z}{\partial r^2} \right) \Big|_{r=r1}$$

The case when incident angle θ is different to 0 is explained in following section.

4.5 Poynting vector and piezoelectric sensor outputs

How to link Poynting vector with piezoelectric sensor outputs is an open issue. If the spatial derivative of Equation (4.12) can be linked from piezoelectric sensor outputs, the energy flow direction can be obtained with a simple expression from the sensor voltages.

Chapter 4 Force detection using energy flow direction estimator with piezoelectric sensors

Let us consider two piezoelements and the surface S , $abcd$ arranged as shown in Figure 4.4. The sensor centers are placed in parallel on $a-b$ and $c-d$ lines.

The voltages of these sensors are then given by (the value of the derivative of the displacement in the space domain $\frac{\partial^2 u_z}{\partial r^2}$ is assumed to be larger than the displacement divided by distance $\frac{1}{r} \frac{\partial u_z}{\partial r}$):

$$\begin{aligned}
 V_1 &= \alpha \int_{r_1-\Delta r_1}^{r_1+\Delta r_1} \left(\frac{\partial^2 u_z}{\partial r^2} + \frac{1}{r} \frac{\partial u_z}{\partial r} \right) L_{pie} dr & (4.13) \\
 &\approx \int_{r_1-\Delta r_1}^{r_1+\Delta r_1} \left(\frac{\partial^2 u_z}{\partial r^2} \right) L_{pie} dr \\
 V_2 &= \alpha \int_{r_2-\Delta r_2}^{r_2+\Delta r_2} \left(\frac{\partial^2 u_z}{\partial r^2} + \frac{1}{r} \frac{\partial u_z}{\partial r} \right) L_{pie} dr \\
 &\approx \int_{r_2-\Delta r_2}^{r_2+\Delta r_2} \frac{\partial^2 u_z}{\partial r^2} L_{pie} dr
 \end{aligned}$$

With

$$\alpha = \frac{l_{pie} e_{31} h_{pla}}{2 \epsilon_{33}^s S_{pie}} \left(\frac{1-2\nu}{1-\nu} \right) \quad (4.14)$$

L_{pie} , l_{pie} , S_{pie} , e_{31} , h_{pla} , ϵ_{33}^s are respectively defined as the piezoelectric sensor length, the piezoelectric sensor thickness, the piezoelectric sensor surface, the voltage coefficient, the plate thickness and the piezoelement permittivity.

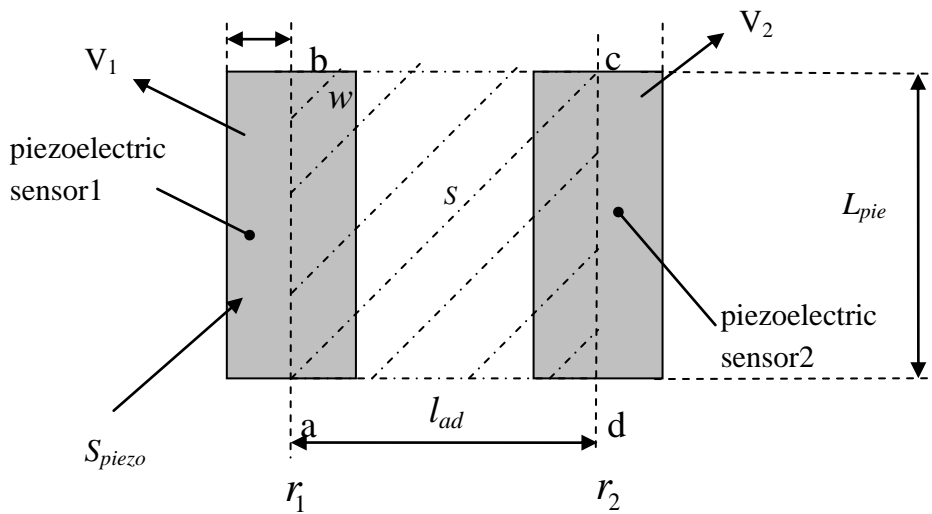


Figure 4.4: Integrated surface with 2 piezoelectric sensors.

Chapter 4 Force detection using energy flow direction estimator with piezoelectric sensors

If the sensor half width w and the distance between two sensors l_{ad} are small enough compared to the wavelength of bending wave, the two piezoelectric sensor voltages become:

$$V_1 \approx \alpha \left. \frac{\partial^2 u_z}{\partial r^2} S_{pie} \right|_{r=r_1} \quad (4.15)$$

$$V_2 \approx \alpha \left. \frac{\partial^2 u_z}{\partial r^2} S_{pie} \right|_{r=r_2}$$

The voltage difference is :

$$V_2 - V_1 = \alpha S_{pie} \left(\left. \frac{\partial^2 u_z}{\partial r^2} \right|_{r=r_2} - \left. \frac{\partial^2 u_z}{\partial r^2} \right|_{r=r_1} \right) \quad (4.16)$$

$$\approx \alpha S_{pie} l_{ad} \frac{\partial^3 u_z}{\partial r^3}$$

The spatial integral of the time derivative of the displacement as a function of the voltage can be expressed from Equation (4.13) as:

$$\int_{r_1}^{r_2} \frac{\partial^2 \dot{u}_z}{\partial r^2} dr \approx \frac{1}{\alpha L_{pie}} (\dot{V}_1 + \dot{V}_2) \frac{1}{2} \quad (4.17)$$

$$= \frac{1}{\alpha S} (\dot{V}_1 + \dot{V}_2) \frac{l_{ad}}{2}$$

where S is the surface between these two sensors corresponding to the covered area shown in Figure 4.4 which is the surface of the $abcd$ parallelogram.

The term $\int_{r_1}^{r_2} \frac{\partial^2 \dot{u}_z}{\partial r^2} dr$ can also be written as:

$$\int_{r_1}^{r_2} \frac{\partial^2 \dot{u}_z}{\partial r^2} dr = \left. \frac{\partial \dot{u}_z}{\partial r} \right|_{r=r_2} - \left. \frac{\partial \dot{u}_z}{\partial r} \right|_{r=r_1} \quad (4.18)$$

From Equations (4.17) (4.18) and, the Equation (4.19) can be obtained as:

$$\left. \frac{\partial \dot{u}_z}{\partial r} \right|_{r=r_2} - \left. \frac{\partial \dot{u}_z}{\partial r} \right|_{r=r_1} = \frac{1}{\alpha S} (\dot{V}_1 + \dot{V}_2) \frac{l_{ad}}{2} \quad (4.19)$$

Assuming that the distance l_{ad} between the two center lines of the piezoelements is small enough compared to the bending wavelength, the output voltage of the piezoelectric can be approximated by a linear function of the radial distance, so that

Chapter 4 Force detection using energy flow direction estimator with piezoelectric sensors

the term $\left. \frac{\partial^3 u_z}{\partial r^3} \right|_{r=r_1, r_2}$ becomes almost constant over the considered distance.

The term $\frac{\partial^4 u_z}{\partial r^4}$ is nil and it is therefore possible to obtain the derivative of the first term of the right member of Equation (4.12) from Equations (4.16) and (4.19):

$$\begin{aligned} \left. \frac{\partial}{\partial r} \left(\frac{\partial^3 u_z}{\partial r^3} \frac{\partial \dot{u}_z}{\partial r} \right) \right|_{r=r_1} &= \left. \frac{\partial^3 u_z}{\partial r^3} \right|_{r=r_1} \frac{1}{l_{ad}} \left(\left. \frac{\partial \dot{u}_z}{\partial r} \right|_{r=r_2} - \left. \frac{\partial \dot{u}_z}{\partial r} \right|_{r=r_1} \right) \\ &= \frac{V_2 - V_1}{\alpha S_{pie} l_{ad}} \cdot \frac{1}{l_{ad}} \cdot \frac{1}{\alpha S} \frac{l_{ad}}{2} (\dot{V}_1 + \dot{V}_2) \\ &= \frac{1}{2 l_{ad} S_{pie} S \alpha^2} (V_2 - V_1) (\dot{V}_1 + \dot{V}_2) \end{aligned} \quad (4.20)$$

As well, the derivative of the second term of the right member of Equation (4.12) is given as:

$$\begin{aligned} \left. \frac{\partial}{\partial r} \left(\frac{\partial^2 u_z}{\partial r^2} \frac{\partial^2 \dot{u}_z}{\partial r^2} \right) \right|_{r=r} &= \frac{1}{l_{ad}} \left(\left. \frac{\partial^2 u_z}{\partial r^2} \frac{\partial^2 \dot{u}_z}{\partial r^2} \right|_{r=r_2} - \left. \frac{\partial^2 u_z}{\partial r^2} \frac{\partial^2 \dot{u}_z}{\partial r^2} \right|_{r=r_1} \right) \\ &= \frac{1}{l_{ad}} \frac{1}{S_{pie}^2 \alpha^2} (V_2 \dot{V}_2 - V_1 \dot{V}_1) \end{aligned} \quad (4.21)$$

The spatial derivative of the energy difference $\frac{\partial}{\partial r} P_{in-out}$ expressed by Poynting vector can be rewritten as:

$$\begin{aligned} \frac{\partial}{\partial r} (P_{in-out}) &= A \left(\frac{I}{2 S_{piezo} S \alpha^2} (V_2 - V_1) (\dot{V}_1 + \dot{V}_2) + \right. \\ &\quad \left. \frac{I}{(S_{piezo})^2 \alpha^2} (\dot{V}_2 V_2 - \dot{V}_1 V_1) \right) \end{aligned} \quad (4.22)$$

If l_{ad} is small enough as the assumption before, S_{piezo} becomes equal to S , and the Equation (4.22) can be rewritten as :

$$\frac{\partial}{\partial r} (P_{in-out}) = A \frac{1}{S_{pie}^2 \alpha} \left(\frac{1}{2} (V_2 - V_1) (\dot{V}_1 + \dot{V}_2) + \dot{V}_2 V_2 - \dot{V}_1 V_1 \right) \quad (4.23)$$

Integrating Equation (4.23) in the time domain, the energy density difference is expressed by:

$$\int_0^T \frac{\partial}{\partial r} (P_{in-out}) dt = \int_0^T A \frac{1}{S_{pie}^2 \alpha} \left(\frac{1}{2} (V_2 - V_1) (\dot{V}_1 + \dot{V}_2) + \dot{V}_2 V_2 - \dot{V}_1 V_1 \right) dt \quad (4.24)$$

We finally obtain here an expression between the energy difference initially expressed from the pointing vector (cf (4.10) and the piezoelements voltage V_1 and V_2 .

The left term of Equation (4.24) decreases with the distance from the impact location. When an impact is applied to the left area of piezoelectric sensor 1 the energy density decrease from piezoelectric sensors 1 to 2. Thus, the right term of Equation (4.24) will be negative. On the other hand, when an impact is applied to the right area of sensor 2 the energy density increase from sensor 1 to 2. Thus, the right term of Equation (4.24) will be positive.

4.6 Impact area location detection with piezoelectric sensors output

Let us consider now the specific arrangement in 2 clusters of 2 sensors as introduced in figure 1b. This arrangement, reminded in Figure 4.5 permits to evaluate the impact location by the areas related to the location of piezoelectric sensors 1 to 4. Area 1 is located as the left side of sensor 1. Area 2 is located between sensor 2 and 3. Area 3 is located as the right area of sensor 3.

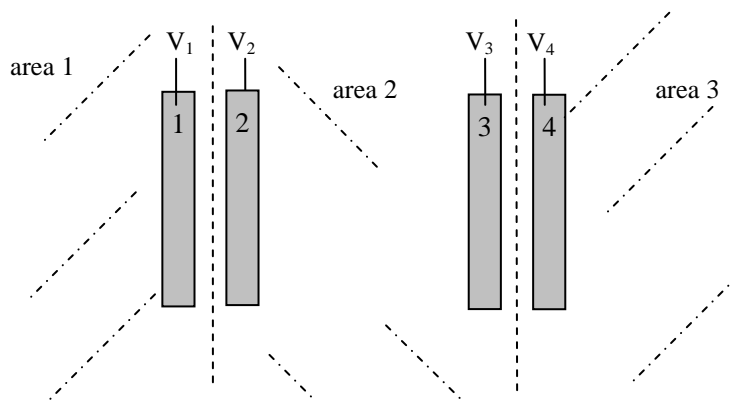


Figure 4.5: Integrated surface with 4 piezoelectric sensors-four outputs

Because of the system symmetry, it is possible to connect sensor 2 with 3 and 1 with 4 (Figure 4.6) to reduce computational requirements. When an impact is applied between these pairs, area 2, the right term of Equation (4.24) becomes positive. On the other hand, the cases of impact applied in outer of these pairs, area 1 or 3, the right

Chapter 4 Force detection using energy flow direction estimator with piezoelectric sensors

term of Equation (4.24) becomes negative.

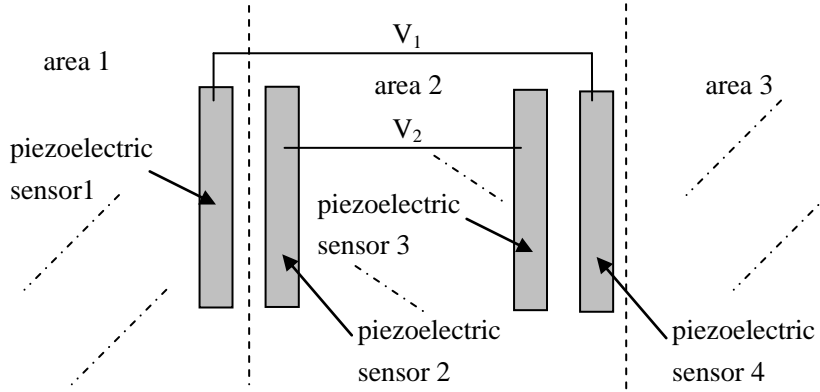


Figure 4.6: Integrated surface with 4 piezoelectric sensors-two output

Let us consider now the specific arrangement using eight sensors and electrically connected as shown in Figure 4.7.

Two pairs of sensors are used in each vertical and horizontal direction. Area 1 is defined the inner surface of these sensors. This arrangement defines 9 areas (1 to 9) and permits to know if the impact is located in area 1 or not.

The disadvantage of this structure (Figure 4.7) is that it needs four sensor outputs. If the object is only to know if the force location is inside or outside the integrated surface, it is possible to reduce computational requirements. Two vertical directions are considered at the same time. They are independent from each other because of the far field assumption. When the inner surface width l_{ad} (Figure 4.3) is small enough compared to radial distance r , it is possible to define the energy density difference estimator $Q = Q_1 + Q_2$ within the surface in the time domain from Equation (4.9) and (4.24) as:

$$Q_1 = \beta \int_0^T \left(\frac{1}{2} (V_2 - V_1) (\dot{V}_1 + \dot{V}_2) + \dot{V}_2 V_2 - \dot{V}_1 V_1 \right) dt \quad (4.25)$$

$$Q_2 = \delta \int_0^T \left(\frac{1}{2} (V_3 - V_4) (\dot{V}_3 + \dot{V}_4) + \dot{V}_3 V_3 - \dot{V}_4 V_4 \right) dt$$

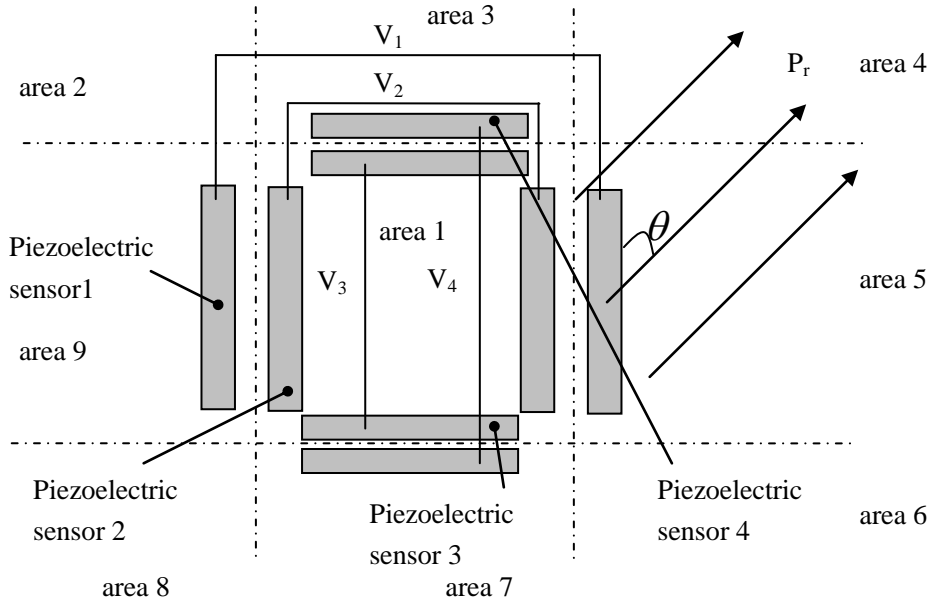


Figure 4.7: Integrated surface with eight piezoelectric sensors-four outputs

where β and δ equal to $A \frac{1}{(S_0)^2 a^2} \cos \theta$ and $A \frac{1}{(S_0)^2 a^2} \sin \theta$, respectively. If the

impact is applied in area 8 ($0 \leq \theta \leq \frac{\pi}{2}$), β and δ becomes positive. The signs of

Q_1 and Q_2 , however, do not depend on β and δ . Here, Q_1 and Q_2 values are negative, which lead to a negative value of Q . Analogous results can be obtained when the impact is applied in area 2, 4 or 6. Moreover, if the impact is applied in left area to that surface, area 5, or right area, area 9, the absolute Q_1 value becomes higher than Q_2 value because of the great radial distance. Thus, the value of Q becomes negative. The same operation can be applied for the area 3 and 7. Based on the above results, we can simplify the energy density difference as (Figure 4.8), where only two sensor outputs are necessary:

$$q = \int_0^T \left(\frac{1}{2} (V_2 - V_1) (\dot{V}_1 + \dot{V}_2) + \dot{V}_2 V_2 - \dot{V}_1 V_1 \right) dt \quad (4.26)$$

In other words, Q_1 and Q_2 depend on the V_1 , V_2 and V_3 , V_4 voltages respectively. It is therefore possible to know the impact location whether inside or outside with the sign of q simply from two piezoelectric sensors output. When an impact is applied inside of the structure (Figure 4.8), q value is positive.

When an impact is applied outside of the structure, q value becomes negative. The

Chapter 4 Force detection using energy flow direction estimator with piezoelectric sensors

absolute value of q increases with the force magnitude (and same impact location if the impact is outside), because more energy flows through the sensors. When an impact is applied outside, the q amplitude also decreases with the distance of impact location for the same magnitude impact, since less energy flows to the sensors. However, it seems that this technique has limited sensitivity for low damping.

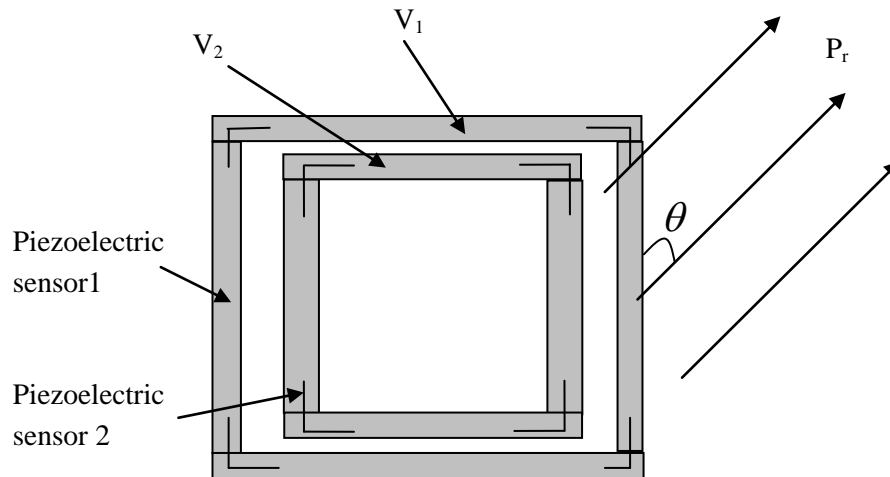


Figure 4.8: Integrated surface with 8 piezoelectric sensors-2

4.7 Numerical simulation validation

4.7.1 Impact location and q value determination

In order to validate the theoretical model, simulations using *Matlab*® software were carried out. The modelled infinite plate is shown in Figure 4.9. Two piezoelectric framed sensors are glued on the plate. Coordinate origin is on the centre of the sensors contour. The physical properties and dimensions are given in Table 4.1. The impact as shown in Figure 4.10 is applied near the centre of the contour (coordinate (0.01, 0.01)), inside the sensors contour. To avoid symmetry problem, the impact was not applied in the coordinate origin. When the energy flows from inside to outside of the contour, q value becomes positive. When all the energy pass the sensors, there are no energy flow anymore so that q becomes a constant value. The simulated result which

Chapter 4 Force detection using energy flow direction estimator with piezoelectric sensors

is shown in Figure 4.11 gives a good agreement.

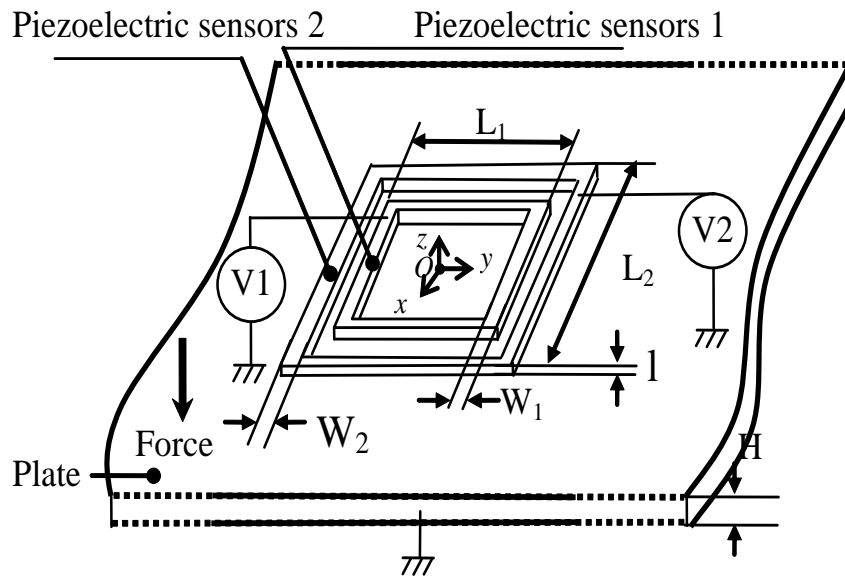


Figure 4.9: Schematics of the considered structure-infinite plate

On the other hand, when the same impact force is applied outside of the contour, the q becomes negative as shown in Figure 4.12 and Figure 4.13.

In Figure 4.12, the force is applied at location (0.38, 0.35), outside area of the contours. In Figure 4.13 the force is applied at location (0.40, 0.40), farther distance from contours than the force of Figure 4.12 q tends to a constant value from a certain time t_{out} as there is no more energy flow through the sensors from that time. t_{out} is greater than t_{in} because of the distance. It is also seen that the absolute value of q magnitude decreases with the distance of impact location. It is because less energy flows through the sensors when the distance increases.

Chapter 4 Force detection using energy flow direction estimator with piezoelectric sensors

Table 4.1: Matlab simulation parameters

Parameter	Value	Parameter	Value
Plate surface density m	$6.4Kg/m^2$	Outside sensor surface length L_2	$0.14m$
Plate elastic modules E	$1.95 \cdot 10^{11} Pa$	Outside sensor surface width W_2	$0.003m$
Plate thickness H	$8 \cdot 10^{-4} m$	Inside sensor surface length L_1	$0.132m$
Poisson ratio ν	0.33	Inside sensor surface width W_1	$0.003m$
Damping ratio ξ_n	0.1	Relative permittivity $\epsilon_{33}^s / \epsilon_0$	1142
Voltage coefficient e_{31}	$-4.3C.m^{-1}$		
Sensor thickness l	$5 \cdot 10^{-4} m$		

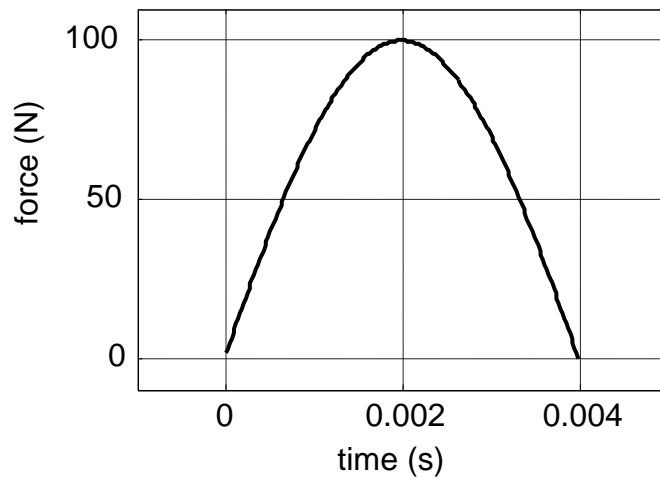


Figure 4.10: Impact force applied to the considered-infinite plate

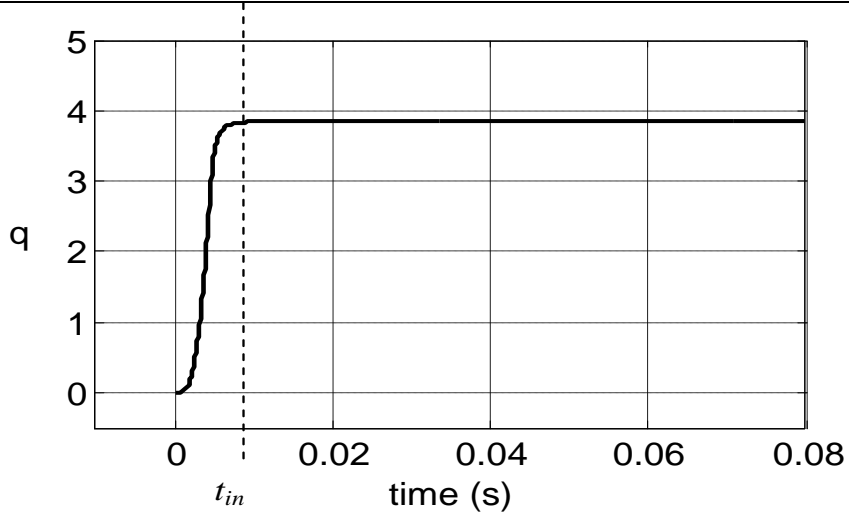


Figure 4.11: q value response to an impact excitation at the (0.01,0.01)-location inside-1

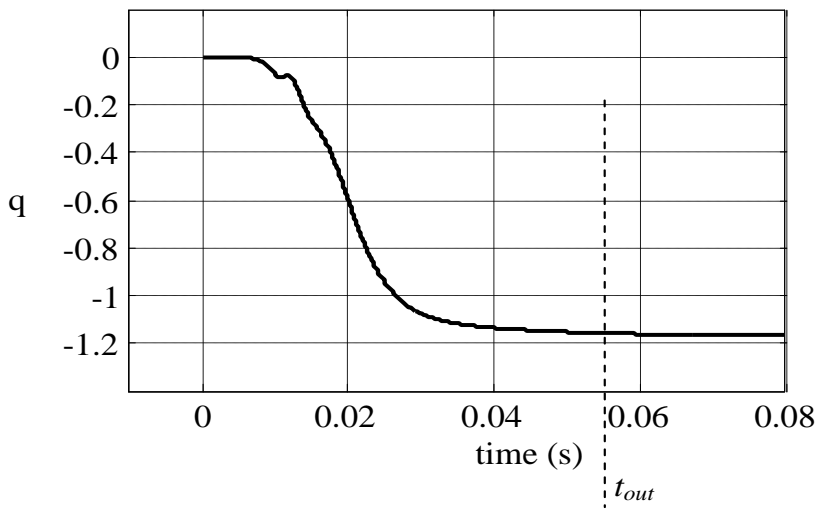


Figure 4.12: q value response to a pulse force excitation at (0.38, 0.35)-location outside

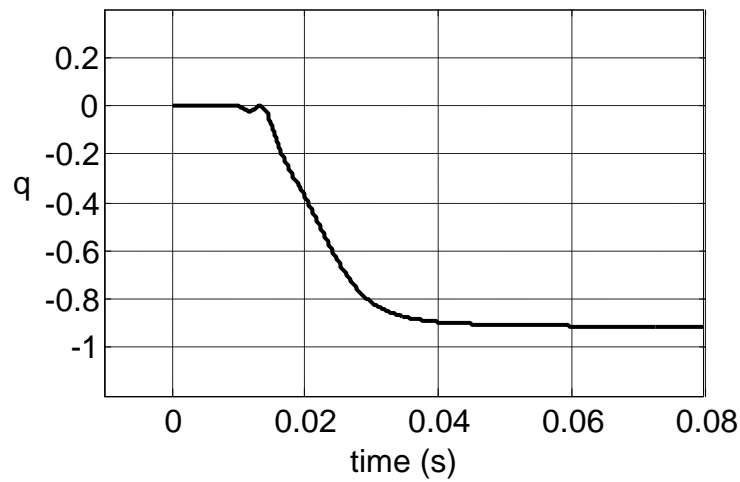


Figure 4.13: q value response to a pulse force excitation at (0.40, 0.40)-location outside

The impact force in the simulated data from Figure 4.11 to Figure 4.13 has a 100N magnitude.

With a 200N impact magnitude, simulation results are shown Figure 4.14 when applied at (0.01, 0.01) and in Figure 4.15 when applied at (0.40, 0.40). They correspond to Figure 4.11 and Figure 4.13, respectively.

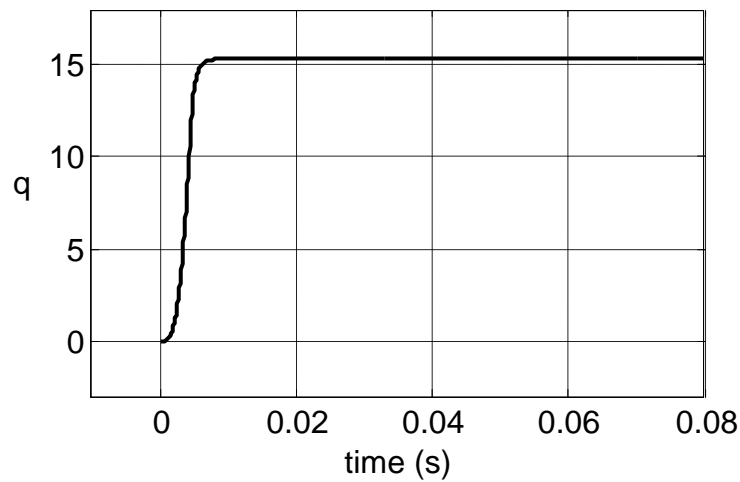


Figure 4.14: q value response to a pulse force excitation at the origin (0.01, 0.01)-location inside-2 with a 200 N force

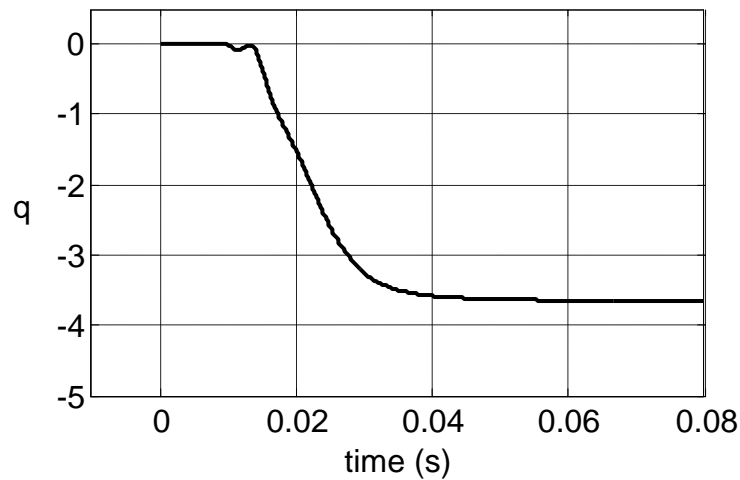


Figure 4.15: q value response to a pulse force excitation at (0.40, 0.40)-location outside-2 with a 200 N force

It is clearly seen that the max/min peak q value increases with the force magnitude. The reason is that more energy flows through the sensors. The value of q is four times greater since the energy depends on the squared force magnitude. Finally the q -estimator is sensitive to the impact amplitude. Thus, this approach can estimate quantity of the input energy.

4.7.2 q -estimator value with different location inside

A same impact applied at different locations in the inside area (Figure 4.16) leads to the results shown in Figure 4.17 and Figure 4.18. The peak value of q stays constant with different the impact inside location. Hence, this shows that the criterion also gives an idea of the relative impact force magnitude for the same impact location when outside, and whatever the location inside.

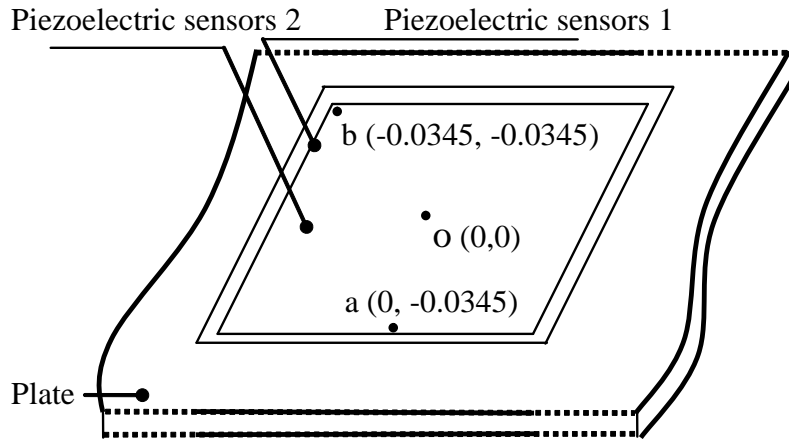


Figure 4.16: Schematics of different location inside

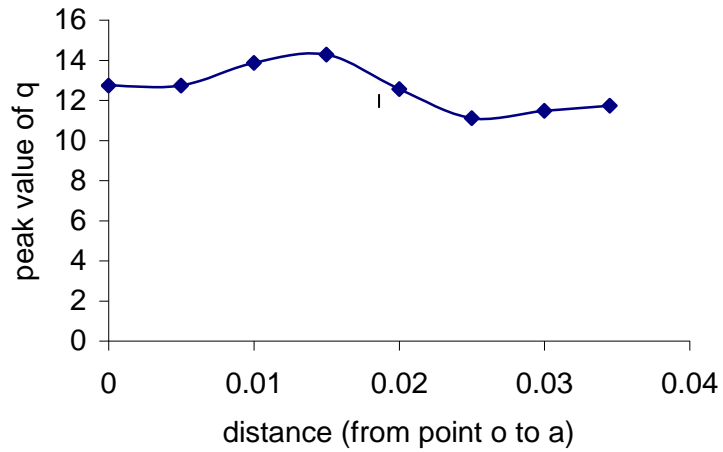


Figure 4.17: peak of q value response to different location inside from point o to a

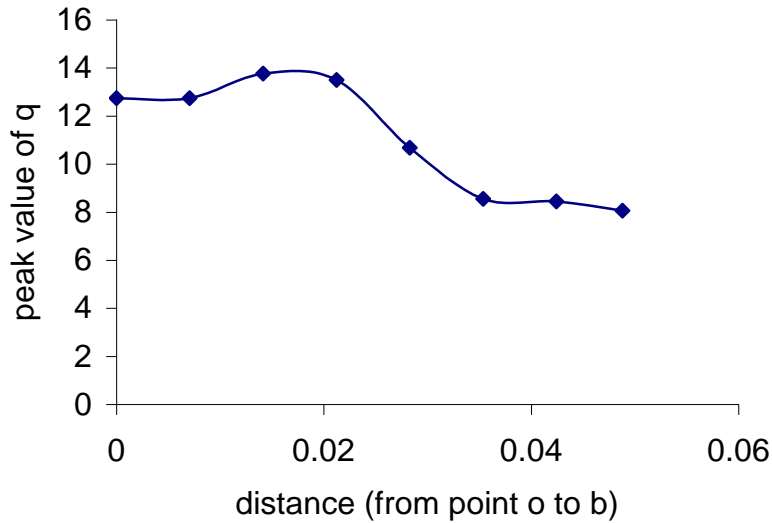


Figure 4.18: peak of q value response to different location inside from point *o* to *b*

4.8 Experimental validation

4.8.1 Experimental set-up

Experiments have been carried out to confirm the previously introduced model. The infinite dimension condition is fulfilled by using a plate with very large dimensions, preventing reflection phenomena in the transient state in the considered spatial domain. A $1.2m \times 0.8m$ steel thin plate was used whose four corners were suspended by elastic fasteners. The piezoelectric sensors were bonded to its surface (Figure 4.19). The experimental parameters were those used in the previous simulations (Table 4.1). 16 unitary elements were connected each other to determine one closed contour. There are 4 in each line (in the same way than Figure 4.9).

An impulse hammer (Dytran 5850B) was used for applying the impact. The hammer had a flat head of $6mm$ in diameter and the impact force exerted by this hammer was approximated as a localized load. It is important to note that all received signals were not processed by any filters, nor were the environmental noises handled with special care.

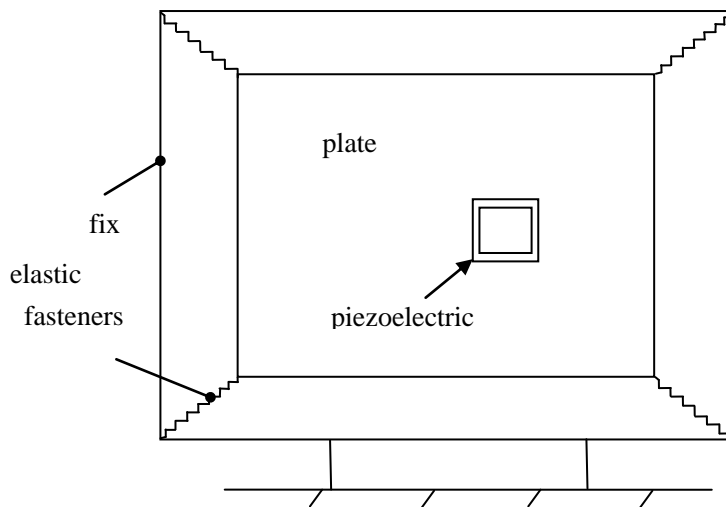


Figure 4.19: Experimental structure

4.8.2 Result & Discussion

Four impact tests were performed. One was performed using a steel hammer tip and three using plastics hammer tip, which gives lower pseudo-frequency impacts. First, the steel tip was used with impact waveforms shown in Figure 4.20. This impact is applied both inside and outside of area delimited by the sensors. The coordinate origin is placed at the centre of the surface. The results are given in Figure 4.21. These results demonstrate that the positive (resp. negative) value of q effectively corresponds to an impact applied inside surface of sensor (resp. outside), allowing an effective impact monitoring as expected.

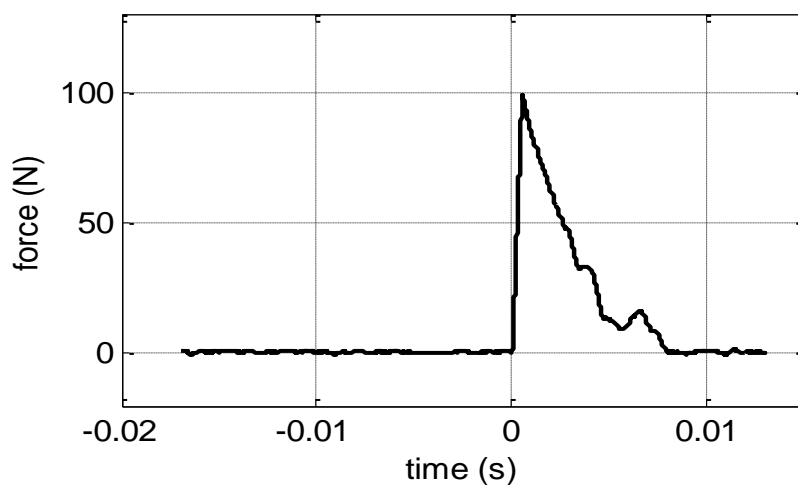


Figure 4.20: Impact force to the considered structure-finite plate-1

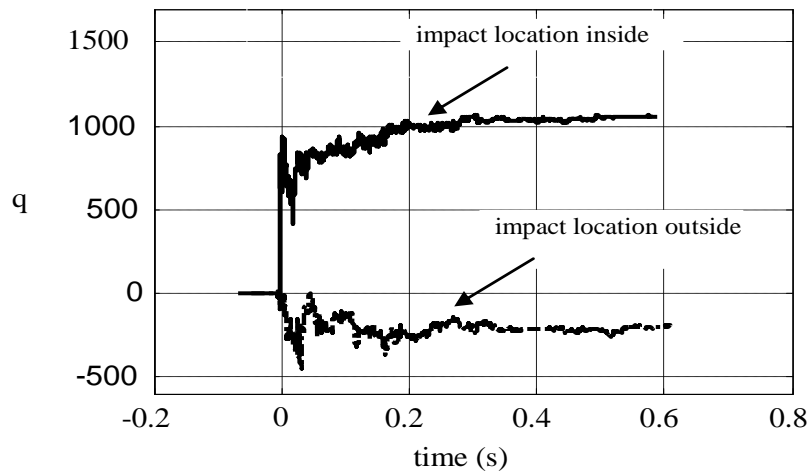


Figure 4.21: q value response to the pulse force outside and inside-1
force outside at (0.4, 0.4)-force inside at (0, 0.01)

Then the plastic tip is used to give another type of force as shown in Figure 4.22. The plastic tip, which is not as stiff as the steel tip, gives lower pseudo-frequency impacts. The results are given from Figure 4.23 to Figure 4.25. These Figures clearly demonstrate that the impact location can be efficiently detected from the value of the proposed criterion.

These figures also show good agreement between simulation and experimental results. From these results, it seems that high pseudo-frequencies have more reflections due to fewer losses. Thus, the reflection on the plate boundaries makes the value of q oscillating.

As well, these series of tests show that the force magnitude can also be estimated by the value of q . The peak value gives the impact energy received by the sensor (if the impact is applied inside). All these results show that the value of q decreases with the time because of the reflection in the plate and dielectric losses of the piezoelectric sensors. The reflections can besides be thought as the outside impact.

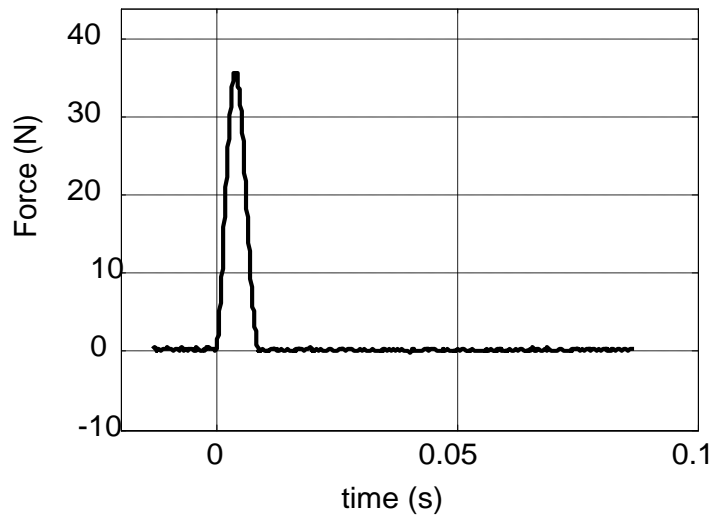


Figure 4.22: Impact force to the considered structure-finite plate-2

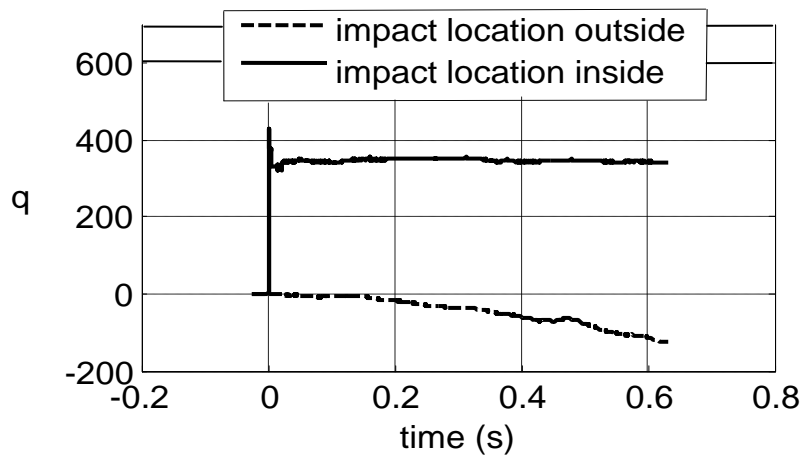


Figure 4.23: q value response to the pulse force - force outside at (0.25, 0.3)-force inside at (0, 0.01)

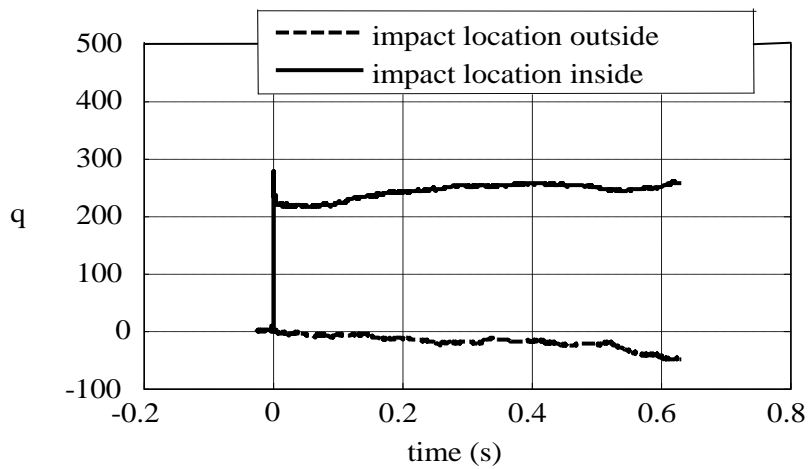


Figure 4.24: q value response to the pulse force - force outside at (0.4, 0.4)-force inside at (0.01, 0.01)

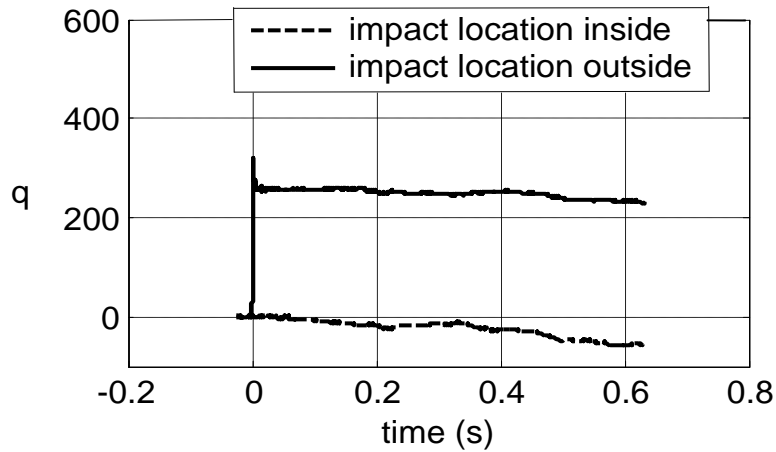


Figure 4.25: q value response to the pulse force - force outside at (0.4, 0.35)-force inside at (0.02, 0.01)

4.9 Conclusion

This chapter introduced a new model for detecting impact location by estimating the energy flow direction with piezoelectric sensors.

Based on a Poynting vector approach, we show that the energy flow difference can be approximated from the electric response of piezoelectric sensors with a specific geometric arrangement.

This approach is a low cost technique with low computational requirements and it is easy to embed in structures.

Simulations and experimental measurements show that the proposed model gives a interesting tool for estimating impact location and eventually impact force magnitude.

5 Force detection using energy flow estimator with piezoelectric sensors

5.1 Introduction

As the before chapters introduce, we can identify the force using energy flow direction with piezoelectric sensors. It is seems that the approach proposed in before chapter is not sensitive in few energy density derivative case. Therefore, this chapter proposes an approach using energy flow with piezoelectric sensors. This approach is more responsive for low loss system.

The present chapter is organized as follow. First, energy flow analysis is proposed in bending wave. Secondly, numerical simulation is shown to verify the theoretical approach. Thirdly, an approach using piezoelectric outputs to express the energy flow is proposed. Finally, simulation and experimental confirmation is demonstrated using some piezoelectric devices put on a thin steel plate.

5.2 Principles

Application of Poynting vector for power flow expression has been investigated in the previous sections. Extension for impact energy transmission will be developed in this chapter. To obtain the impact location and history, the estimation of the power flux through the closed surface (S) is considered as shown in Figure 5. 1a. The structure here is, first of all, infinite plate. Integral energy from inside surface (S) to outside in time domain is defined as name of Q . When the impact is located inside the frame (for example, point I), the mechanical energy flows out of the structural surface. The value Q becomes positive with outgoing power flow. In the case of an impact outside the frame as see in point O , the induced energy quantity flows in and out through the closed surface (S). The outgoing energy quantity and the energy losses in the structure consists ingoing energy. The value Q turns to negative. The reflexion phenomenon by each plate edges has to be taken into account. It behaves as secondary external sources. Reflected waves arrive latter on as shown in Figure 5. 1b, the first power flow are not modified if we see in time domain. Consequently, the value Q associated to the first transition carries direct information with the impact location. The reflexion does not change the value Q . Thus, this approach is able to use in a finite plate as shown in Figure 5. 1b.

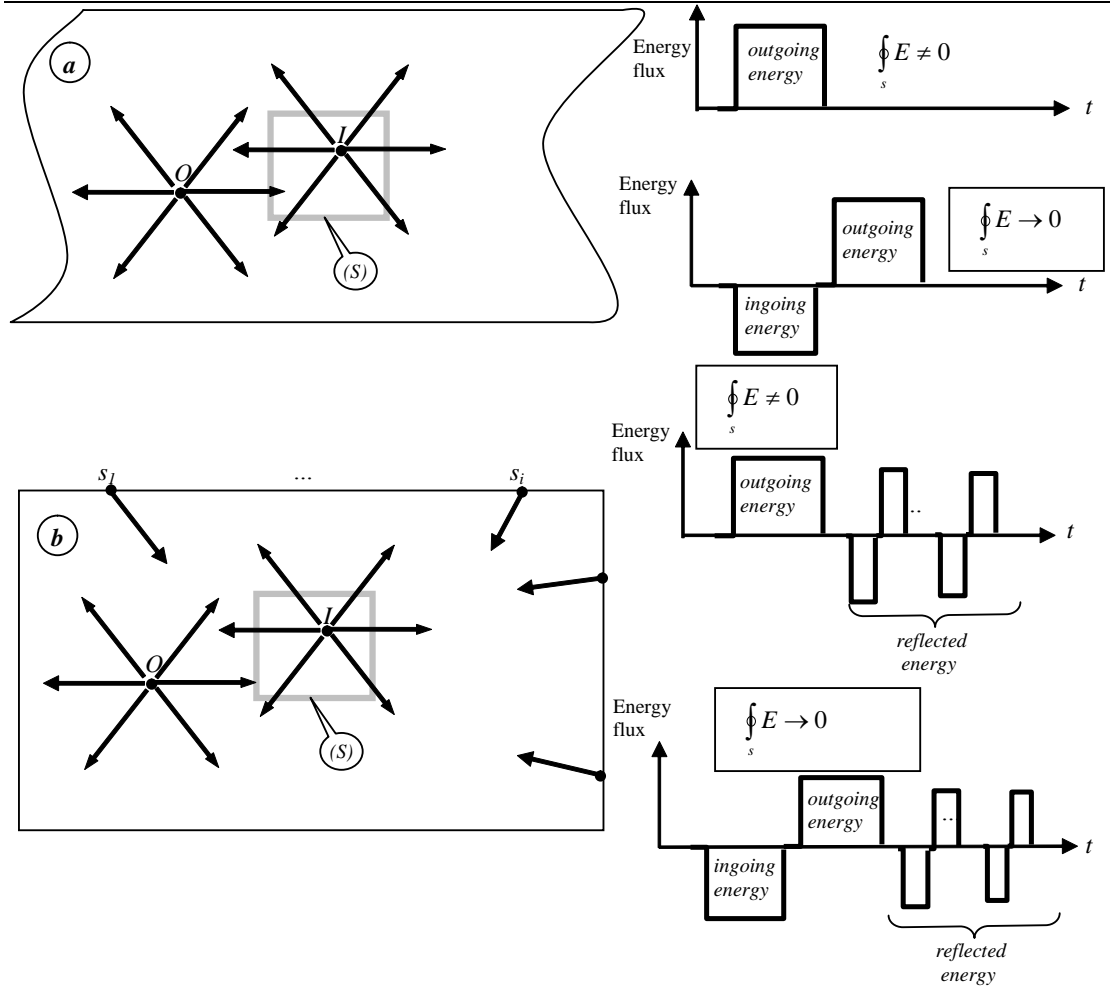


Figure 5. 1: principle of the energy flux expressed by Poynting vector in an infinite structure (a) without consideration of losses. Sum of energy flux trough the surface (S) is null for an outside impact (O -point) and not null for an inside impact (I -point). For a finite structure (b), reflexion phenomena induce secondary sources ($s_1..s_i$) which are the associated null energy flux total

5.3 Poynting vector applied with bending wave

The Poynting vector associated with the bending equation is calculated by a standard procedure that consists to start from the propagation general equation to get the energy equation. We start from the bending equation⁷²,

$$m\ddot{u}_z + D\Delta^2 u_z = f(x, y, t) \quad (5.1)$$

where ε is the flexural displacement, f is the applied load, Δ is the Laplacian

Chapter 5 Force detection using energy flow estimator with piezoelectric sensors

operator and m is defined as the surface mass density. D represents the bending stiffness that can be expressed as a function of the Young modulus Y , the Poisson ratio ν and the plate thickness h .

$$D = \frac{Yh^3}{12(1-\nu^2)} \quad (5.2)$$

In order to get the energy flow in the plates, Equation (5.1) is multiplied by the displacement yields:

$$m\ddot{u}_z\dot{u}_z + D\left(\frac{\partial^4 u_z}{\partial x^4}\dot{u}_z + \frac{\partial^4 u_z}{\partial y^4}\dot{u}_z + 2\frac{\partial^4 u}{\partial x^2\partial y^2}\dot{u}_z\right) = f \cdot \dot{u}_z \quad (5.3)$$

We are now going to transform the equation to introduce the Poynting vector.

The term $\frac{\partial^4 u_z}{\partial x^4}\dot{u}_z$ can be also written as:

$$\frac{\partial^4 u_z}{\partial x^4}\dot{u}_z = \frac{\partial}{\partial x}\left(\frac{\partial^3 u_z}{\partial x^3}\dot{u}_z\right) - \frac{\partial^3 u_z}{\partial x^3}\frac{\partial \dot{u}_z}{\partial x} \quad (5.4)$$

where the second right member term is given by:

$$\frac{\partial^3 u_z}{\partial x^3}\frac{\partial \dot{u}_z}{\partial x} = \frac{\partial}{\partial x}\left(\frac{\partial^2 u_z}{\partial x^2}\frac{\partial \dot{u}_z}{\partial x}\right) - \frac{\partial^2 u_z}{\partial x^2}\frac{\partial^2 \dot{u}_z}{\partial x^2} \quad (5.5)$$

since

$$\frac{\partial^2 u_z}{\partial x^2}\frac{\partial^2 \dot{u}_z}{\partial x^2} = \frac{1}{2}\frac{\partial}{\partial t}\left(\frac{\partial^2 u_z}{\partial x^2}\right)^2 \quad (5.6)$$

Equation (5.4) turns to;

$$\frac{\partial^4 u_z}{\partial x^4}\dot{u}_z = \frac{\partial}{\partial x}\left(\frac{\partial^3 u_z}{\partial x^3}\dot{u}_z - \frac{\partial^2 u_z}{\partial x^2}\frac{\partial \dot{u}_z}{\partial x}\right) + \frac{1}{2}\frac{\partial}{\partial t}\left(\frac{\partial^2 u_z}{\partial x^2}\right)^2 \quad (5.7)$$

We can get the same result for the y coordinates since the plate is isotropic.

$$\frac{\partial^4 u_z}{\partial y^4}\dot{u}_z = \frac{\partial}{\partial y}\left(\frac{\partial^3 u_z}{\partial y^3}\dot{u}_z - \frac{\partial^2 u_z}{\partial y^2}\frac{\partial \dot{u}_z}{\partial y}\right) + \frac{1}{2}\frac{\partial}{\partial t}\left(\frac{\partial^2 u_z}{\partial y^2}\right)^2 \quad (5.8)$$

One term in Equation (5.3) $2\frac{\partial^4 u_z}{\partial x^2\partial y^2}\dot{u}_z$ is still rest to solve. It can be written as following.

$$2 \frac{\partial^4 u_z}{\partial x^2 \partial y^2} \dot{u}_z = \frac{\partial}{\partial x} \left(\frac{\partial^3 u_z}{\partial x \partial y^2} \dot{u}_z \right) + \frac{\partial}{\partial y} \left(\frac{\partial^3 u_z}{\partial x^2 \partial y} \dot{u}_z \right) - \left(\frac{\partial^3 u_z}{\partial x \partial y^2} \frac{\partial \dot{u}_z}{\partial x} + \frac{\partial^3 u_z}{\partial x^2 \partial y} \frac{\partial \dot{u}_z}{\partial y} \right) \quad (5.9)$$

The last right term of Equation (5.9) can be given as:

$$\frac{\partial^3 u_z}{\partial x \partial y^2} \frac{\partial \dot{u}_z}{\partial x} = \frac{\partial}{\partial y} \left(\frac{\partial^2 u_z}{\partial x \partial y} \frac{\partial \dot{u}_z}{\partial x} \right) - \frac{\partial^2 u_z}{\partial x \partial y} \frac{\partial^2 \dot{u}_z}{\partial x \partial y} \quad (5.10)$$

with

$$\frac{\partial^3 u_z}{\partial x^2 \partial y} \frac{\partial \dot{u}_z}{\partial y} = \frac{\partial}{\partial x} \left(\frac{\partial^2 u_z}{\partial x \partial y} \frac{\partial \dot{u}_z}{\partial y} \right) - \frac{\partial^2 u_z}{\partial x \partial y} \frac{\partial^2 \dot{u}_z}{\partial x \partial y} \quad (5.11)$$

It yields the expression:

$$2 \frac{\partial^2 u_z}{\partial x \partial y} \frac{\partial^2 \dot{u}_z}{\partial x \partial y} = \frac{\partial}{\partial t} \left(\frac{\partial u_z}{\partial x \partial y} \right)^2 \quad (5.12)$$

Therefore, the Equation (5.9) can be developed as:

$$2 \frac{\partial^4 u_z}{\partial x^2 \partial y^2} \dot{u}_z = \frac{\partial}{\partial x} \left(\frac{\partial^3 u_z}{\partial x \partial y^2} \dot{u}_z - \frac{\partial^2 u_z}{\partial x \partial y} \frac{\partial \dot{u}_z}{\partial y} \right) + \frac{\partial}{\partial y} \left(\frac{\partial^3 u_z}{\partial x^2 \partial y} \dot{u}_z - \frac{\partial^2 u_z}{\partial x \partial y} \frac{\partial \dot{u}_z}{\partial x} \right) + \frac{\partial}{\partial t} \left(\frac{\partial^2 u_z}{\partial x \partial y} \right)^2 \quad (5.13)$$

Equation (5.3) can be, thus, rewritten as:

$$m \frac{\partial}{\partial t} \left(\frac{\dot{u}_z^2}{2} + \frac{D}{2} \left(\left(\frac{\partial^2 u_z}{\partial x^2} \right)^2 + \left(\frac{\partial^2 u_z}{\partial y^2} \right)^2 \right) + D \left(\frac{\partial^2 u_z}{\partial x \partial y} \right)^2 \right) + D \frac{\partial}{\partial x} \left(\frac{\partial^3 u_z}{\partial x^3} - \frac{\partial^2 u_z}{\partial x^2} \frac{\partial \dot{u}_z}{\partial x} + \frac{\partial^3 u_z}{\partial x \partial y^2} \dot{u}_z - \frac{\partial^2 u_z}{\partial x \partial y} \frac{\partial \dot{u}_z}{\partial y} \right) + D \frac{\partial}{\partial y} \left(\frac{\partial^3 u_z}{\partial y^3} \dot{u}_z - \frac{\partial^2 u_z}{\partial y^2} \frac{\partial \dot{u}_z}{\partial y} + \frac{\partial^3 u_z}{\partial x^2 \partial y} \dot{u}_z - \frac{\partial^2 u_z}{\partial x \partial y} \frac{\partial \dot{u}_z}{\partial x} \right) = f \cdot \dot{u}_z = \frac{dw}{dt} \quad (5.14)$$

where w is the energy supplied to the plate.

The volume integral of Equation (5.14) leads to:

$$D \int_V \text{div} P dV + \int_V m \frac{\partial}{\partial t} [E_p + E_c] dV = \int_V \frac{dw}{dt} dV \quad (5.15)$$

$$\text{or } D \int_C P dC + \int_V m \frac{\partial}{\partial t} [E_p + E_c] dV = \int_V \frac{dw}{dt} dV$$

Chapter 5 Force detection using energy flow estimator with piezoelectric sensors

where C is the surface closing the volume V .

The P corresponds to power flow. E_p , E_c correspond to potential and kinetic energy of the bending wave. If there are no losses, the second left term of Equation (5.15) equals to zero. The right term of Equation (5.15) corresponds supplied energy.

Thus, the Poynting vector expressed by following two equations:

$$P_x = \frac{\partial^3 u_z}{\partial x^3} \dot{u}_z - \frac{\partial^2 u_z}{\partial x^2} \frac{\partial \dot{u}_z}{\partial x} + \frac{\partial^3 u_z}{\partial x \partial y^2} \dot{u}_z - \frac{\partial^2 u_z}{\partial x \partial y} \frac{\partial \dot{u}_z}{\partial y} \quad (5.16)$$

$$P_y = \frac{\partial^3 u_z}{\partial y^3} \dot{u}_z - \frac{\partial^2 u_z}{\partial y^2} \frac{\partial \dot{u}_z}{\partial y} + \frac{\partial^3 u_z}{\partial x^2 \partial y} \dot{u}_z - \frac{\partial^2 u_z}{\partial x \partial y} \frac{\partial \dot{u}_z}{\partial x} \quad (5.17)$$

It is should note that this Poynting vector expression is not same with the general one⁷³ because we calculated from flexural wave equation in thin plate. Other methods derive express directly from the stress and strain expression. It seems that the expression of the Poynting vector is not unique.

Four terms in Equation (5.16) and (5.17) correspond to three wave types.

$\frac{\partial^3 u_z}{\partial x^3} \dot{u}_z + \frac{\partial^3 u_z}{\partial x \partial y^2} \dot{u}_z$, $\frac{\partial^2 u_z}{\partial x^2} \frac{\partial \dot{u}_z}{\partial x}$, $\frac{\partial^2 u_z}{\partial x \partial y} \frac{\partial \dot{u}_z}{\partial x}$ correspond to shearing wave, bending waves and twisting waves respectively.

It can be clearly seen that the Poynting vector is related only to the flexural displacement u of the plate.

Let's see again the Equation (5.15). We assume that the system is static state at the beginning time. If the impact is applied to the integral volume; the first left term equal to the supplied energy. If the impact is not applied to the integral volume, the first left term equal to zero. The vertical coordinate (P_z) is zero since we consider a flectional structure coupling. The integral volume can be considered as integral surface (A) shown in Figure 5.2

Now, the integral Poynting vector from inside surface to outside in time domain can be obtained as:

$$Q = \int_0^T \iint \left(\frac{\partial^3 u_z}{\partial x^3} \dot{u}_z - \frac{\partial^2 u_z}{\partial x^2} \frac{\partial \dot{u}_z}{\partial x} + \frac{\partial^3 u_z}{\partial x \partial y^2} \dot{u}_z - \frac{\partial^2 u_z}{\partial x \partial y} \frac{\partial \dot{u}_z}{\partial y} \right) + \left(\frac{\partial^3 u_z}{\partial y^3} \dot{u}_z - \frac{\partial^2 u_z}{\partial y^2} \frac{\partial \dot{u}_z}{\partial y} + \frac{\partial^3 u_z}{\partial x^2 \partial y} \dot{u}_z - \frac{\partial^2 u_z}{\partial x \partial y} \frac{\partial \dot{u}_z}{\partial x} \right) d\vec{A} dt \quad (5.18)$$

where A is the integral surface shown Figure 5.2.

When an impact is applied inside of the structure (see Figure 5.2), the value Q becomes positive, with an outside impact, Q becomes negative

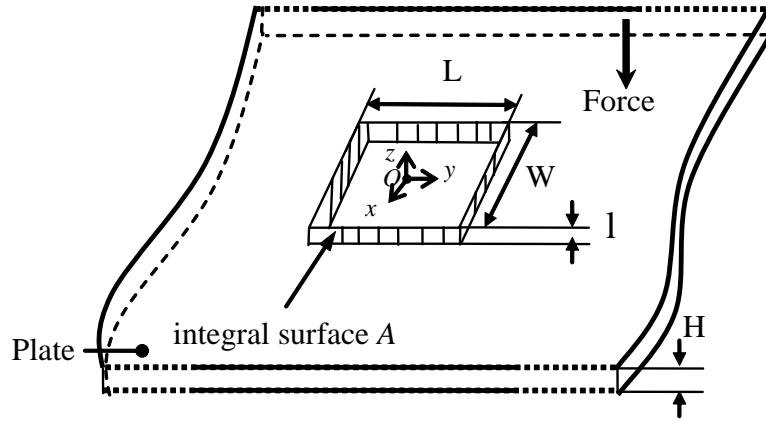


Figure 5.2: Schematics of the considered structure-infinite plate

5.4 Numerical simulation based on Poynting vector

Simulations using Matlab R2006a are carried out in order to confirm the present theoretical model. The plate presented in Figure 5.2 is modeled using Matlab. The physical properties and dimensions of the target plate are given in Table 5. 1. The impact as shown in Figure 5.3 is supposed to be applied in the center of the contour (the coordinate is (0, 0), see Figure 5.2). The energy flows from inside to outside the contour, Q value becomes positive. When all the energy pass the contour, there are not energy flow anymore, Q becomes a constant value. The simulated result which is shown in Figure 5.4 gives a good correspondence.

Table 5. 1: Matlab simulation parameters

Parameter	Value	Parameter	Value
Plate surface density m	$6.4Kg/m^2$	Integral surface length L	$0.18m$
Plate elastic modules E	$1.95 \cdot 10^{11} Pa$	Integral surface width W	$0.18m$
Plate thickness H	$8 \cdot 10^{-4} m$		
Poisson ratio μ	0.33		
Damping ratio ξ_n	0.1		

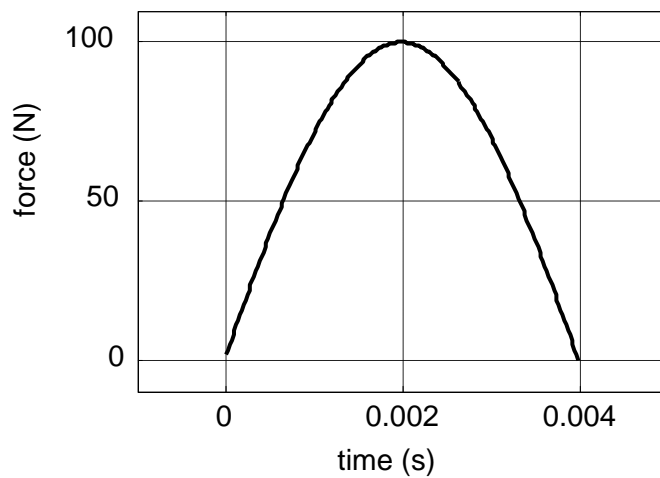


Figure 5.3: Impact force to the considered structure-infinite plate

On the other hand, when the same impact force is applied outside of the contours, Q becomes negative as shown in Figure 5.5. It can be read that Q tends to a constant value. It will be discussed later.

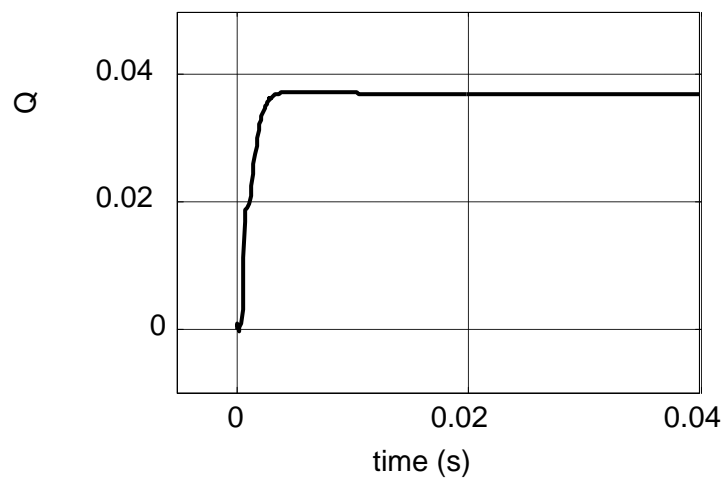


Figure 5.4: energy response to a pulse force excitation at the origin (0, 0)-location inside

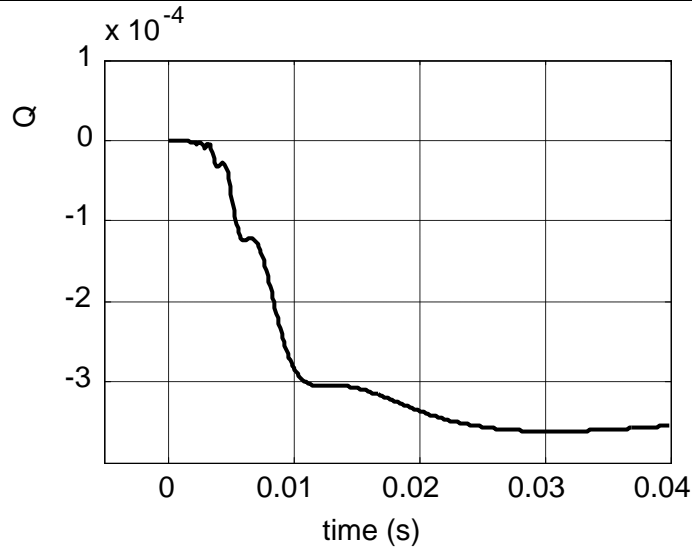


Figure 5.5: energy response to a pulse force excitation at (0.14, 0.14)-location outside

The time of occurrence of the maximum value of Q increases with the propagation distance between the impact location and the contour, and the magnitude of the maximum value of Q decreases with the distance. The reason of is that, due to damping, the longer the distance the less energy goes through the integration surface as shown in Figure 5. 6. This figure shows the relation between Poynting vector vs time with some different locations of the impact source. All impacts were outside of contour. The wave propagation distance effects two factors: one is in time and the other is in amplitude. It is clearly seen that Q achieves quickly to its first peak when the distance is smaller. It is also clearly demonstrated that the amplitude of Q is bigger when the distance is smaller. As it was mentioned above, the reason for the second case is supposed that there is damping effect. It seems that longer the distance, less energy propagate through the surface. To verify it, the relation between Poynting vector Q and damping coefficient variation are investigated. Figure 5. 7 shows its result.

It is seems that saturated Q value decreases with increase of damping factor. This simulation result verifies well that the overall magnitudes of Q curves would be decreased if the magnitude of the damping ratio increases.

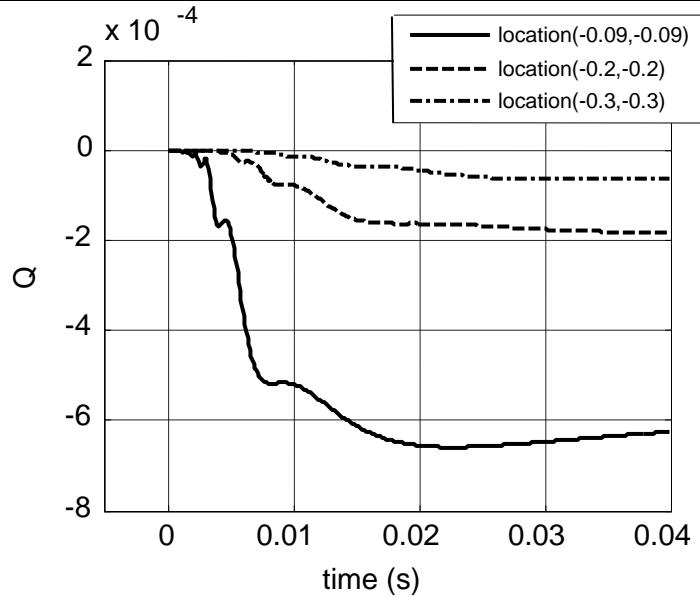


Figure 5. 6: Energy for various force locations outside (damping coefficient is 0.1)

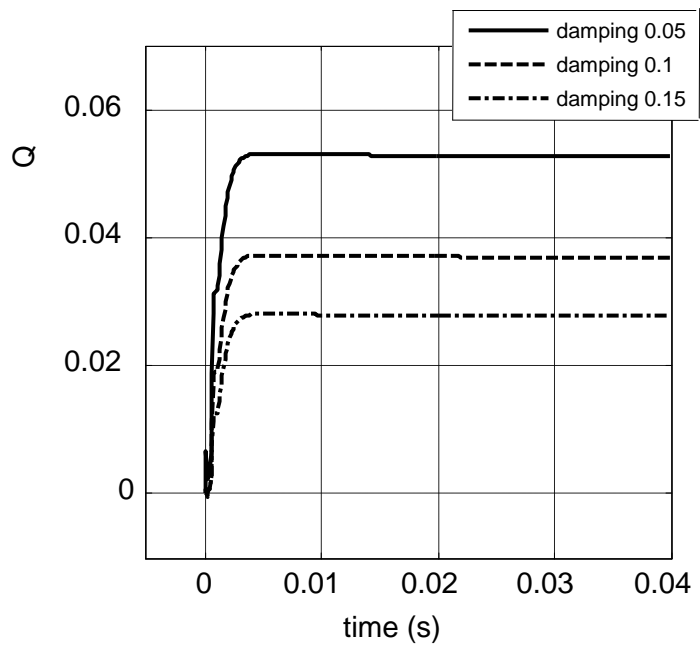


Figure 5. 7: Energy for various damping coefficient -force locations at the origin (0, 0).

In a similar way, Figure 5.8 shows that the overall magnitudes of Q curves would be increased if we increase the force peak as shown in Figure 5.3. The reason is that more energy flows through the contour. The value of Q is four times greater since the energy depends on the squared force magnitude. Needless to say, Figure 5.8 shows Q

increase with higher energy given in the structure as expected.

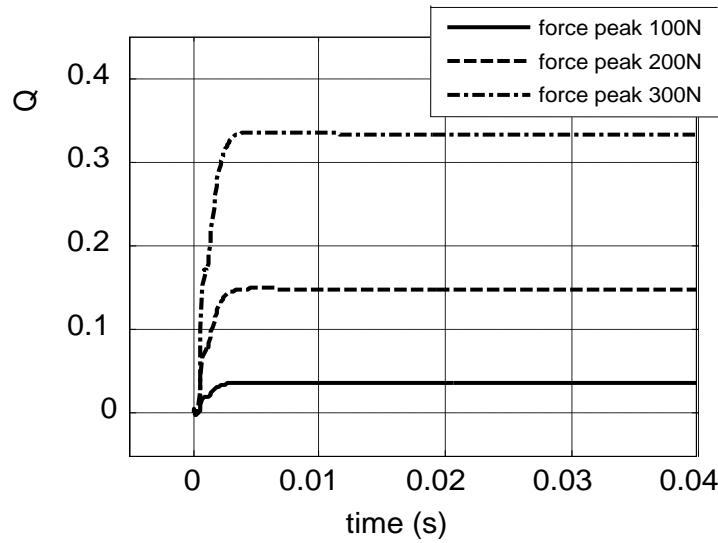


Figure 5.8: Energy for various force curve peak-force locations at the origin (0, 0).

5.5 Approximation of Poynting vector and piezoelectric sensors outputs

How to link Poynting vector with piezoelectric sensor outputs is an open issue. If the Equation (5.18) can be linked from piezoelectric sensor outputs, the energy flow can be obtained with easy expression from the sensor voltages. This section proposes the connection between the Poynting vector and piezoelectric output voltage.

From the simulation result, the third and fourth terms of Equation (5.16) are negligible compare to the first and second terms.

The velocity of flexural deflection can be expressed by:

$$\dot{u}_z = \frac{1}{2tm} \sqrt{\frac{2\pi m}{D(1-\xi^2)}} e^{-\frac{r^2 \xi}{4t} \sqrt{\frac{m}{D}}} \sin\left(\frac{r^2}{4t} \sqrt{\frac{m}{D}} (1-\xi^2)\right) \quad (5.19)$$

Chapter 5 Force detection using energy flow estimator with piezoelectric sensors

From the Equation (5.19), we can be obtained:

$$\begin{aligned} \frac{\partial \dot{u}_z}{\partial x} = & \frac{1}{2tm} \sqrt{\frac{2\pi m}{D(1-\xi^2)}} \left(e^{-\frac{x^2+y^2}{4t}\xi\sqrt{\frac{m}{D}}} \left(-\frac{2x}{4t}\xi\sqrt{\frac{m}{D}} \right. \right. \\ & \left. \left. \sin\left(\frac{x^2+y^2}{4t}\sqrt{\frac{m}{D}(1-\xi^2)}\right) + e^{-\frac{x^2+y^2}{4t}\xi\sqrt{\frac{m}{D}}} \right. \right. \\ & \left. \left. \cos\left(\frac{x^2+y^2}{4t}\sqrt{\frac{m}{D}(1-\xi^2)}\right) \frac{2x}{4t}\sqrt{\frac{m}{D}(1-\xi^2)} \right) \right) \end{aligned} \quad (5.20)$$

Because ξ equals to 0.05~0.1, that, the first right term of Equation (5.20) is negligible compare to the second term.

Equation (5.20) turns to:

$$\begin{aligned} \frac{\partial \dot{u}_z}{\partial x} \approx & \frac{1}{2tm} \sqrt{\frac{2\pi m}{D(1-\xi^2)}} \left(e^{-\frac{x^2+y^2}{4t}\xi\sqrt{\frac{m}{D}}} \right. \\ & \left. \cos\left(\frac{x^2+y^2}{4t}\sqrt{\frac{m}{D}(1-\xi^2)}\right) \frac{2x}{4t}\sqrt{\frac{m}{D}(1-\xi^2)} \right) \end{aligned} \quad (5.21)$$

From the Equation (5.21), we can obtain:

$$\begin{aligned} \frac{\partial^2 \dot{u}_z}{\partial x^2} \approx & \frac{1}{2tm} \sqrt{\frac{2\pi m}{D(1-\xi^2)}} \left(e^{-\frac{x^2+y^2}{4t}\xi\sqrt{\frac{m}{D}}} \left(-\frac{2x}{4t}\xi\sqrt{\frac{m}{D}} \right) \right. \\ & \left. \cos\left(\frac{x^2+y^2}{4t}\sqrt{\frac{m}{D}(1-\xi^2)}\right) \frac{2x}{4t}\sqrt{\frac{m}{D}(1-\xi^2)} \right. \\ & \left. + e^{-\frac{x^2+y^2}{4t}\xi\sqrt{\frac{m}{D}}} \left(-\sin\left(\frac{x^2+y^2}{4t}\sqrt{\frac{m}{D}(1-\xi^2)}\right) \left(\frac{2x}{4t}\sqrt{\frac{m}{D}(1-\xi^2)} \right)^2 \right. \right. \\ & \left. \left. e^{-\frac{x^2+y^2}{4t}\xi\sqrt{\frac{m}{D}}} \cos\left(\frac{x^2+y^2}{4t}\sqrt{\frac{m}{D}(1-\xi^2)}\right) \frac{2}{4t}\sqrt{\frac{m}{D}(1-\xi^2)} \right) \right) \end{aligned} \quad (5.22)$$

Because it is transient problem, when time t turns to zero and r is big enough compare to the time t , the velocity of deformation can be simple as:

$$\begin{aligned} \frac{\partial^2 \dot{u}_z}{\partial x^2} \approx & \frac{1}{2tm} \sqrt{\frac{2\pi m}{D(1-\xi^2)}} \left(e^{-\frac{x^2+y^2}{4t}\xi\sqrt{\frac{m}{D}}} \right. \\ & \left. \left(-\sin\left(\frac{x^2+y^2}{4t}\sqrt{\frac{m}{D}(1-\xi^2)}\right) \left(\frac{2x^2}{4t^2} \frac{m}{D} (1-\xi^2) \right) \right) \right) \end{aligned} \quad (5.23)$$

As the same assumption,

$$\frac{\partial^3 \dot{u}_z}{\partial x^3} \approx \frac{1}{2tm} \sqrt{\frac{2\pi n}{D(1-\xi^2)}} \left(e^{-\frac{x^2+y^2}{4t} \xi \sqrt{\frac{m}{D}}} \right) \quad (5.24)$$

$$\left(-\cos\left(\frac{x^2+y^2}{4t} \sqrt{\frac{m}{D}(1-\xi^2)}\right) \frac{2x}{4t} \sqrt{\frac{m}{D}(1-\xi^2)} \left(\frac{2x^2}{4t^2} \frac{m}{D}(1-\xi^2)\right) \right)$$

From the Equations (5.19), (5.23) and (5.20) (5.24) we can obtain:

$$\frac{\partial^2 \dot{u}_z}{\partial x^2} \approx -\dot{\varepsilon} \left(\frac{2x^2}{4t^2} \frac{m}{D} (1-\xi^2) \right) \quad (5.25)$$

$$\frac{\partial^3 \dot{u}_z}{\partial x^3} \approx -\frac{\partial \dot{u}_z}{\partial x} \left(\frac{2x^2}{4t^2} \frac{m}{D} (1-\xi^2) \right) \quad (5.26)$$

Thus, The Poynting vector can be express by:

$$P_x = \left(\frac{\partial^3 u_z}{\partial x^3} \frac{\partial^2 \dot{u}_z}{\partial x^2} - \frac{\partial^2 u_z}{\partial x^2} \frac{\partial^3 \dot{u}_z}{\partial x^3} \right) \cdot (-1) \cdot \left(\frac{2x^2}{4t^2} \frac{m}{D} (1-\xi^2) \right) \quad (5.27)$$

On the other hand, two piezoelectirc sensors and the surface S , $abcd$, between them are considered as shown in Figure 5.9. Sensor centre is put on $a-b$ and $c-d$ in parallel.

The voltages of these sensors are given as:

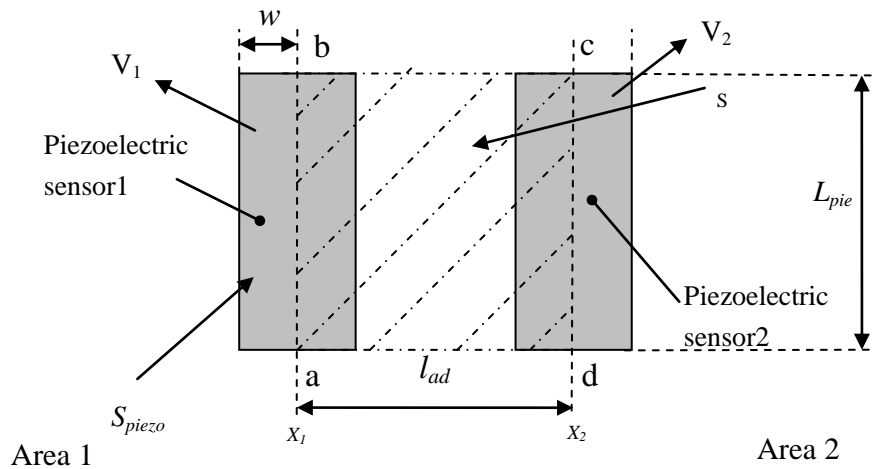


Figure 5. 9: Integrated surface with 2 piezoelectric sensors

$$V_1 = \alpha \int_{x_1-w}^{x_1+w} \frac{\partial^2 u_z}{\partial x^2} L_{pie} dx \quad (5.28)$$

$$V_2 = \alpha \int_{x_2-w}^{x_2+w} \frac{\partial^2 u_z}{\partial x^2} L_{pie} dx$$

with $\alpha = \frac{l_{pie} e_{31} h_{pla}}{2 \mathcal{E}_{33}^s S_{pie}} \left(\frac{1-2\nu}{1-\nu} \right)$ L_{pie} , l_{pie} , S_{pie} , e_{31} , h_{pla} , \mathcal{E}_{33}^s are defined as the piezoelectric sensor length, the piezoelectric sensor thickness, piezoelectric sensor surface, voltage coefficient, plate thickness and permittivity respectively.

If the half width of sensor w and the distance between two sensors l_{ad} are small enough compared to wavelength of bending wave, the two piezoelectric sensor voltages turn to:

$$V_1 \approx \alpha \frac{\partial^2 u_z}{\partial x^2} S_{pie} \Big|_{x=x_1} \quad (5.29)$$

$$V_2 \approx \alpha \frac{\partial^2 u_z}{\partial x^2} S_{pie} \Big|_{x=x_2}$$

Hence,

$$\begin{aligned} V_2 - V_1 &= \alpha S_{pie} \left(\frac{\partial^2 u_z}{\partial r^2} \Big|_{x=x_2} - \frac{\partial^2 u_z}{\partial r^2} \Big|_{x=x_1} \right) \\ &\approx \alpha S_{pie} l_{ad} \frac{\partial^3 u_z}{\partial x^3} \end{aligned} \quad (5.30)$$

The spatial integral of the time derivative of the displacement as a function of the voltage can be expressed as:

$$\begin{aligned} \int_{r_1}^{r_2} \frac{\partial^2 \dot{u}_z}{\partial r^2} dr &\approx \frac{1}{\alpha L_{pie}} (\dot{V}_1 + \dot{V}_2) \frac{1}{2} \\ &= \frac{1}{\alpha S} (\dot{V}_1 + \dot{V}_2) \frac{l_{ad}}{2} \end{aligned} \quad (5.31)$$

From the Equation (5.27), (5.30) and (5.31), the Poynting vector P_x can be express by:

$$\begin{aligned}
 P_x &= ((V_2 - V_1)(\dot{V}_1 + \dot{V}_2) - (V_2 + V_1)(\dot{V}_2 - \dot{V}_1))(-1) \frac{\left(\frac{2x^2}{4t^2} \frac{m}{D}(1 - \xi^2)\right)}{2S \cdot S_{pie} \cdot \alpha^2} \\
 &= ((V_1 - V_2)(\dot{V}_1 + \dot{V}_2) - (V_2 + V_1)(\dot{V}_1 - \dot{V}_2)) \frac{\left(\frac{2x^2}{4t^2} \frac{m}{D}(1 - \xi^2)\right)}{2S \cdot S_{pie} \cdot \alpha^2}
 \end{aligned} \tag{5.32}$$

Integrating the Equation (5.32) in the time domain, the energy flow is given:

$$\begin{aligned}
 \int_0^t P_x dt &= \int_0^t ((V_1 - V_2)(\dot{V}_1 + \dot{V}_2) - \\
 &\quad (V_2 + V_1)(\dot{V}_1 - \dot{V}_2)) \frac{\left(\frac{2x^2}{4t^2} \frac{m}{D}(1 - \xi^2)\right)}{2S \cdot S_{pie} \cdot \alpha^2} dt
 \end{aligned} \tag{5.33}$$

Because the term $\frac{2x^2}{4t^2} \frac{m}{D}(1 - \xi^2)$ is a positive value, hence, the signs of P_x do not

depend of this term. Based on the above results, we can simplify the energy flow as:

$$Q \approx \int_0^t ((V_1 - V_2)(\dot{V}_1 + \dot{V}_2) - (V_2 + V_1)(\dot{V}_1 - \dot{V}_2)) dt \tag{5.34}$$

When an impact is applied the area 1 (in Figure 5.9), the Q value is positive (resp. negative).

When 4 piezoelectric sensors is used as shown in Figure 5.10, using Equation (5.34), the impact location can be obtained in area 1, 2 or 3.

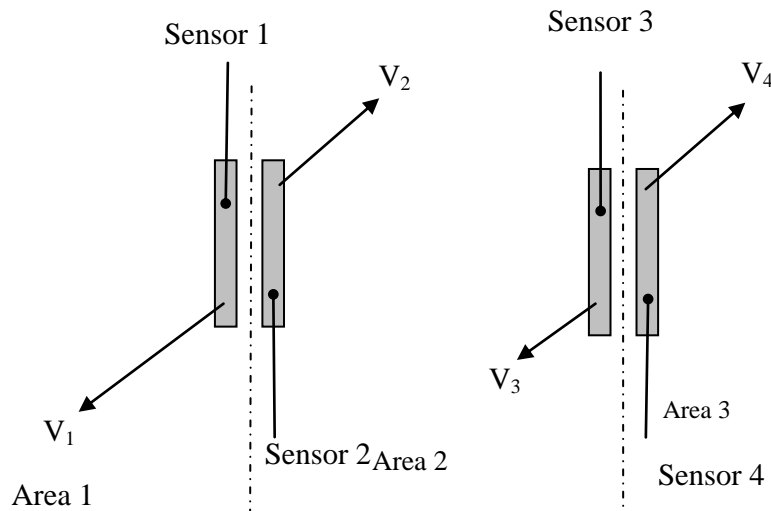


Figure 5.10: Integrated surface with 4 piezoelectric sensor-1

Chapter 5 Force detection using energy flow estimator with piezoelectric sensors

Because of the symmetry of the system, it is possible to connect sensor 2 with 3 and 1 with 4 shown in to reduce computational requirements.

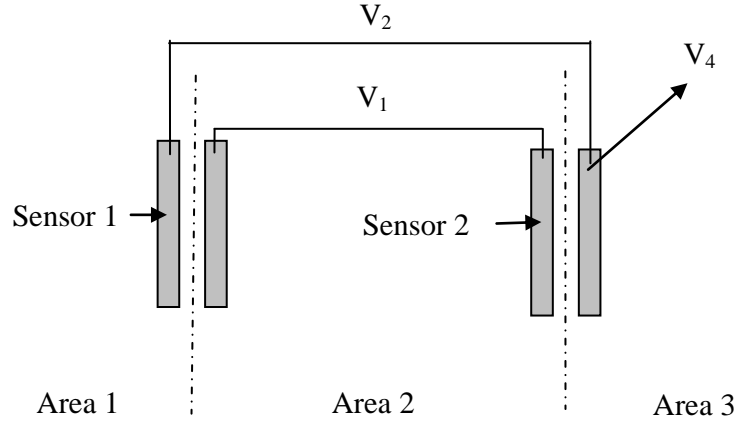


Figure 5.11: Integrated surface with 4 piezoelectric sensor-2

When an impact is applied in the area 2, the Q value is positive. Otherwise, for the case of an impact applied in area 1 or 3, the Q value is negative.

When eight sensors are connected shown in Figure 5.12, the impact location can be known in area 1 or not with the energy flow value Q_x and Q_y :

$$Q_x = \int_0^t ((V_1 - V_2)(\dot{V}_1 + \dot{V}_2) - (V_2 + V_1)(\dot{V}_1 - \dot{V}_2))dt \quad (5.35)$$

$$Q_y = \int_0^t ((V_3 - V_4)(\dot{V}_3 + \dot{V}_4) - (V_3 + V_4)(\dot{V}_3 - \dot{V}_4))dt \quad (5.36)$$

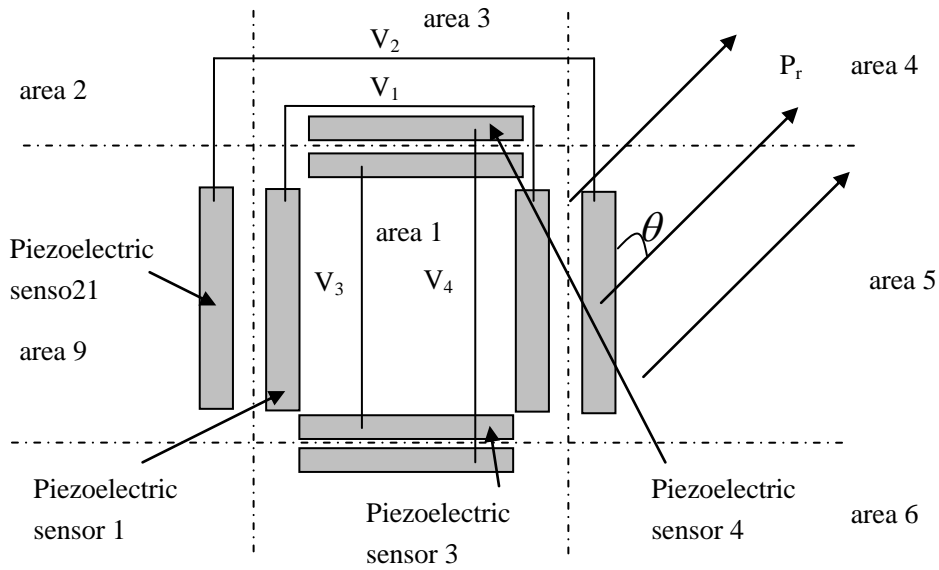


Figure 5.12: Integrated surface with 8 piezoelectric sensors-1

However, this necessitates four sensors output. In order to reduce computational requirements, P_x and P_y are considered together and independent from each other because of the far field assumption. In the other word, Q_1 and Q_2 depend on the V_1 , V_2 and V_3 , V_4 respectively.

Thus, we can simplify the energy flow as shown in Figure 5.13.

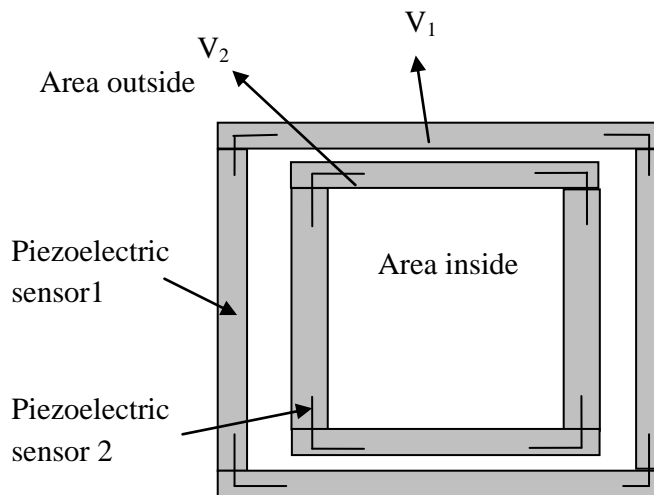


Figure 5.13: Integrated surface with 8 piezoelectric sensors-2

It is therefore possible to know the impact location whether inside or outside with the sign of Q simply from two piezoelectric sensors output. When the impact is applied

inside (resp. outside) of the structure (Figure 5.13), Q is positive (resp. negative). The absolute value of Q increases with the force magnitude (and same impact location if the impact is outside), because more energy flows through the sensors. When applying a force outside, the absolute value of Q also decreases with the distance of impact location for the same magnitude impact, since less energy flows to the sensors.

5.6 Numerical simulation and experimental results based on piezoelectric sensors outputs

5.6.1 Numerical simulation

The simulation parameters are those used in the previous simulations (Table 5. 1) except for the piezoelectric sensor bonded in the integral surface seen Figure 5.14. The other parameters are shown in Table 5.2.

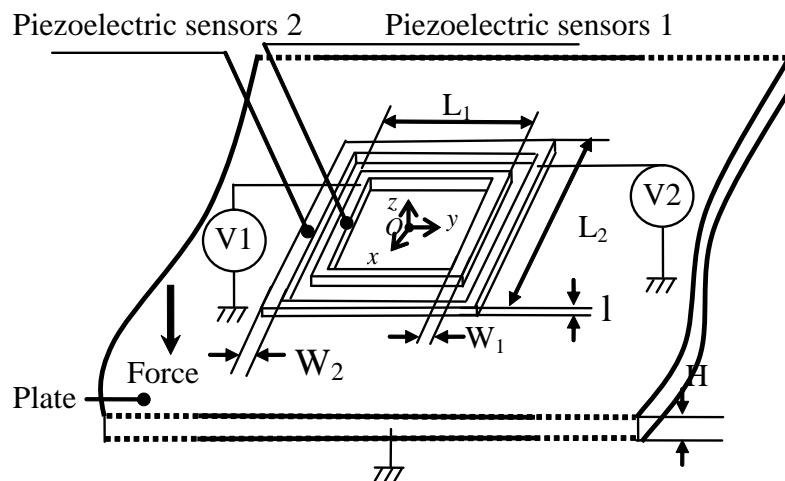


Figure 5.14: Schematics of the considered structure-infinite plate with surface-bonded piezoelectric element

Chapter 5 Force detection using energy flow estimator with piezoelectric sensors

Table 5.2: Matlab simulation parameters of the piezoelectric element

Parameter	Value	Parameter	Value
Plate surface density m	$6.4Kg/m^2$	Integral surface length $L2$	$0.14m$
Plate elastic modules E	$1.95 \cdot 10^{11} Pa$	Integral surface width $W2$	$0.003m$
Plate thickness h	$8 \cdot 10^{-4} m$	Integral surface length $L1$	$0.138m$
Poisson ratio ν	0.33	Integral surface width $W1$	$0.003m$
Damping ratio ξ_n	0.1	Relative permittivity $\epsilon_{33}^s / \epsilon_0$	1142
Voltage coefficient e_{31}	$-4.3C.m^{-1}$		

5.6.2 Experimental set-up

The experimental set-up consists of a steel thin plate with surface-bonded piezoelectric device, it is suspended at its four corners by elastic fasteners. Experimental parameters are the same in the Table 5. 1 and Table 5.2. The plate dimension is $0.8 \times 1.2m$. The squared piezoelectric sensor of size is made of 16 elements. They are connected separately, the one of inside and the one of outside.

The impact force was exerted at the target by an instrumented hammer (Dytran company, 5850B, minimum force 50 lbs, maximum force 8000 lbs, three impact tips) which contained a force transducer to measure the impact force directly. The Integrated Circuit Piezoelectric (ICP) Conditioning Module M32 provided the necessary power supply for the electronic circuit of the sensor. The hammer had a flat head of 6mm in diameter and the impact force exerted by this hammer was approximated as a point load. It is important to note that all received signals were not processed by any filters, nor were the environmental noises handled with special care. Based these reasons, the approach can easily use as self-power system.

5.6.3 Result & Discussion

A simple impact force as shown in Figure 5.15 is applied to the plates. Because the impact is given by hammer, the impact amplitude and the instantaneous frequency are

Chapter 5 Force detection using energy flow estimator with piezoelectric sensors

not the exactly same every times, thus, it is not care about the amplitude.

The approximation results based on the simulation and experimental data are given in Figure 5.16 and Figure 5.19. In both of these figures, two locations of impact force in side and outside are given. The inside force location is at (0, 0). The outside force location is at (0.2, 0.2).

These figures show good agreements between previous theory and approximation based on simulation and experiment data from piezoelectric sensors.

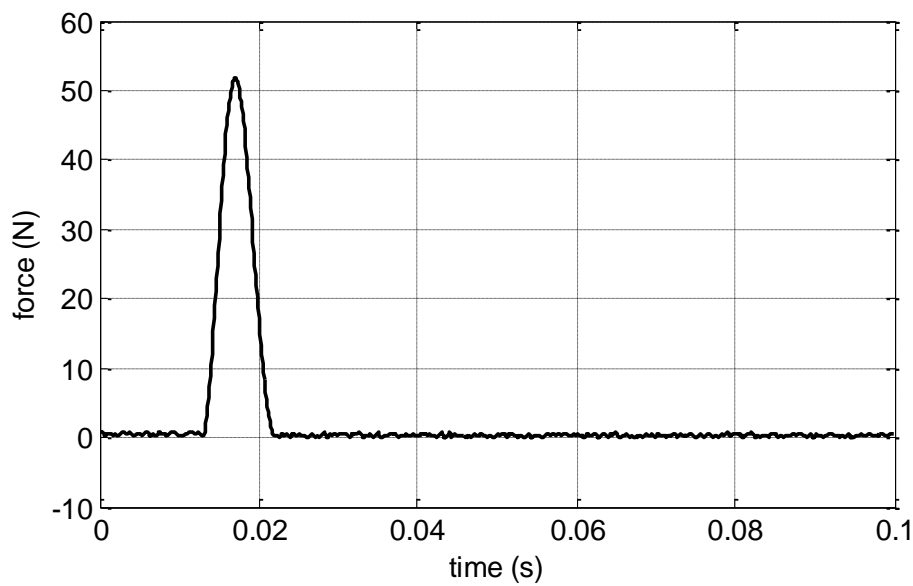


Figure 5.15: Impact force to the structure (with piezoelectric sensor)

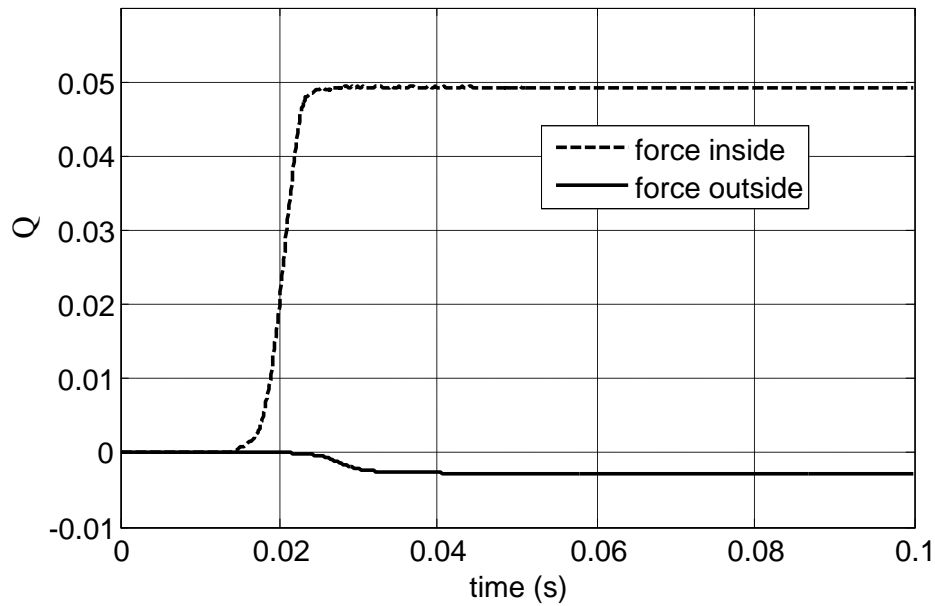


Figure 5.16: approximation energy response to a pulse force (simulation)

The max peak of Poynting vector increases with the force amplitude, because the more energy flows through the sensors and the energy depends on the squared force magnitude. The simulation results as shown in Figure 5.17 correspond to the theory very well. It is interesting because it mean that we can quantity the energy of the impact.

The pointing vector decreases with increase of damping factor, because the less energy flows through the sensors. The simulation results verify well that the overall magnitudes of Poynting vector would be decreased if the magnitude of the damping ratio increases.

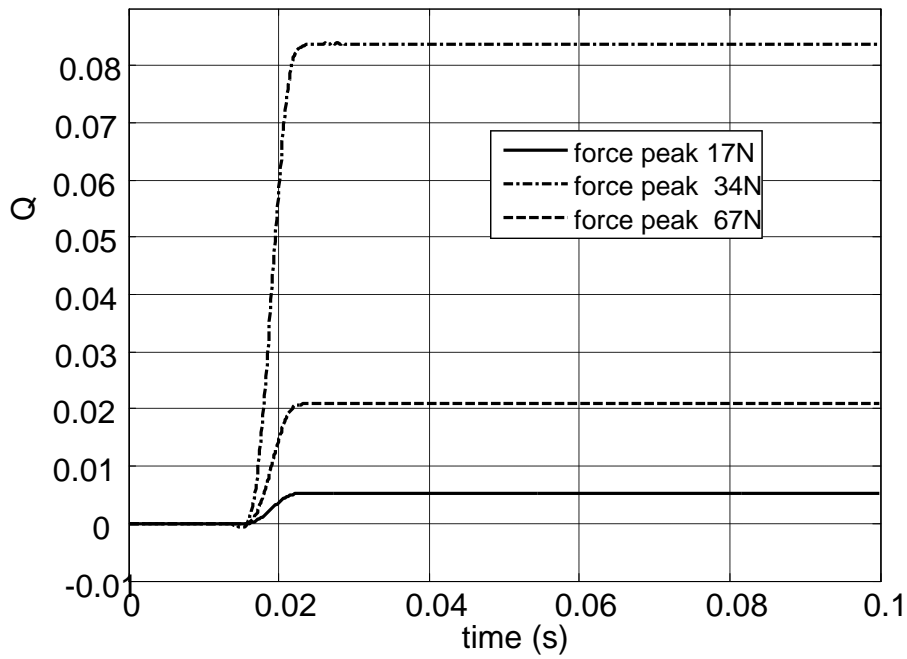


Figure 5.17: approximation energy response to different peak pulse force

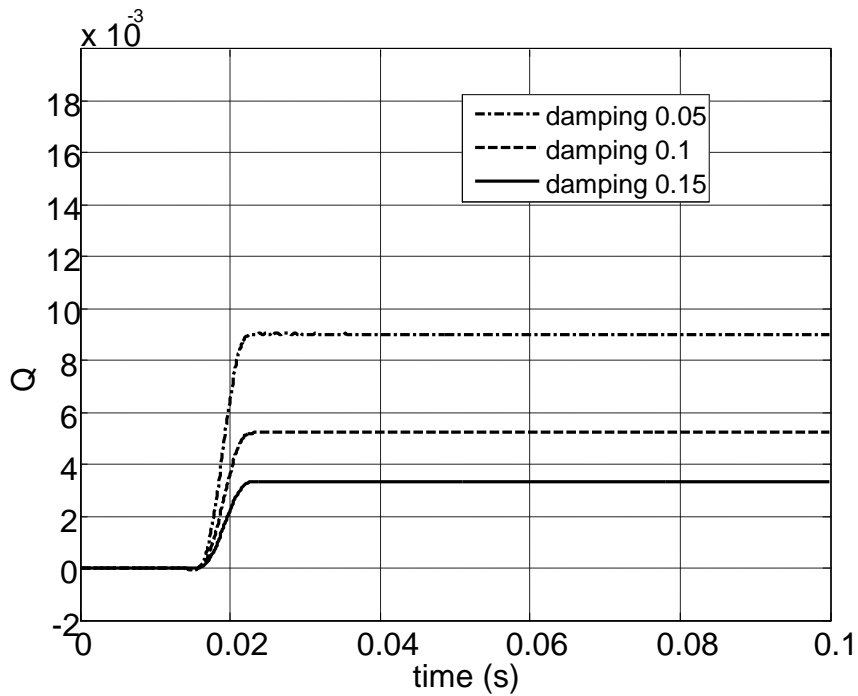


Figure 5.18: approximation energy for various damping coefficient
-force location at the origin (0,0)

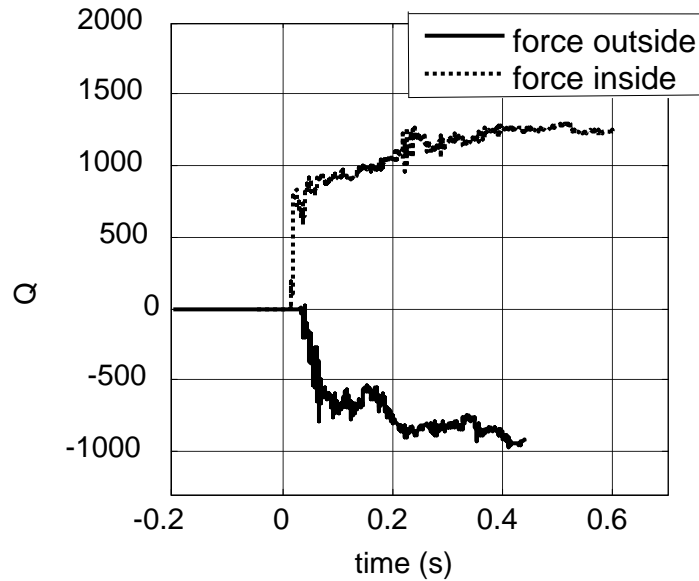


Figure 5.19: approximation energy response to a pulse force-1 (experimental, steel tip of hammer)

First, the steel tip was used. Coordinate origin is placed at the centre of the surface. The results are given in Figure 5.19 and Figure 5.20. These results demonstrate that the positive (resp. negative) value of Poynting vector corresponds to an impact applied inside surface of sensor (resp outside). The steel tip generates an impact that leads to short time duration. Its spectrum is broad band and consequently lamb waves modes higher than the bending mode one generated: That might explain the oscillating behaviour of the curves.

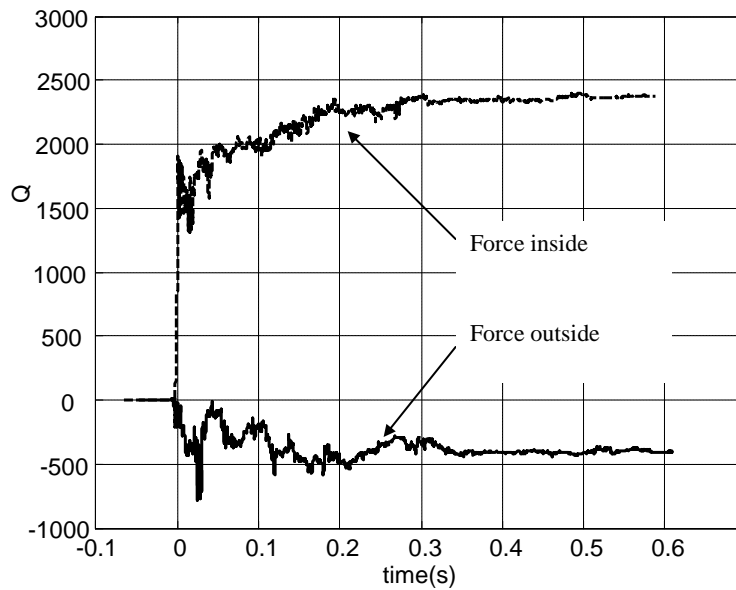


Figure 5.20: energy response to a pulse force -2 (experimental, steel tip of hammer)

When the pseudo-frequency of impact is decrease, if there are bending wave in the plate, the approach can detect the force location area inside the sensor or not. Based on above ideal, the plastic tip is used to give low frequency impact because is not as stiff as the steel tip. Figure 5.21-Figure 5.23 show the results. These results clearly demonstrate that the impact location area can be efficiently detected from the value of the proposed criterion.

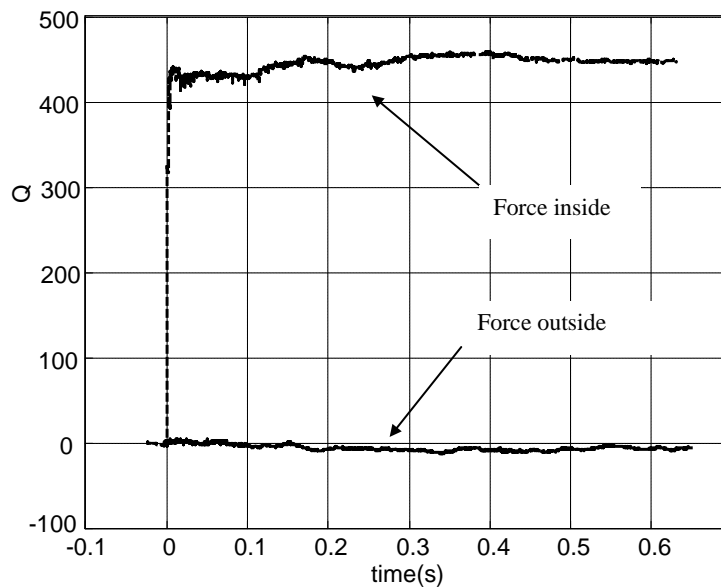


Figure 5.21: energy response to a pulse force -1 (experimental, plastic tip of hammer)

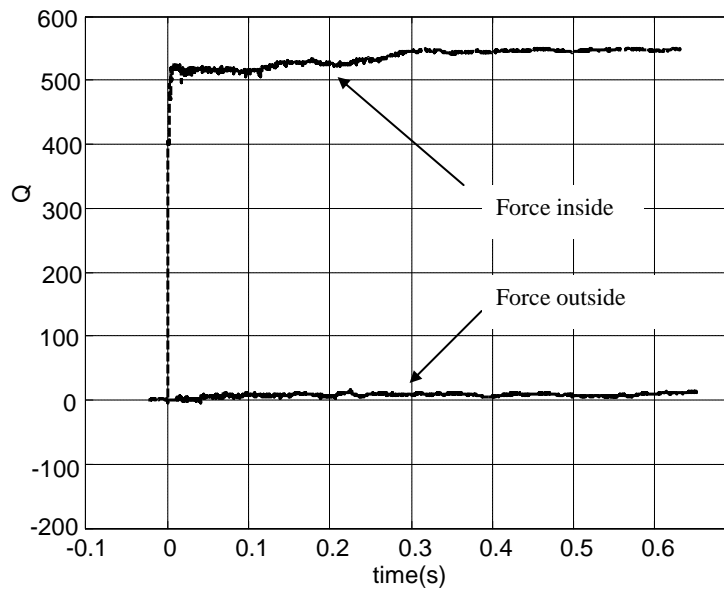


Figure 5.22: energy response to a pulse force -2 (experimental, plastic tip of hammer)

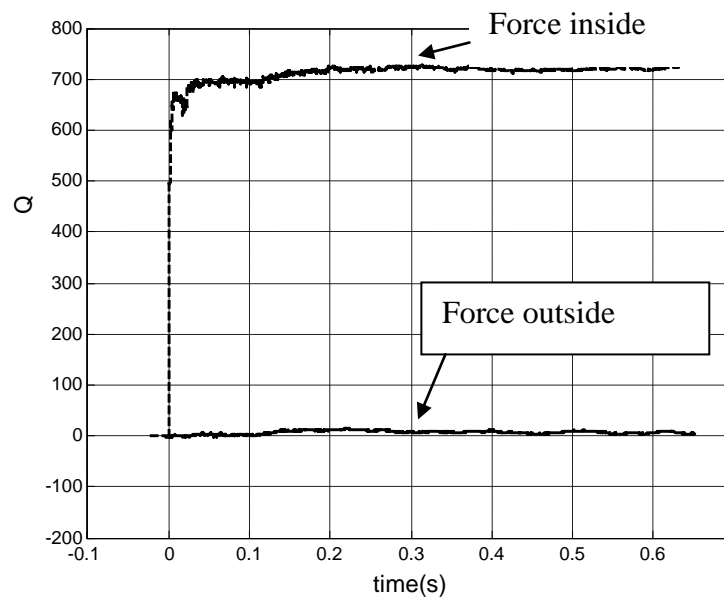


Figure 5.23: energy response to a pulse force -3 (experimental, plastic tip of hammer)

It should be note that this technique can estimate the time history of input energy. The several forces are applied to the inside of structural at different time, which means several mechanical energies are input to the system. The schema of Poynting vector will show several levels as shown in Figure 5. 24. For example, in Figure 5. 24 b, when

Chapter 5 Force detection using energy flow estimator with piezoelectric sensors

time is close to 0, 0.18, and 0.36 second, there are the force input to the inside of the structure. The value of Poynting vector is increase quickly.

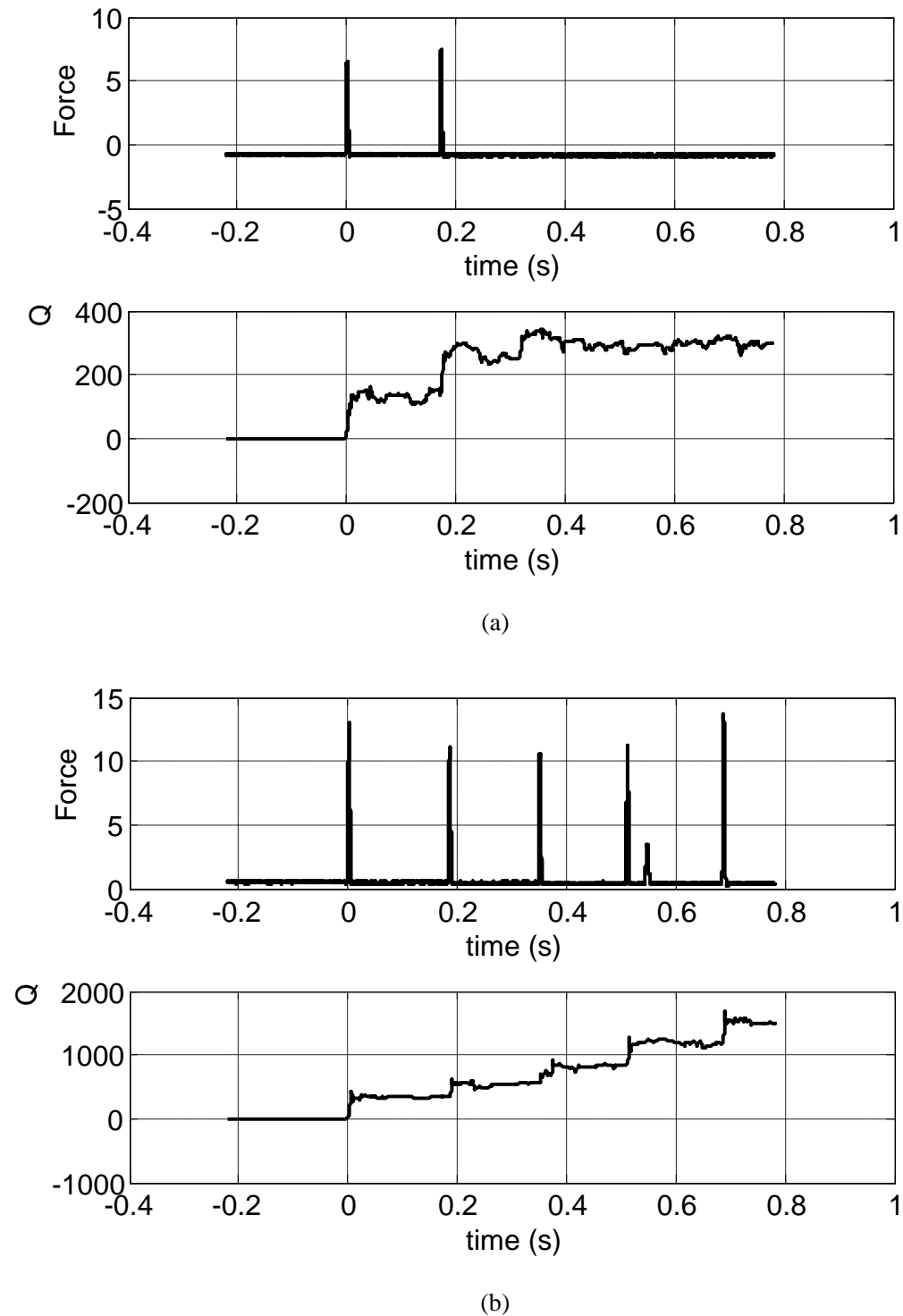
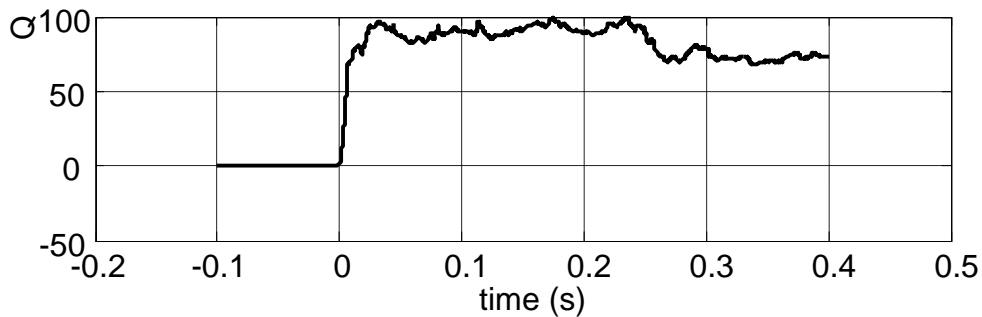
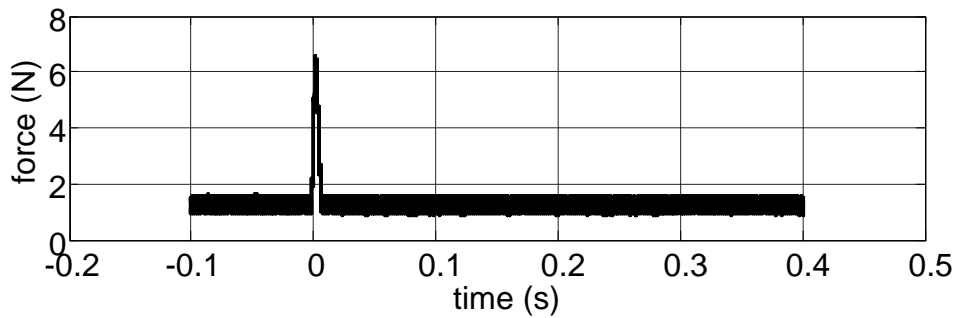


Figure 5. 24 energy response to different pulse force

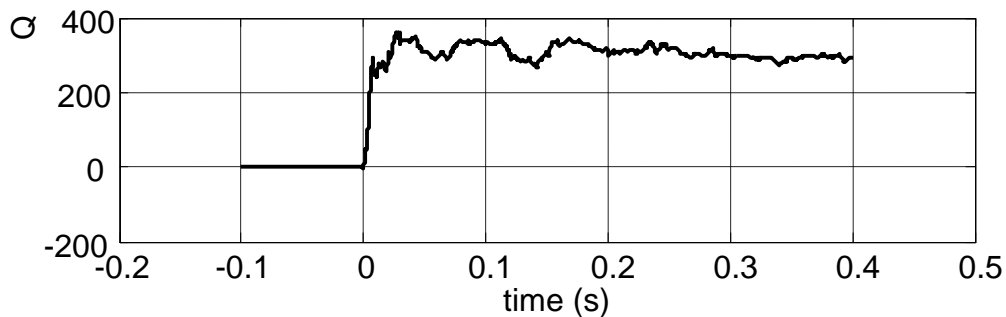
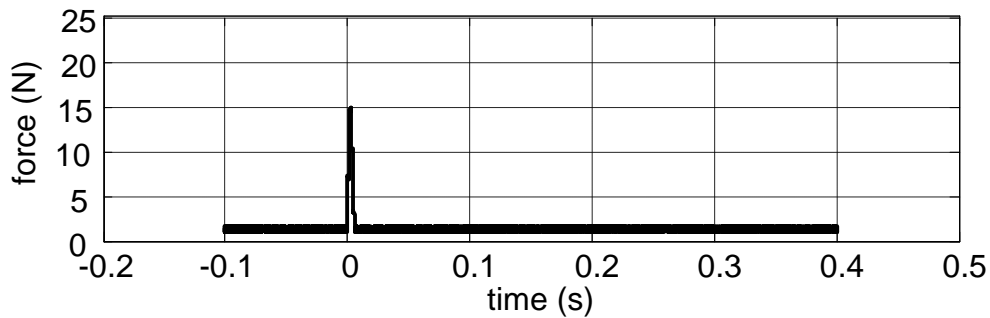
As the same reason we discuss before, this approach can estimate the force amplitude. The Poynting vector depends on the squared force magnitude, when the input force

Chapter 5 Force detection using energy flow estimator with piezoelectric sensors

increases two times, the Poynting vector increases four times. As it is shown in Figure 5.25 (a) and (b), when the force amplitude increases close to two times (from 7N to 15N), the max peak of Poynting vector increases four times (from 90 to 350). The same result can be obtained from Figure 5.25 (b) and (c).



(a)



(b)

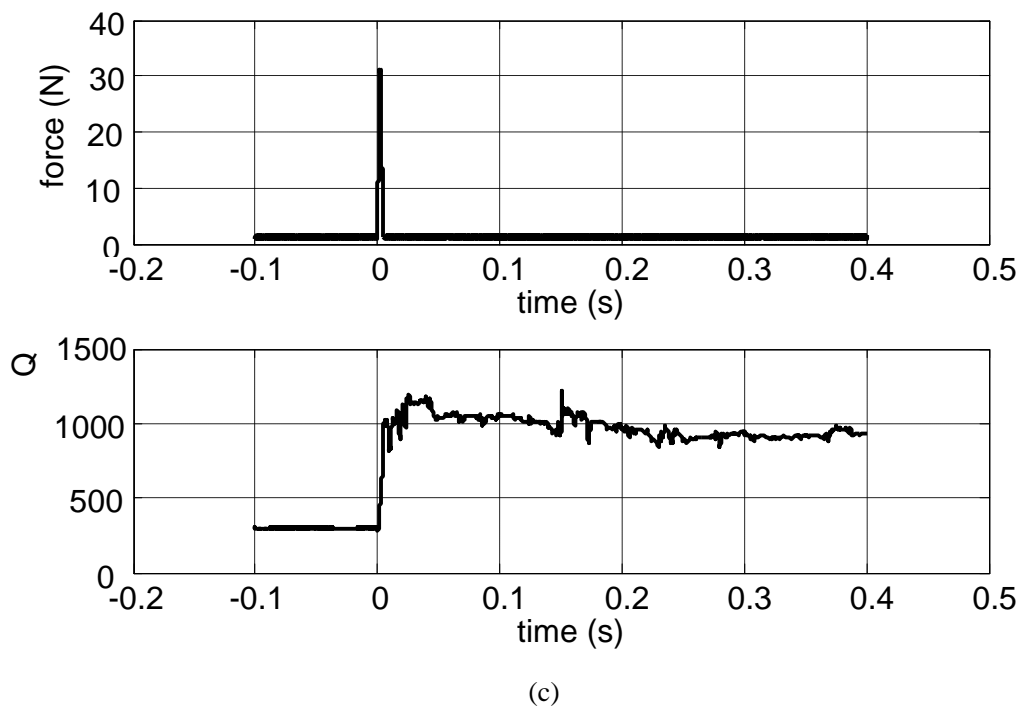


Figure 5.25 energy response to different amplitude pulse force (force inside of frame)

5.7 Conclusion & Further Work

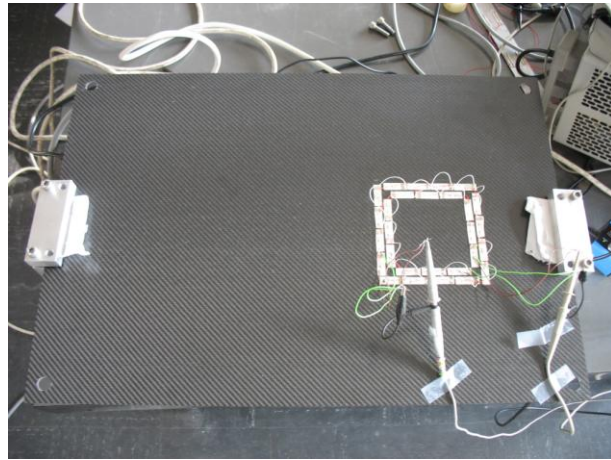
A simple, fast and efficient technique for identifying the impact location and force amplitude using Poynting vector is proposed and an approximation way to calculate the Poynting vector is given in this research. The present work demonstrates that it is quite easy to estimate whereas the impact location is inside or outside the chosen contour. When the value of the energy flow Q is positive, the impact location is inside of the contour, and the opposite. In the future, the model of piezoelectric sensors will be empirical in theory, or maybe find another better approach.

Future work may be considering anisotropic materials.

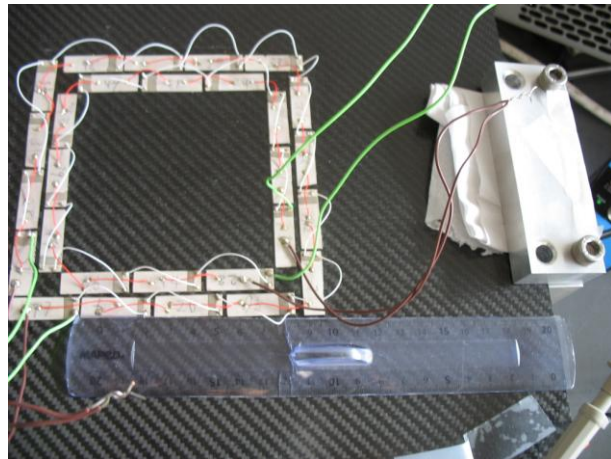
5.8 Anisotropic plate

Using the approach (5.35) and (5.36), we also do some investigation in anisotropic plate. We have good experiment result, and the theory approach is developing.

A composite plate (fabric 0 / 90, rate of fibre 60%, Density: 1600 kg/m³) is considered in current research as shown in Figure 5.26.



(a)



(b)

Figure 5.26 experiment set-up for composite plate-1

The plastic tip is used in this experiment. The result is shown in Figure 5.27. This result demonstrates that the positive (resp. negative) value of approximation vector corresponds to an impact applied inside frame. This result also show that the impact location area can be efficient detected from the value of the proposed criterion.

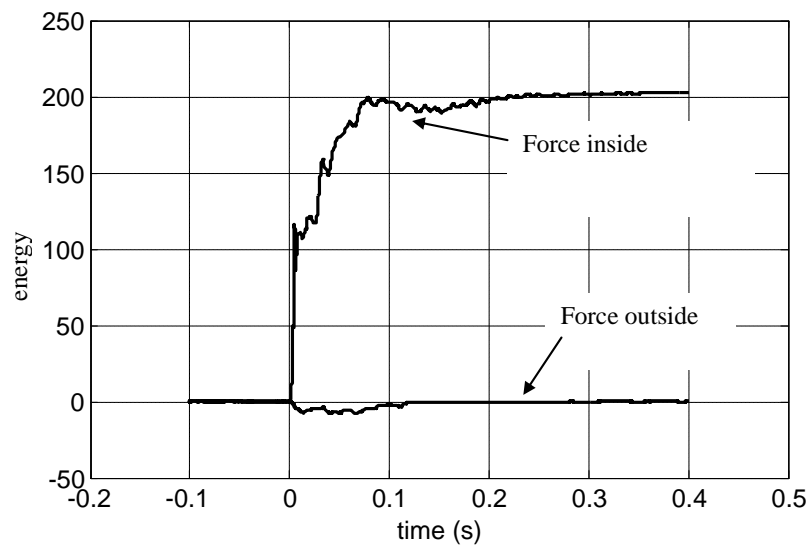


Figure 5.27 energy response to a pulse force -1 (composite plate)

We also change the boundary limit in Figure 5.28. The result is shown in Figure 5. 29. This result show proposed model gives a interesting tool for estimating location and magnitude impact.

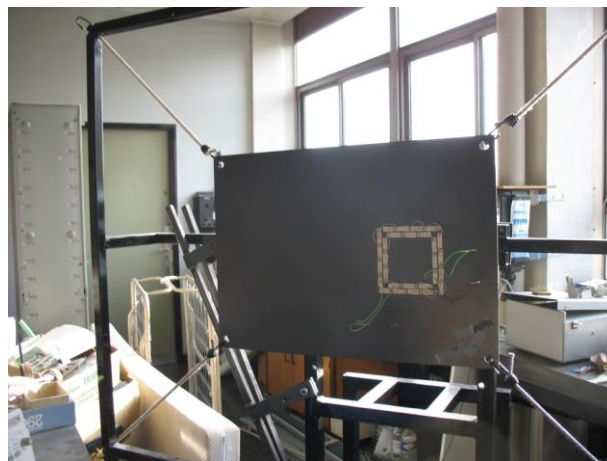


Figure 5.28 experiment set-up for composite plate-2

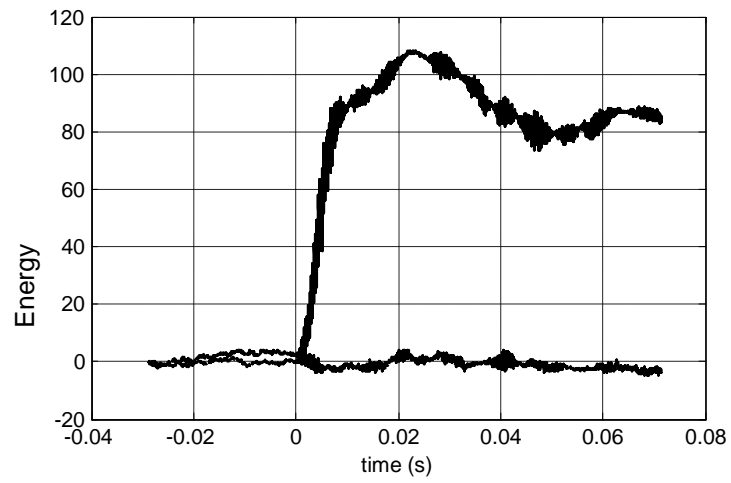


Figure 5. 29 energy response to a pulse force -2(composite plate)

6 Conclusions

The objective of this work was to develop a technique to detect the location of an impact on a structure (plate) and quantify the shock energy. The identification should be simple enough to lead to a self power wireless system. This construct restricts the data processing to basic mathematical operations.

We selected piezoelectric elements to detect the shock history. To get these requirements, we followed several routes that are presented in chapters 2, 4, and 5. The basic idea of the research was to extract energy, by means of a resistance in parallel with the piezo elements, bonded on a beam (1D) and aligned with a constant spacing. A straight comparison between piezoelements' response leads to the impact location on the beam. This process can be self-powered quite easily (Energy can be harvested on the beam or the plate shunt).

In chapter 3, we develop a modelling of the mechanical impulse response between a force applied at some location in an infinite plate and the displacement (or the displacement speed) at a different location. We consider the bending mode and ignore all the other bands' modes. This modelling, based on a 2D Fourier transform of the bending equation, leads to a closed form expression of the displacement speed. The modelling allows getting the displacement response to any arbitrary signals and overcomes the problem encountered with the finite element approach. Once the impulse response is known, the voltage on an element bonded to the plate can be easily calculated. It must be stressed that we consider the piezoelement as a pure one that we neglect the coupling between the piezoelement and the plate structure.

The method presented in chapter 4 is based on the variation of the global wave energy measured at successive points. Clearly, the energy variation is directly related to the wave losses deriving from propagation. Using a set of piezoelements measuring the voltage difference, the wave propagation direction can be estimated. Four sets of these piezoelements can be used to form a square frame thus generating the wave

Chapter 6 Conclusions

direction detect in 2D. Based on this simple concept, we can derive an approximate relating the power flow (Poynting vector) to the voltage on the piezoelements. These approximate takes a positive value when the impact occurs inside the piezo frame and negative when the impact is located outside the piezo frame, thus providing an easy way to locate the impact location. Clearly the impact location resolution is of the order of the frame dimension but the processing is very simple and demands small energy requirement since only basic operation involved.

In chapter 5, we introduced a technique based on the power flow for the impact location and energy quantification. We first derived an expression of the Poynting vector from the equation supporting bending wave propagation. Then approach leads to a theoretical energy equation and clearly shows that the power flow is different from zero if the impact occurs inside the frame and zero if it occurs outside. A parallel with the Gauss theorem applied to location of an electrical charge can be made.

From the above mentioned approach, we can derive a new estimation that relates the power to the piezo voltage of the elements constituting the frame. It leads to experimental results that confirm the detection scheme. In this case also, the power requirements to drive the system are low. The approach developed for isotropic plate was used on anisotropic plate (composite). The experimental results show that detection is also quite straightforward in this case.

To conclude, we would say that we developed a set of method to estimate the impact location and quantification on a plate structure. The three proposed approaches show the feasibility of the impact location with detection schemes that requires a small amount of energy to be self-powered and wireless. Extension of this work will concern a more precise quantification estimation. So far we worked with plate structure. It would be very interesting to develop an approach for 3D structure or plate with variable thickness.

Lists of figure

Figure 1.1. Beam acceleration response under impulse force..... 14

Figure 1.2 sensor network for the detection of the energy flow direction in a 1D structure...18

Figure 1.3: principle of the energy flux expressed by Poynting vector in an infinite structure
 (a) without consideration of losses. Sum of energy flux trough the surface (S) is null for an outside impact (O-point) and not null for an inside impact (I-point). For a finite structure (b), reflection on the boundaries induce secondary sources (s1..si) with a null associated energy flow. 19

Figure 1.4. Piezoelectric element used as bending sensor.....21

Figure 1.5. primary forms of piezoelectric material.....22

Figure 1.6: Massive ceramic: industrial standard materials.23

Figure 1.7. piezoelectric fibers (a) and an example of integration (b)24

Figure 2.1: The studied structure. The PZT elements are uniformly bound on the beam with a Δx – step. E_{in} is the stored energy in the beam due to the impact at the point A. E_{pi} is the energy extracted by the i -element and dissipated in the resistor. E_b is the mechanical energy in the beam.27

Figure 2. 2: Spring-Mass representation of an infinite beam.28

Figure 2.3 Energy flow in the beam, differentiating the energy over sensor 1 to 2 is negative ($\Delta E_{p12} < 0$), sensor 2 to 3 is null ($\Delta E_{p23} = 0$), 3 to 4 and 4 to 5 is positive ($\Delta E_{p23} > \Delta E_{p34} > \Delta E_{p45}$).....31

Figure 2.4 Normalized evolutions of the extracted energy (dotted) and the proposed criterion (plain)—force location at $x_0=7.5$31

Figure 2.5: The simulated model. Dimensions are in mm33

Figure 2.6: Meshing of the structure (Zoomed area).....33

Figure 2.7: Example of a sensor (PZT2) response for an impact in part 0..... 34

Figure 2.8: simulation results: 1-2 means ΔE_{p12} (the differentiating energy over sensor 1 and 2 (Figure 2.5)). As the same, 2-3, 3-4, 4-5 mean ($\Delta E_{p23}, \Delta E_{p34}, \Delta E_{p45}$).....40

Figure 2.9 Experimental set-up41

Figure 2.10: Experimental (plain) and results for the proposed criterion using a- 530KHz piezoelectric moveable source.43

Figure 3.1: Schematics of the considered infinite plate45

Figure 3.2: Impulse response at the point (0.2, 0.2).....49

Figure 3.3: Impulse response at the point (0.4, 0.4).....50

Figure 3.4: Schematics of the considered structure with surface-bonded piezoelectric element

List of figure

.....	51
Figure 3.5: Voltage response to a pulse force excitation at different location.....	54
Figure 3.6: Simulated sensor voltage for a half period-burst impact (a), 1 period-burst impact (b) and 2 periods-burst impact (c). The impact location coordinates are (0, 0).	55
Figure 3.7: Meshed plate and piezoelectric element-I point is the inside point impact and O point is the output point impact.....	57
Figure 3. 8: Deformation of the plate obtained with the FEM for an outside impact at different time ($t = 0.228\text{ms}$ (a); 1.2ms (b); 2.15ms (c) and 5ms (d)).....	58
Figure 3.9: Comparison between FEM and analytical model for a burst force inside the piezo frame	58
Figure 3.10: Comparison between FEM and analytical model for a burst force outside the piezo frame.....	59
Figure 3.11: the experimental set-up. Plate dimension is $1200 \times 800 \times 0.1 \text{ mm}^3$	60
Figure 3.12: Experimental results and analytical and FEM prediction for a force applied at location (0, 0)	61
Figure 4.1. (a) detection of energy flow direction for 1D propagation;	65
Figure 4.2: Integrated surface-1	68
Figure 4.3: Integrated surface for an incident angle $\theta = 0$	69
Figure 4.4: Integrated surface with 2 piezoelectric sensors.	70
Figure 4.5: Integrated surface with 4 piezoelectric sensors-four outputs.....	73
Figure 4.6: Integrated surface with 4 piezoelectric sensors-two output.....	74
Figure 4.7: Integrated surface with eight piezoelectric sensors-four outputs.....	75
Figure 4.8: Integrated surface with 8 piezoelectric sensors-2	76
Figure 4.9: Schematics of the considered structure-infinite plate	77
Figure 4.10: Impact force applied to the considered-infinite plate	78
Figure 4.11: q value response to an impact excitation	79
Figure 4.12: q value response to a pulse force excitation	79
Figure 4.13: q value response to a pulse force excitation	80
Figure 4.14: q value response to a pulse force excitation	80
Figure 4.15: q value response to a pulse force excitation	81
Figure 4.16: Schematics of different location inside.....	82
Figure 4.17: peak of q value response to different location inside from point o to a.....	82
Figure 4.18: peak of q value response to different location inside from point o to b.....	83
Figure 4.19: Experimental structure.....	84
Figure 4.20: Impact force to the considered structure-finite plate-1	84
Figure 4.21: q value response to the pulse force outside and inside-1	85
Figure 4.22: Impact force to the considered structure-finite plate-2.....	86
Figure 4.23: q value response to the pulse force - force outside	86
Figure 4.24: q value response to the pulse force - force outside.....	86
Figure 4.25: q value response to the pulse force - force outside	87
Figure 5. 1: principle of the energy flux expressed by Poynting vector in an infinite structure (a) without consideration of losses. Sum of energy flux trough the surface (S) is null for an outside impact (O -point) and not null for an inside impact (I -point). For a finite structure (b), reflexion phenomena induce secondary sources (s_j, s_i) which are the	

List of figure

associated null energy flux total.....	90
Figure 5.2: Schematics of the considered structure-infinite plate	94
Figure 5.3: Impact force to the considered structure-infinite plate	95
Figure 5.4: energy response to a pulse force excitation	95
Figure 5.5: energy response to a pulse force excitation	96
Figure 5. 6: Energy for various force locations outside	97
Figure 5. 7: Energy for various damping coefficient	97
Figure 5.8: Energy for various force curve peak-force locations	98
Figure 5. 9: Integrated surface with 2 piezoelectric sensors	100
Figure 5.10: Integrated surface with 4 piezoelectric sensor-1	102
Figure 5.11: Integrated surface with 4 piezoelectric sensor-2	103
Figure 5.12: Integrated surface with 8 piezoelectric sensors-1	104
Figure 5.13: Integrated surface with 8 piezoelectric sensors-2	104
Figure 5.14: Schematics of the considered structure-infinite plate with surface-bonded piezoelectric element.....	105
Figure 5.15: Impact force to the structure (with piezoelectric sensor).....	107
Figure 5.16: approximation energy response to a pulse force (simulation)	108
Figure 5.17: approximation energy response to different peak pulse force	109
Figure 5.18: approximation energy for various damping coefficient.....	109
Figure 5.19: approximation energy response to a pulse force-1 (experimental, steel tip of hammer)	110
Figure 5.20: energy response to a pulse force -2 (experimental, steel tip of hammer)	111
Figure 5.21: energy response to a pulse force -1 (experimental, plastic tip of hammer)	111
Figure 5.22: energy response to a pulse force -2 (experimental, plastic tip of hammer)	112
Figure 5.23: energy response to a pulse force -3 (experimental, plastic tip of hammer)	112
Figure 5. 24 energy response to different pulse force	113
Figure 5.25 energy response to different amplitude pulse force (force inside of frame)	115
Figure 5.26 experiment set-up for composite plate-1.....	116
Figure 5.27 energy response to a pulse force -1(composite plate).....	117
Figure 5.28 experiment set-up for composite plate-2.....	117
Figure 5. 29 energy response to a pulse force -2(composite plate).....	118

Lists of table

Table 2.1: Nomenclature of the lumped model	29
Table 2.2: FEM simulation parameters	33
Table 2.3: Experimental parameters	41
Table 3.1: Simulation parameters of the plate.....	52
Table 3. 2: Simulation parameters of the piezoelectric element.....	53
Table 3.3 Dimensions (in mm) of the FEM model.....	56
Table 4.1: Matlab simulation parameters	78
Table 5. 1: Matlab simulation parameters	94
Table 5.2: Matlab simulation parameters of the piezoelectric element	106

Reference

¹ Chang F-K and Markmiller F.C, A new look in design of intelligent structures with SHM, Proceedings of the third European workshop on structural health monitoring,2006, Pennsylvania, USA, 5-20.

² Victor Giurgiutiu, SPIE's, Lamb wave generation with piezoelectric wafer active sensors for structural health monitoring, 10th Annual international symposium of smart structures and material and 8th Annual international symposium on NDE for Health Monitoring and Diagnostics, 2-6 March 2002,San Diego, CA.paper# 5056-17

³ Tsal C.C, Hocheng H., Computerized tomography and C-Scan for measuring delamination in the drilling of composite materials using various drills, International Journal of Machine Tools & Manufacture, 45(2005), 1282-1287.

⁴ Claudia S.Baptista, Manuel Villagrasa, Antonio A.Marinho, Standardised B-scan and A-scan echographic evaluation of spontaneous anterior uveal melanomas in the dog, The veterinary Journal, 171(2006), 322-330.

⁵ Monnier T, Lame waves-based impact damage monitoring of a stiffened aircraft panel using piezoelectric transducers, Jouranl intelligent material systems and structures,17(5), 2006, 411-421.

⁶ Goodier JN, Jahsman WE, and Ripperger EA, An experimental surface-wave method for recording force-time curves in elastic impacts, ASME Journal of Applied Mechanics, 26, 3-7, 1959.

⁷ Doyle JF, An experimental method for determining the dynamic contact law, Experimental Mechanics, 24,10-16, 1984.

⁸ Chang C and Sun CT, Determining transverse impact force on a composite laminate

Reference

by signal deconvolution, *Experimental Mechanics* 29, 414-419, 1989.

⁹ Wu E, Tsai T-D, and Yen C-S, Two methods for determining impact-force history on elastic plates, *Experimental Mechanics*, 35,11-18, 1995.

¹⁰ Yen C-S and Wu E, On the inverse problem of rectangular plates subjected to elastic impact, Part II: Experimental verification and further applications, *ASME Journal of applied mechanics*, 62,699-705, 1995.

¹¹ Tanaka H and Ohkami Y, Estimation of impact force on a space vehicle based on an inverse analysis technique (in Japanese), *Trans. Jpn.Soc. Mech.Eng.,Ser C 63C*, 1172-1178, 1997.

¹² Fan Jiangling ,Zhang Zhiyi, Li Wanyou, Hua Hongxing, Multiple periodical impact force identification from single point response (in Chinese), *Journal of vibration engineering*, 17, 785-788, 2004.

¹³ Holzer AJ, A technique for obtaining compressive strength at high strain rates using short load cells, *International Journal of Mechanical Sciences*, 20, 553-560, 1978.

¹⁴ Doyle JF, Further developments in determining the dynamic contact law, *Experimental Mechanics*, 24, 68-72, 1984

¹⁵ Doyle JF, Determining the contact force during the transverse impact of plates, *Experimental Mechanics*, 27, 68-72, 1987

¹⁶ Doyle JF, Experimentally determining the contact force during the transverse impact of an orthotropic plate, *Journal of Sound and Vibration*, 118,441-448, 1987

Reference

- ¹⁷ Doyle JF, Force identification from dynamic responses of a biomaterial beam, *Experimental Mechanics*, 33, 64-69, 1993.
- ¹⁸ Marti MT and Doyle JF, Impact force identification from wave propagation responses, *Journal of Intelligent Material Systems and Structures*, 18, 65-77, 1996.
- ¹⁹ Rizzi SA and Doyle JF, Force identification for impact problems on a half plane, *Computational Techniques for Contact, Impact, Penetration, and Perforation of Solids*, ASME AMD-103,163-182, 1989.
- ²⁰ Inoue H, Watanabe R, Shibuya T, and Koizumi T, Measurement of impact force by the deconvolution method, *Trans JSNDI 2*, 63-73, 1989.
- ²¹ Inoue H, Shibuya T, Koizumi T, and Fukuchi J, Measurement of impact force applied to a plate by the deconvolution method. *Trans JSNDI 2*, 74-83, 1989.
- ²² Wilcox DJ, Numerical Laplace transformation and inversion, *International Journal of Electrical Engineering Education*, 15,247-265, 1978.
- ²³ Inoue H, Kamibayashi M, Kishimoto K, Shibuya T, and Koizumi T, Numerical Laplace transformation and inversion using fast Fourier transform, *JSME International journal. Series 1 Vol 35*, 319-324, 1992.
- ²⁴ Inoue H, Kishimoto K, Shibuya T, and Harada K, Regularization of numerical inversion of the Laplace transform for the inverse analysis of impact force, *JSME International journal. Series A*, 41, 473-480, 1998.
- ²⁵ Inoue H Kishimoto K, Shibuya T, and Koizumi T (1992), Estimation of impact load by inverse analysis (Optimal transfer function for inverse analysis), *JSME International journal. Series 1, 35*, 420-427, 1992.

Reference

- ²⁶ Kishimoto K, Inoue H, Shibuya T, and Koizumi T, An inverse analysis of impact load (Measurement of impact force of cantilever by applying the optimal transfer function), Computational Engineering (1st Pan-Pacific Conference Computer Engineering, Seoul, Korea), Elsevier, 309-314, 1993.
- ²⁷ Whiston GS, Remote impact analysis by use of propagated acceleration signals, I: Theoretical methods, Journal of Sound and Vibration, 97, 35-51, 1984.
- ²⁸ Jordan RW and Whiston GS, Remote impact analysis by use of propagated acceleration signals II: Comparison between theory and experiment, Journal of Sound and Vibration, 97, 53-63, 1984.
- ²⁹ Bateman VI, Carne TG, Gregory DL, Attaway, SW, and Yoshimura HR, Force reconstruction for impact tests, ASME Journal of Vibration and Acoustics, 113, 192-200, 1991.
- ³⁰ Kim JT and Lyon RH, Cepstral analysis as a tool for robust processing, deconvolution and detection of transients, Mechanical Systems and Signal Processing, 6, 1-15, 1992.
- ³¹ Lin SQ and Bapat CN, Extension of clearance and impact force estimation approaches to a beam-stop system, Journal of Sound and Vibration, 163, 423-428, 1993.
- ³² McCarthy DJ and Lyon RH, Recovery of impact signatures in machine structures, Mechanical Systems and Signal Processing, 9, 465-483, 1995.
- ³³ Inoue H, Watanabe R, Shibuya T, and Koizumi T, Measurement of impact force by the deconvolution method, *Trans JSNDI* 2, 63-73, 1989.

Reference

- ³⁴ Inoue H, Shibuya T, Koizumi T, and Fukuchi J, Measurement of impact force applied to a plate by the deconvolution method, *Trans JSNDI* 2, 74-83, 1989.
- ³⁵ Inoue H, Kishimoto K, Shibuya T, and Koizumi T, Estimation of impact force by an inverse analysis, *Inverse Problems in Engineering Mechanics (IUTAM) Symp, Tokyo, Japan*, Springer-Verlag, 169-178, 1993.
- ³⁶ Harrigan JJ, Reid SR, and Reddy TY, Accurate measurement of impact force pulses in deforming structural components, *Experimental Mechanics, Advances in Design, Testing and Analysis, (Proc 11th Int Conf Exp Mech, Oxford, UK)*. Balkema, 149-154, 1998.
- ³⁷ Bateman VI, Carne TG, and McCall DM, Force reconstruction for impact tests of an energy-absorbing nose, Conference 61 shock and vibration symposium. Pasadena, CA (USA), 16-18 Oct 1990.
- ³⁸ Chandrashekhara K, Chukwujekwu Okafor A, and Jiang YP, Estimation of contact force on composite plates using impact-induced strain and neural networks, *Composites. Part B* 29B. 363-370, 1998
- ³⁹ Jordan RW and Whiston GS, Remote impact analysis by use of propagated acceleration signals, II: Comparison between theory and experiment, *Journal of sound and vibration*, 97, 53-63, 1984.
- ⁴⁰ Whiston GS , Remote impact analysis by use of propagated acceleration signals, I: Theoretical methods, *Journal of sound vibration*, 97:35-51 1984.

Reference

- ⁴¹ Doyle JF, An experimental method for determining the location and time of initiation of an unknown dispersing pulse. *Experimental mechanics*, 27:229-233, 1987.
- ⁴² Choi K, Chang FK, Identification of foreign object impact in structures using distributed sensors. *Journal of Intelligent Material Systems and Structures*, 5:864-869, 1994.
- ⁴³ Doyle JF, A genetic algorithm for determining the location of structural impacts, *Experimental Mechanics*, 34:37-44, 1994.
- ⁴⁴ Martin MT and Doyle JF, A genetic algorithm for determining the location of structural impacts. *Exp. Mech.* 34, 37-44, 1996.
- ⁴⁵ Inoue H, Kishimoto K. and Shibuya T. Experimental wavelet analysis of flexural waves in beams, *Experimental Mechanics*, 36:212-217,1996.
- ⁴⁶ Kishimoto K, Inoue H, Hamada M, and Shibuya T, Time-frequency analysis of dispersive waves by means of wavelet transform. *ASME Journal of applied mechanics*, 62,841-8476, 1995.
- ⁴⁷ Inoue H, Kishimoto K, Shibuya T. Experimental wavelet analysis of flexural waves in beams. *Experimental mechanics*, 36:212-7, 1996.
- ⁴⁸ Guyomar D, Lallart M, Wang XJ, Monnier T, Petit L. Energy extraction-based force location estimation. In: Chang FK, editor. *Proceedings of the 6th International Workshop on Structural Health Monitoring*. Stanford (Stanford USA): Destech, p.1711-1718, 2007.
- ⁴⁹ Guyomar D, Lallart M, Monnier T, Wang XJ, Petit L. Passive impact location

Reference

estimation using piezoelectric sensors. *Structural Health Monitoring*, 8:357-367, 2009

⁵⁰ Yen CS, Wu E. On the inverse problem of rectangular plates subjected to elastic impact, Part I: method development and numerical verification. *Journal of Applied Mechanics*, 62:692-8, 1995.

⁵¹ Yen CS, Wu E. On the inverse problem of rectangular plates subjected to elastic impact, Part II: experimental verification and further application. *Journal of Applied Mechanics*, 62:699-705, 1995.

⁵² Ohkami Y and Tanaka H, Estimation of impact force and its location exerted on spacecraft, *JSME International journal Series C, Mechanical systems, machine elements and manufacturing*, 41: 829-835, 1998

⁵³ Gaul L and Hurlebaus S, Identification of the impact location on a plate using wavelets, *Mechanical systems and signal processing*, 12, 783-795, 1998.

⁵⁴ P.T. Coverley, W.J. Staszewski, Impact damage location in composite structures using optimized sensor triangulation procedure, *Smart Materials and Structures* 12(5): 795-803, 2003.

⁵⁵ J. Haywood, P.T. Coverley, W.J. Staszewski, K. Worden, An automatic impact monitor for a composite panel employing smart sensor technology, *Smart Materials and Structures*, 14(1): 265-271, 2005.

⁵⁶ Gang Yan, Li Zhou. Impact load identification of composite structure using genetic algorithms. *Journal of Sound and Vibration*, 319:869-884, 2009.

⁵⁷ Choi K, Chang FK. Identification of impact force and location using distributed sensors. *AIAA Journal*, 34:136-142, 1996.

Reference

- ⁵⁸ Inoue H, Harrigan JJ, Reid SR. Review of inverse analysis for indirect measurement of impact force. *Applied Mechanics Reviews*, 56:503-514, 2001.
- ⁵⁹ Shaw JK, Sirkis JS, Friebele EJ, Jones RT, Kersey AD. Model of transverse plate impact dynamics for design of impact detection methodologies. *AIAA Journal*, 33:1327-1335, 1995.
- ⁶⁰ Shin ES. Real-time recovery of impact force based on finite element analysis. *Computer Structures*, 76:621-627, 2000.
- ⁶¹ Akhavan F, Watkins SE, Chandrashekhara F, Prediction of impact contact forces of composite plates using fiber optic sensors and neural networks. *Mechanics of Advanced Materials and Structures*, 7:195-205, 2000.
- ⁶² Rook T. E and Singh R, Structural intensity calculations for compliant plate-beam structures connected by bearings, *Journal of sound and vibration*, 211(3), 365-387, 1996.
- ⁶³ Nejade A and Singh R, Flexural intensity measurement on finite plates using modal spectrum ideal filtering, *Journal of sound and vibration*, 256(1), 33-63, 2001.
- ⁶⁴ Liu Z.S, Lee H.P, Lu C, Structural intensity study of plates under low-velocity impact, *International journal of impact engineering* 31, 957-975, 2004.
- ⁶⁵ Sang-Woo L, Joo-Hyung K. Jaehwan K. and Heung Soo Ki., Characterization and sensor application of cellulose electro-active paper (EAPap), *Chinese Science Bulletin*, 54 (15), 2009
- ⁶⁶ Timoshenko S. "Theory of Plates and Shells," New York: McGraw-Hill, 1940.
- ⁶⁷ Guyomar D. and Powers J, Transient fields radiated by curved surfaces application to focusing, *Journal of the acoustical society of America*, 76(5):1564-1572, 1984.

Reference

⁶⁸ Guyomar D. and Powers J, Boundary effects on transient radiation fields from vibrating surfaces, *Journal of the acoustical society of America*, 77(3):907-915, 1985.

⁶⁹ Abramowitz M. and Stegun I.A, *Handbook of Mathematical Functions with Formulas, Graphs, and Mathematical Tables*, Government Printing Office Washington U.S, 1964.

⁷⁰ Ventsel E, Krauthammer T, *Thin Plates and Shells: Theory, Analysis and Applications*, M Dekker, New York, 666, 2001.

⁷¹ Anthony J Romano, Phillip B Abraham, Earl G Williams, A Poynting vector formulation for thin shells and plates, and its application to structural intensity analysis and source localization. Part I : Theory, 87 :1166-1175, 1990.

⁷².Royer D, Dieulesaint E, *Elastic Waves in Solids I: Free and Guided Propagation*, 2000. Springer-Verlag Berlin Heidelberg; Germany

⁷³ Anthony J Romano, Phillip B Abraham, and Earl G. Williams, A Poynting vector formulation for thin shells and plates, and its application to structural intensity analysis and source localization. Part I: Theory, *Journal acoustical society of America* 87(3), 1166-1175,1990.